Supporting Information

Thinking Outside the "Blue Box": from Molecular to Supramolecular pH-Responsiveness

Table of Contents:

1. Experimental Procedures

1.1. General procedures

Starting materials were purchased from commercial suppliers and used without further purification. Compounds **1**·2Br[1] and 4-formyl-1-methylpyridinium iodide[2] were prepared according to published procedures. Milli-Q water was purified with a Millipore Gradient A10 apparatus. Merck 60 F_{254} foils were used for thin layer chromatography, and Merck 60 (230-400 mesh) silica gel was used for flash chromatography. NMR spectra were recorder on a Bruker Advance 300, 400 or 500 MHz for ^{1}H, and 75, 101 or 126 MHz for ^{13}C, all equipped with a dual cryoprobe. The solvent used for NMR experiments was D_2O, DMSO-d_6 or CD_3CN. Mass spectrometry experiments were carried out in a LCQ-q-TOF Applied Biosystems QSTAR Elite spectrometer for low and high resolution ESI. UV/Vis spectra were recorded on a Jasco V-650 spectrometer. Potentiometric titration was carried out with CRISON 5028 pH electrode for microsamples with Ag/AgCl reference element. Melting points were measured using a SMP3 Stuart Scientific apparatus and are uncorrected. Microanalyses for C, H and N were performed by the elemental analyses general service of the University of A Coruña, using a Carlo Erba Instruments EA 1108 apparatus.

1.2. Synthesis and characterization data of 2b·2Br.

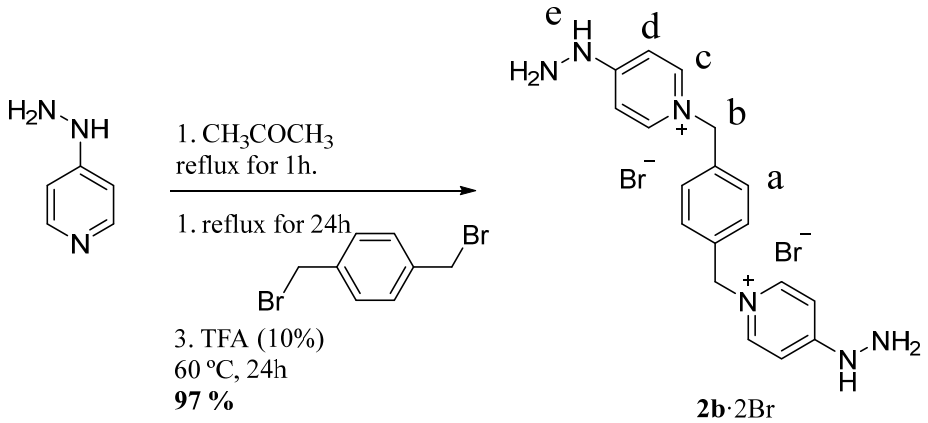

A solution of 4-hydrazinopyridine (116 mg, 1.06 mmol) in 140 mL of acetone was heated at reflux for 1h. After this, *α,α'*-dibromo-*p*-xylene (112 mg, 0.425 mmol), was added to the reaction mixture and heated at reflux for 24 hours. The obtained precipitate was filtrated upon cooling and washed with hot acetone (3 × 20 mL) and diethyl ether (3 × 10 mL). The obtained solid (232 mg) was dissolved in 40 mL of MiliQ water, a catalytic amount of TFA (0.01 eq.) was added, and the resulting mixture was heated at 60 ºC for 24 h. The solvent was removed under reduce pressure to yielding virtually pure **2b**·2Br (200 mg, 97 %) as a white powder. Mp = 250.6 – 252.8 ºC (decomposition).^{1}H NMR (400 MHz, D_2O) δ 8.11 (d, J = 7.1 Hz, 4H), 7.35 (s, 4H), 6.97 (d, J = 7.6 Hz, 4H), 5.34 (s, 4H) ppm. ^{13}C NMR (101 MHz, D_2O) δ 157.44 (C), 142.92 (CH), 135.20 (C), 129.08 (CH), 107.27 (CH), 60.69 (CH_2) ppm. HR-ESI-MS: m/z calculated for $[M+2C_3H_6-2Cl]^{2+}$ 201.1260, found: 201.1251. $[M+2C_3H_6-H-2Cl]^{+}$ 401.2448, found: 401.2436. Analysis calculated for $C_{18}H_{22}Br_2N_6$: C, 44.83; H, 4.60; N, 17.43; Found: C, 44.94; H, 4.57; N 17. 39.

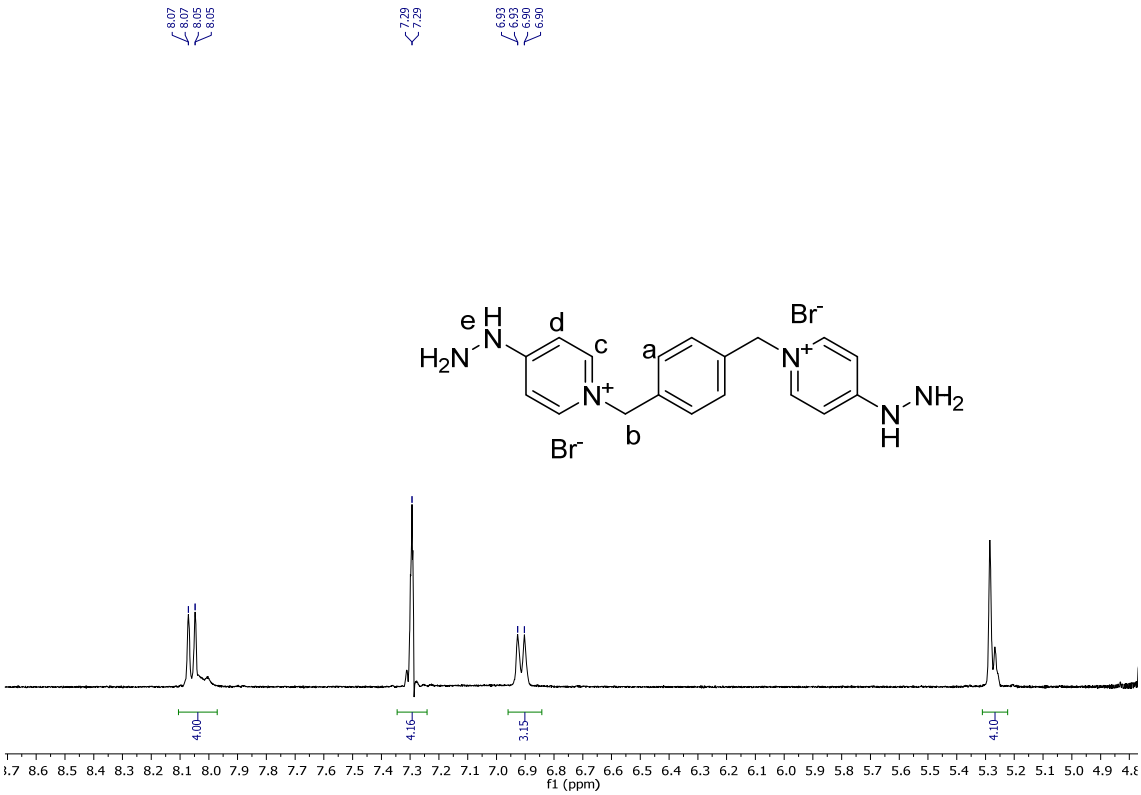

Figure S1. ^{1}H NMR (400 MHz, D_2O) spectrum of **2b**·2Br.

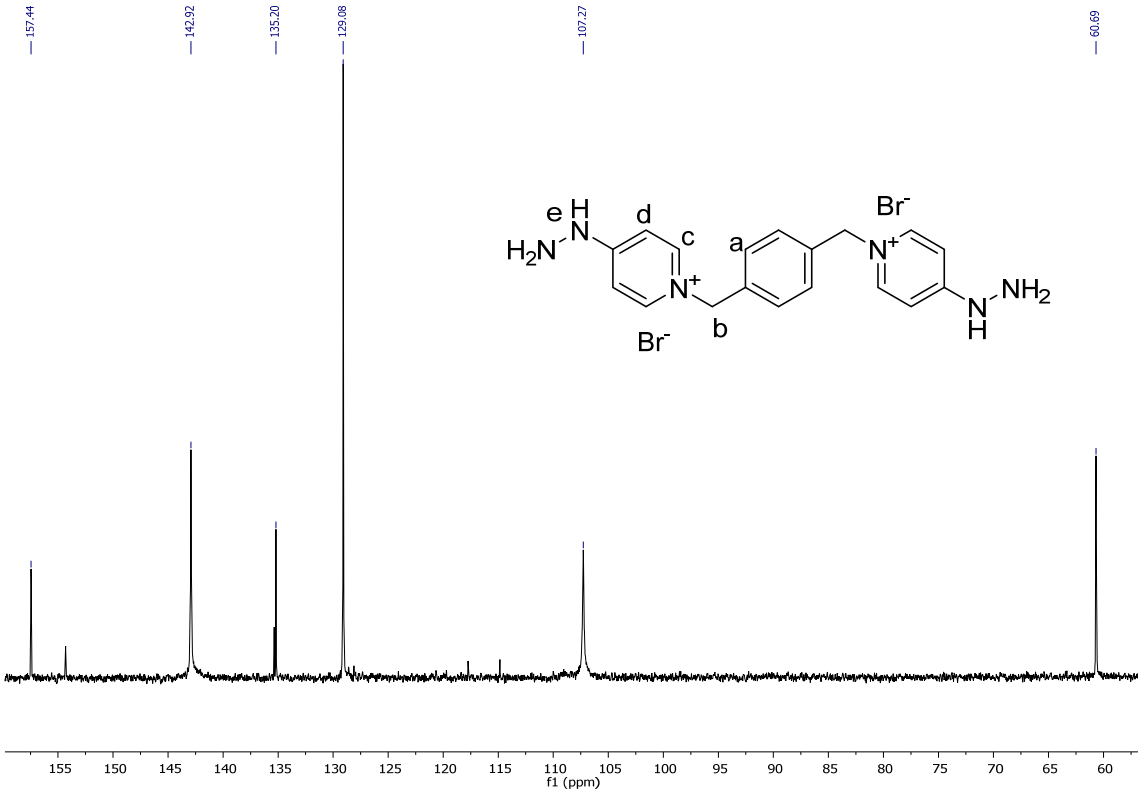

Figure S2. ^{13}C NMR (101 MHz, D_2O) spectrum of **2b**·2Br.

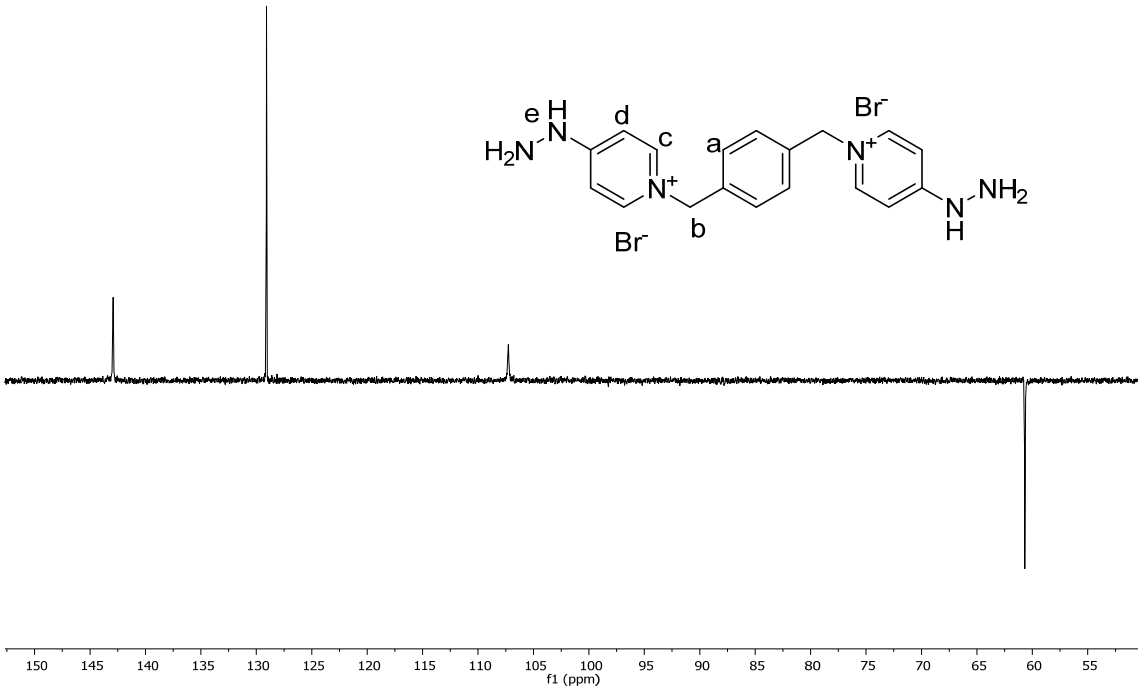

Figure S3. DEPT-135 (101 MHz, D_2O) spectrum of **2b**·2Br.

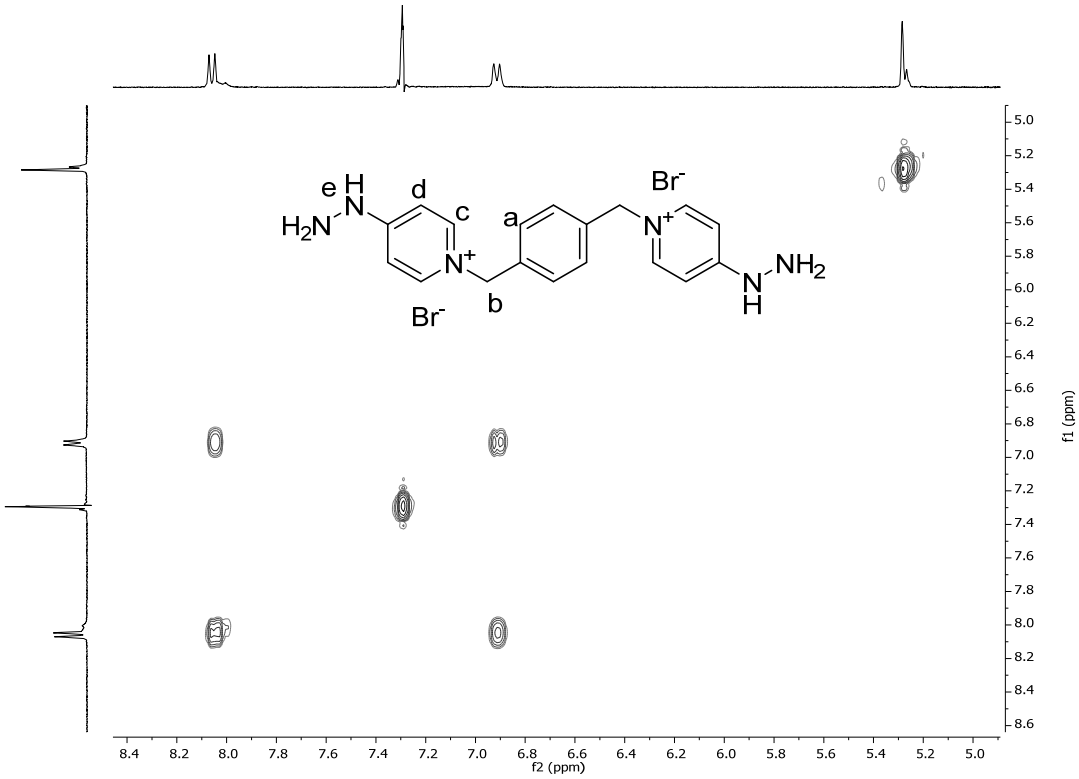

Figure S4. ^{1}H-^{1}H COSY (400 and 101 MHz, D_2O) spectrum of **2b**·2Br.

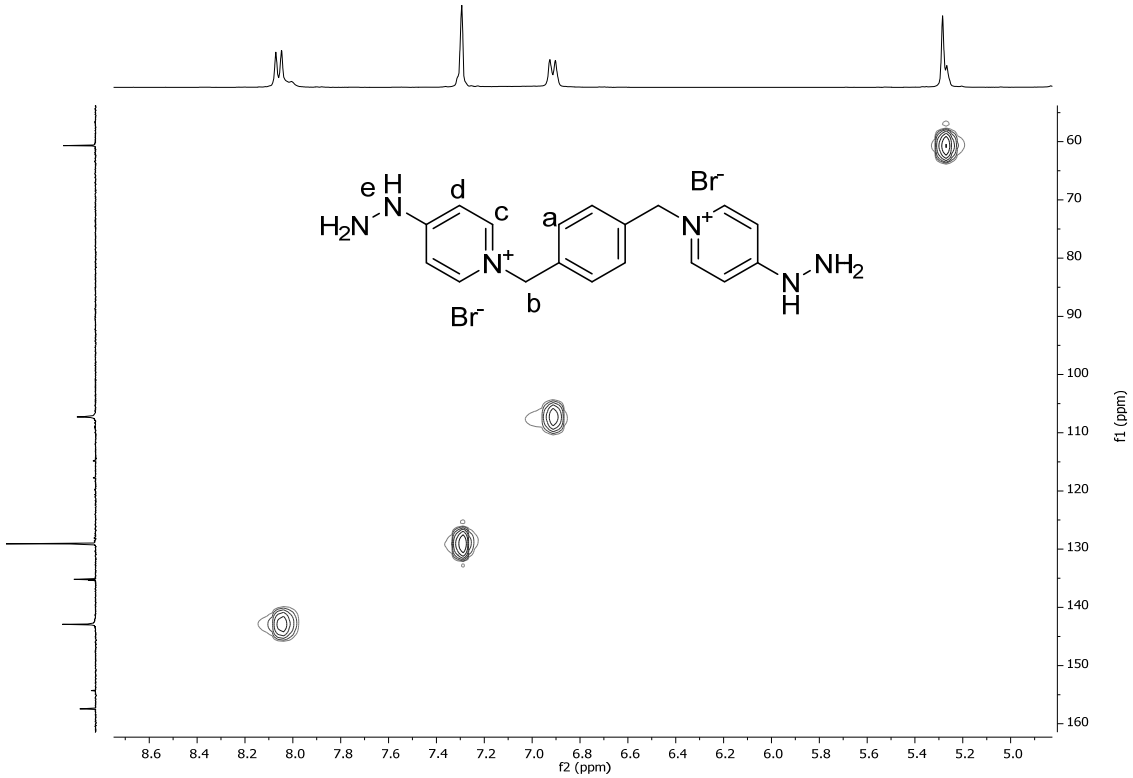

Figure S5. ^{1}H-^{13}C HSQC (400 and 101 MHz, D_2O) spectrum of **2b**·2Br.

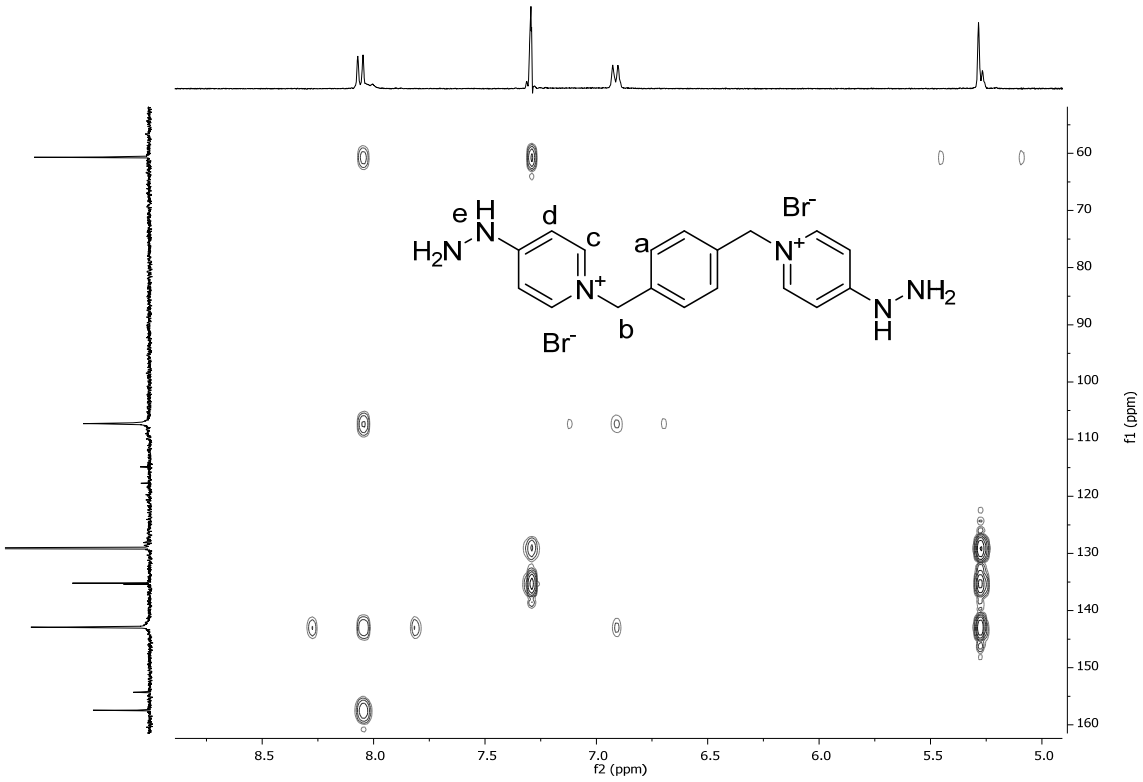

Figure S6. ^{1}H-^{13}C HMBC (400 and 101 MHz, D_2O) spectrum of **2b**·2Br.

1.3. Synthesis and characterization data of 3·I.

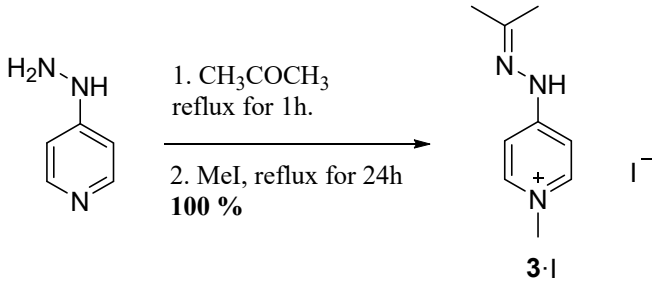

A solution of 4-hydrazinopyridine (220 mg, 2.02 mmol) in 50 mL of acetone was heated at reflux for 1h. After this time, the solution was cooled and then MeI (2 mL, 30 mmol) was added to the reaction mixture and stirred at room temperature for 24 hours. Upon cooling, the solvent was removed under vacuum yielding virtually pure **3**·I (588 mg, 100 %) as a brownish solid. Mp = 178.1-180.5 (decomposition). ^{1}H NMR (300 MHz, D_2O) δ 7.95 (d, J = 5.9 Hz, 2H), 7.07 (s, 2H), 3.85 (broad s, 3H), 2.01 (s, 3H), 1.94 (s, 3H) ppm. ^{13}C NMR (75 MHz, D_2O) δ 161.98 (C=N), 153.94 (C), 143.51 (CH), 107.44 (CH), 44.84 (CH_3), 24.35 (CH_3), 17.37 (CH_3) ppm.

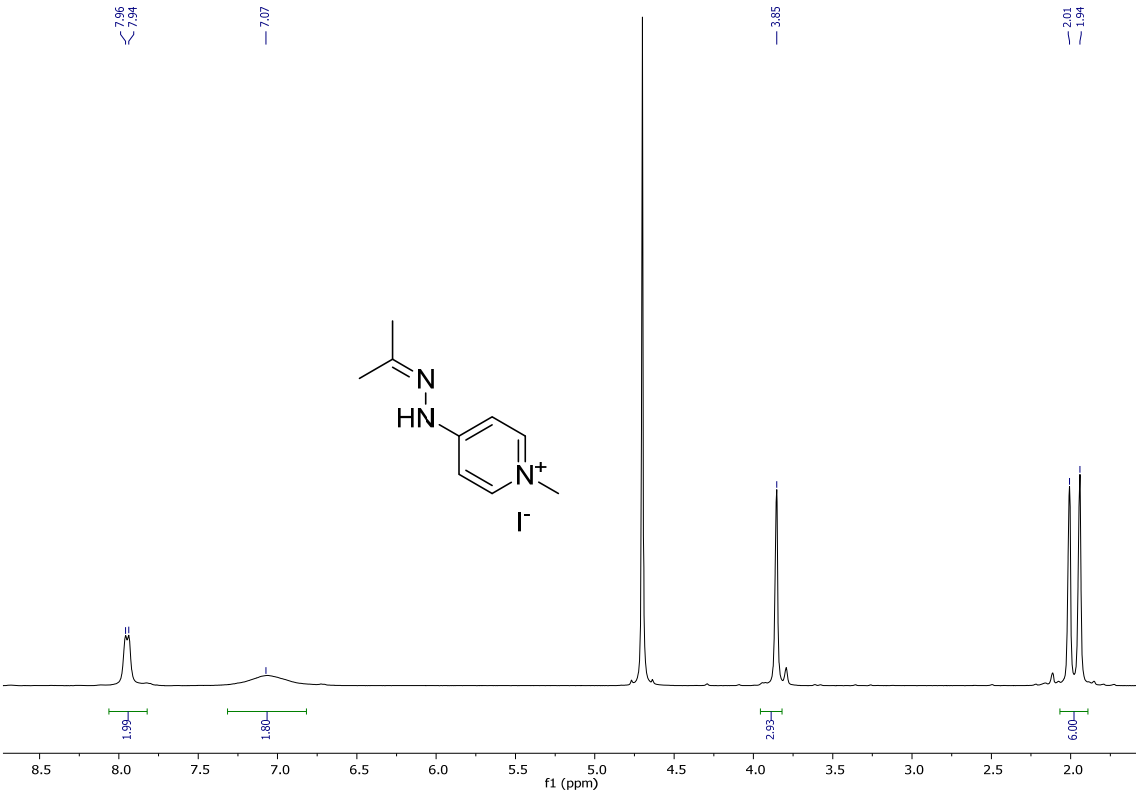

Figure S7. ^{1}H NMR (300 MHz, D_2O) spectrum of **3**·I.

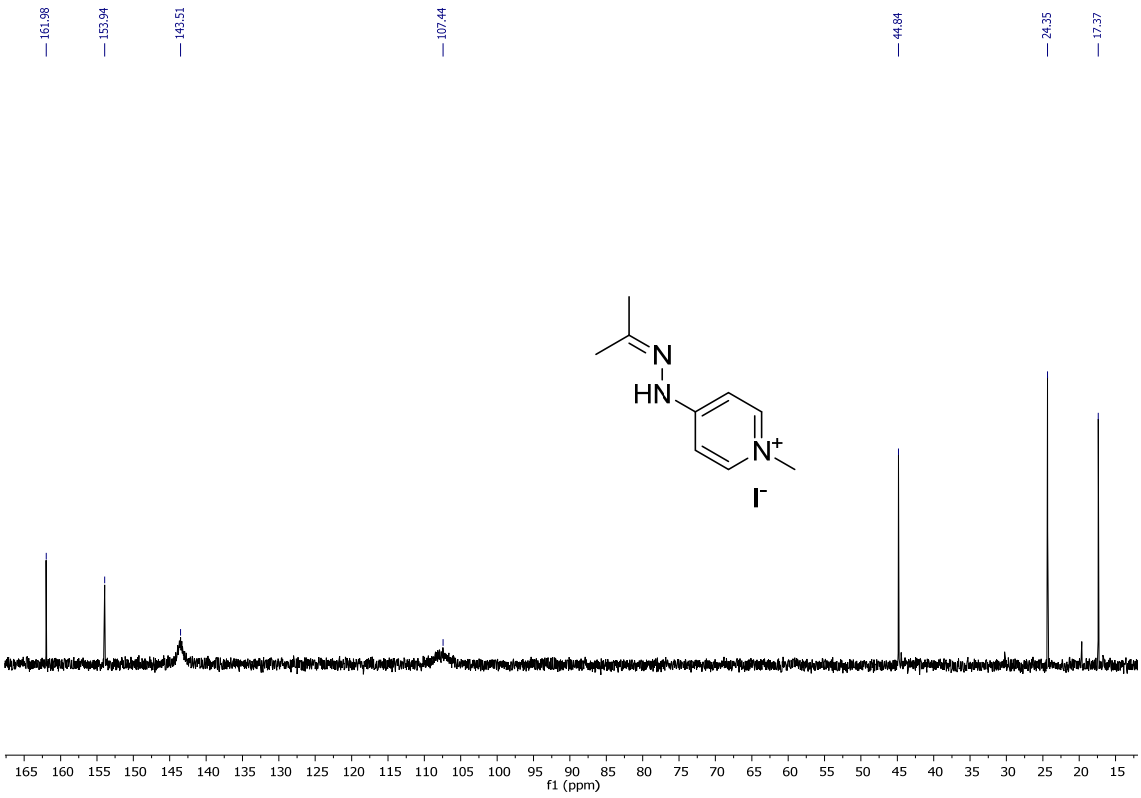

Figure S8. ^{13}C NMR (75 MHz, D_2O) spectrum of **3**·I.

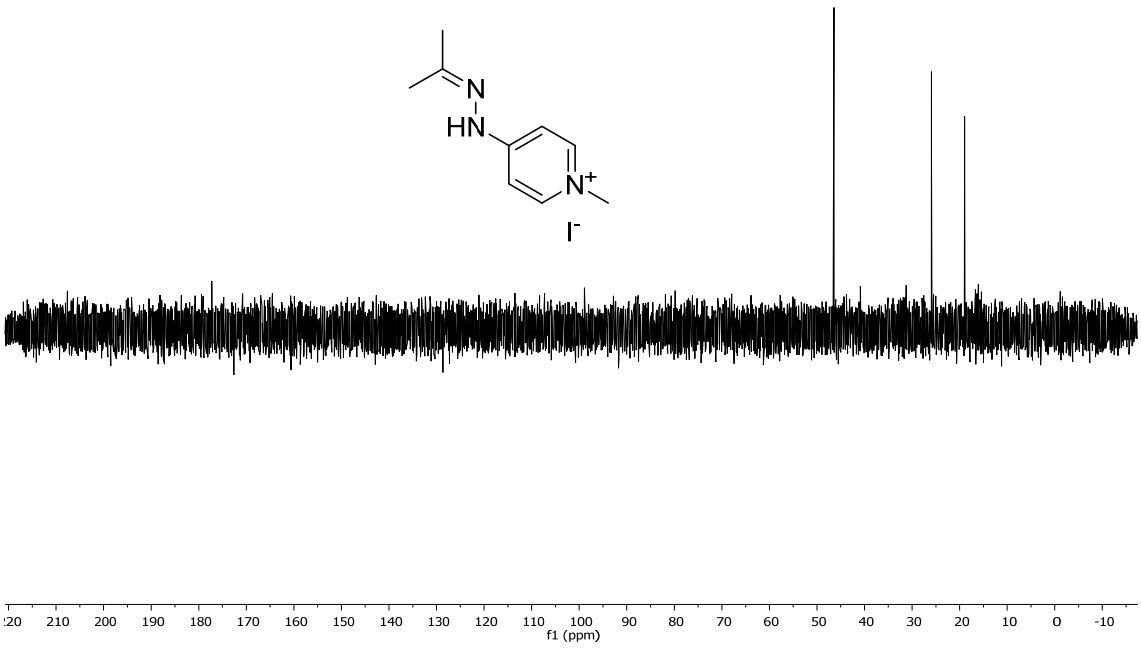

Figure S9. DEPT-135 (75 MHz, D_2O) spectrum of **3**·I.

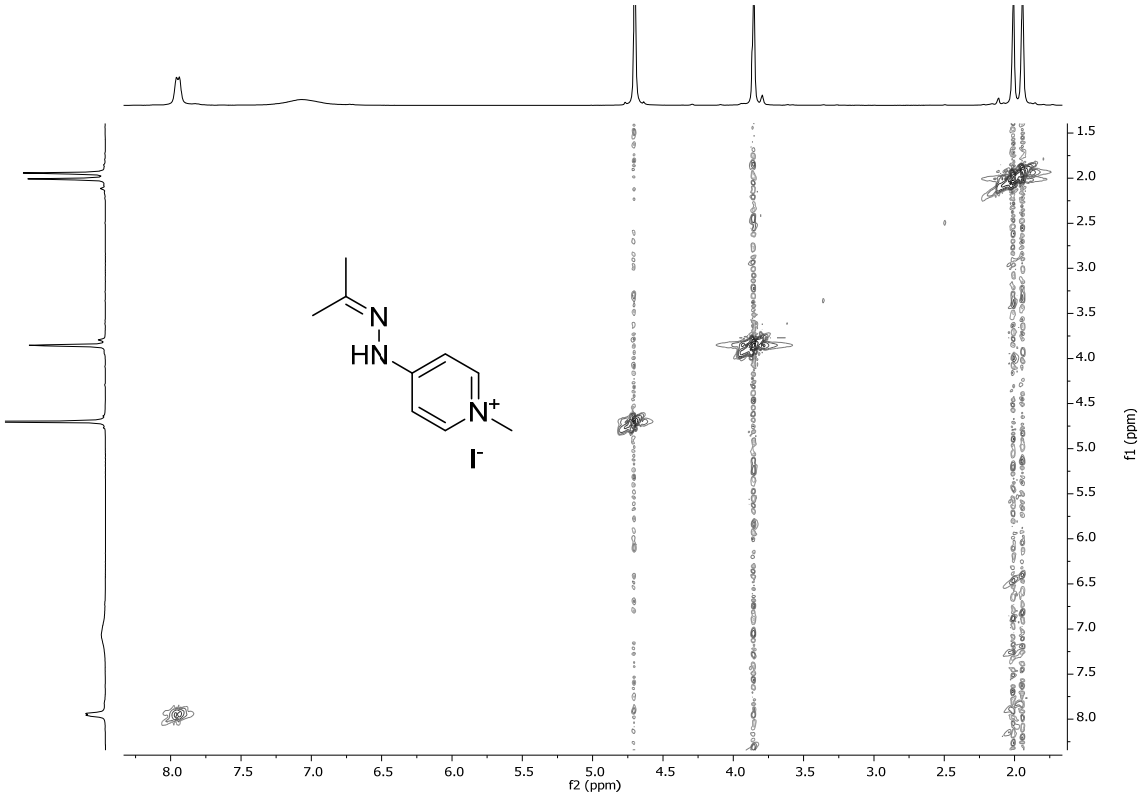

Figure S10. ^{1}H-^{1}H COSY (300 and 75 MHz, D_2O) spectrum of **3**·I.

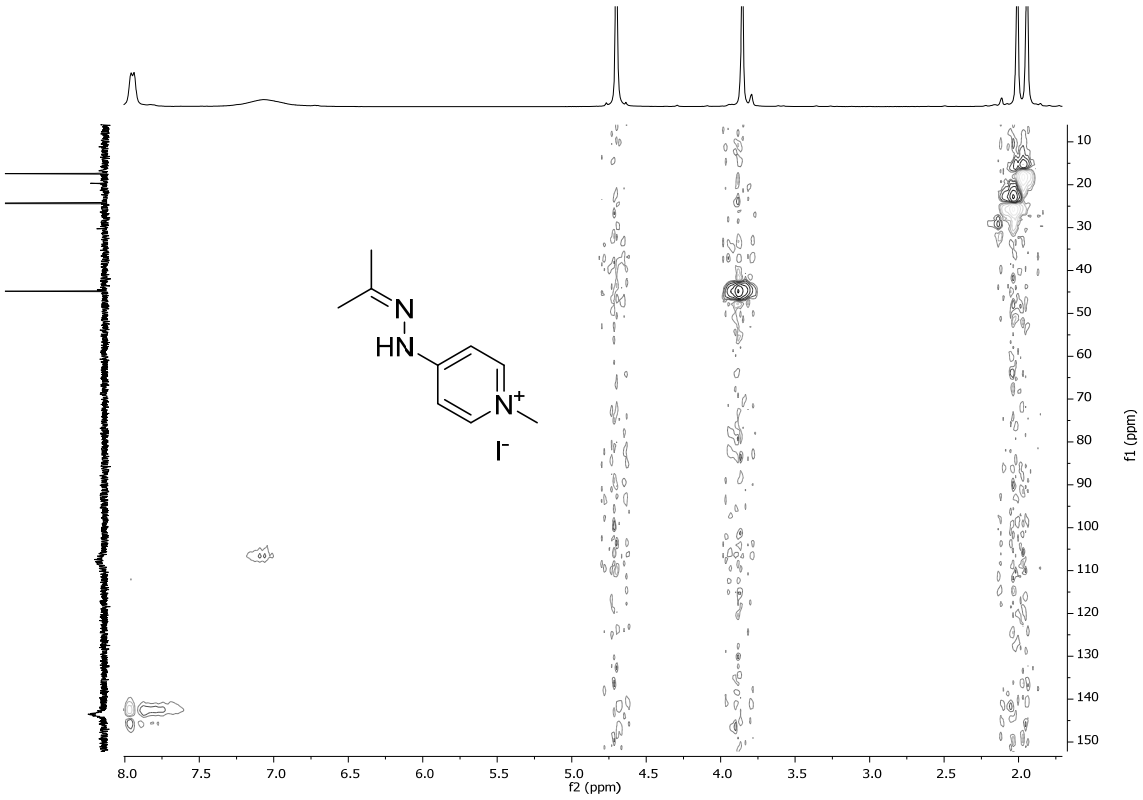

Figure S11. ^{1}H-^{13}C HSQC (300 and 75 MHz, D_2O) spectrum of **3**·I.

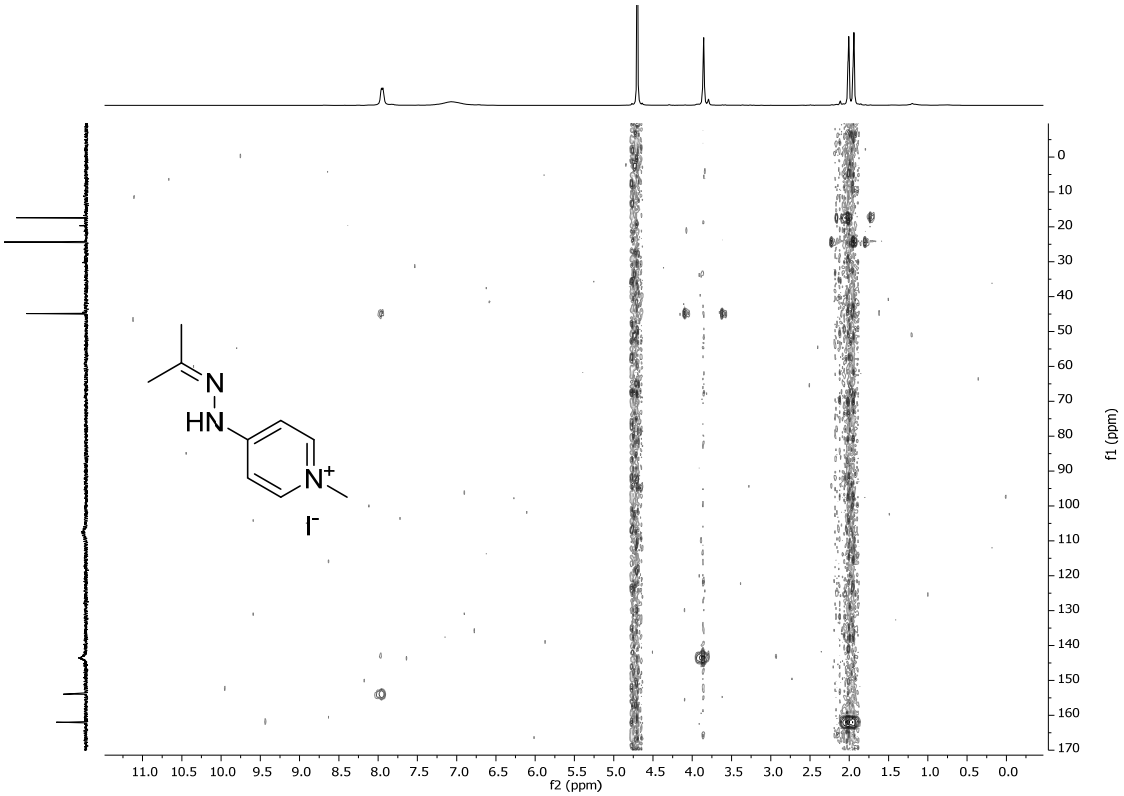

Figure S12. ^{1}H-^{13}C HMBC (300 and 75 MHz, D_2O) spectrum of **3**·I.

1.4. Synthesis and characterization data of L·2Cl.

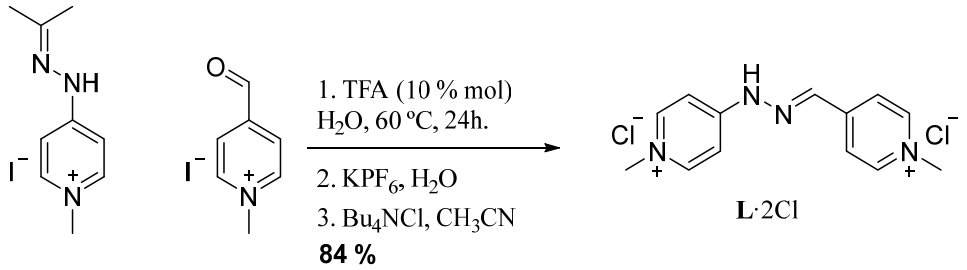

A solution of **3**·I (380 mg, 1.3 mmol), 4-formyl-1-methylpyridinium iodide (390 mg, 1.56 mmol)[S1] and TFA (10% molar) in 260 mL of water was heated at 60 ºC for 24h. After cooling, excess of KPF_6 was added until no further precipitation was observed. The obtained solid was filtrated, washed with water (3 × 15 mL) and dissolved in acetonitrile (20 mL). An excess of Bu_4NCl was added until no further precipitation was observed. The obtained solid was filtrated and washed with acetonitrile (3 × 20 mL) yielding virtually pure **L**·2Cl (328 mg, 84 %) as a yellowish solid. Mp = 220.1-223.4 ºC. ^{1}H NMR (500 MHz, D_2O) δ 8.58 (d, J = 6.6 Hz, 2H), 8.18 – 8.01 (m, 5H), 7.71 (broad s, 1H), 7.01 (broad s, 1H), 4.18 (s, 3H), 3.9 (s, 3H) ppm. ^{13}C NMR (126 MHz, D_2O) δ 154.00 (C), 149.19 (C), 145.08 (CH), 144.43 (CH), 140.71 (HC=N), 124.27 (CH), 110.00 (CH), 108.77 (CH), 47.50 (CH_3), 45.40 (CH_3) ppm. HR-ESI-MS: m/z calculated for $[M-H-2Cl]^+$ 227.1291, found: 227.1302. Analysis calculated for $C_{13}H_{16}Cl_2N_4$: C, 54.19; H, 5.39; N, 18.73; Found: C, 54.31 ; H, 5.37; N 5.29.

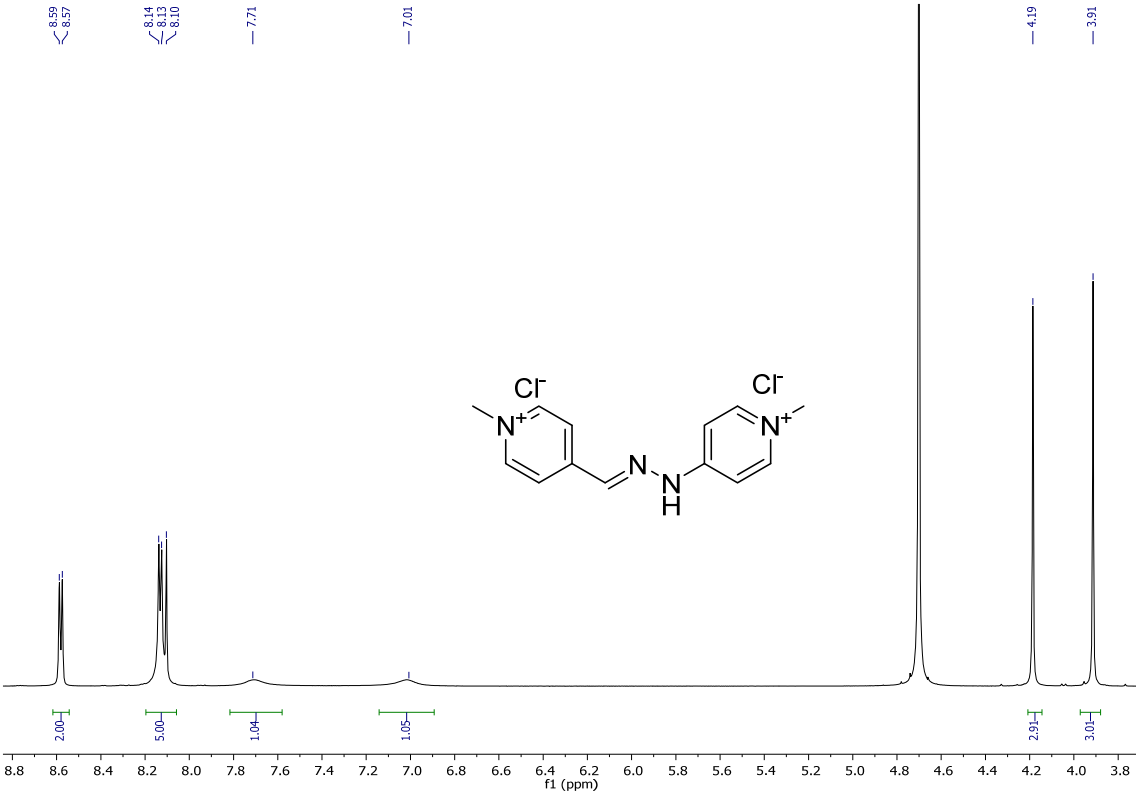

Figure S13. ^{1}H NMR (500 MHz, D_2O) spectrum of **L**·2Cl.

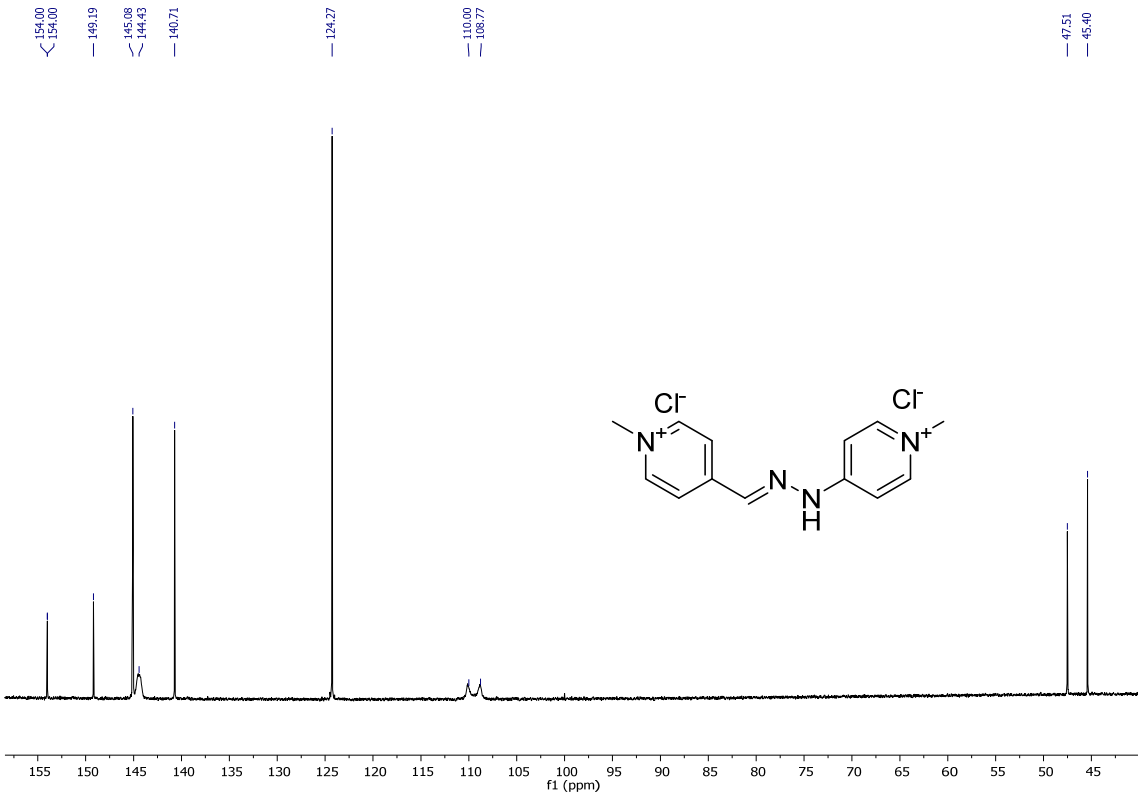

Figure S14. ^{13}C NMR (126 MHz, D_2O) spectrum of **L**·2Cl.

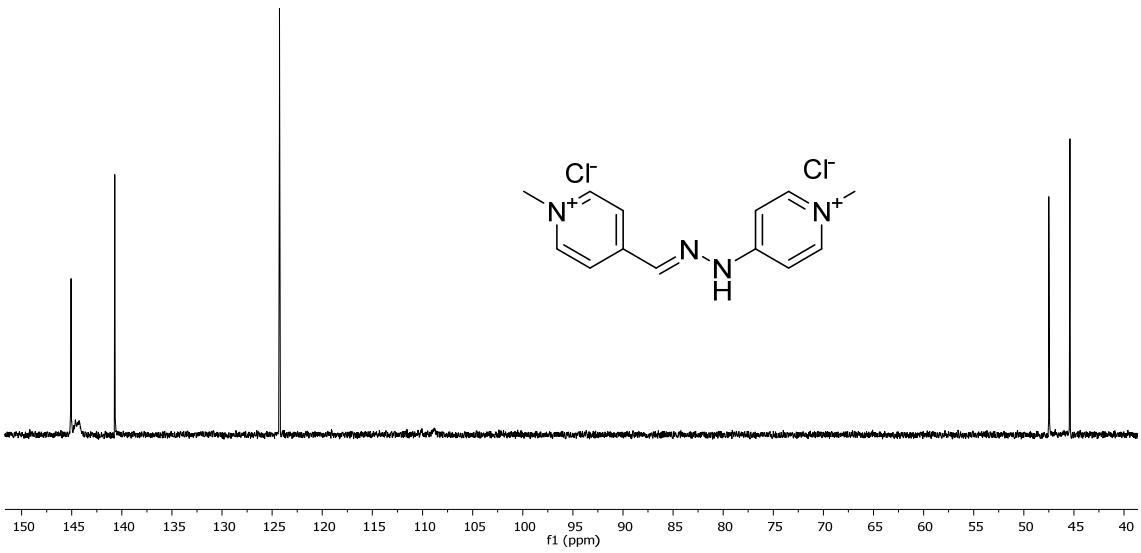

Figure S15. DEPT-135 (126 MHz, D_2O) spectrum of **L**·2Cl.

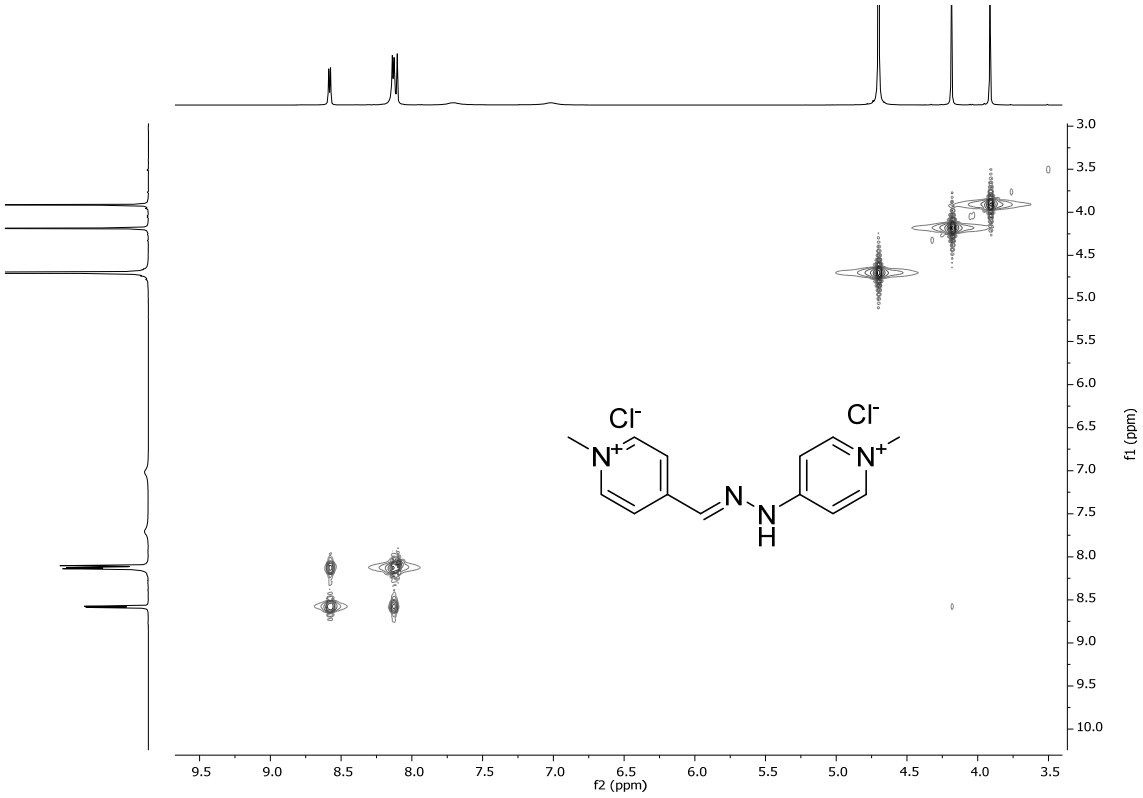

Figure S16. ^{1}H-^{1}H COSY (500 and 126 MHz, D_2O) spectrum of **L**·2Cl.

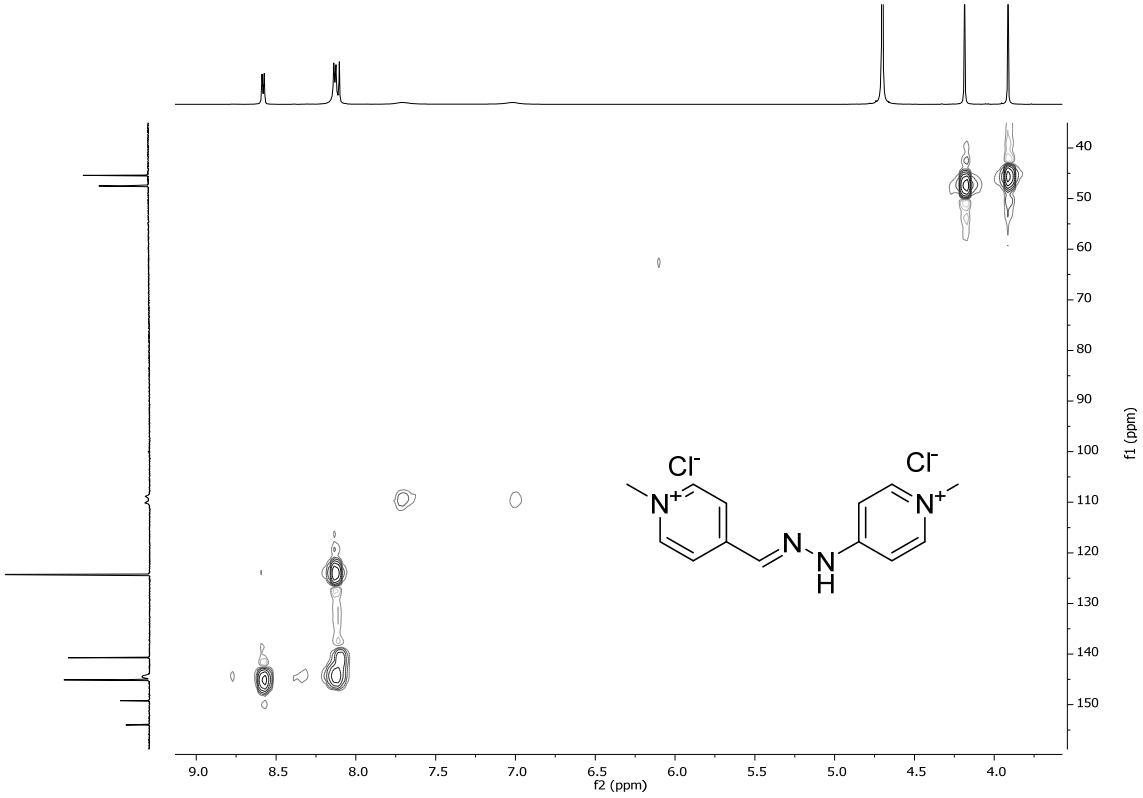

Figure S17. ^{1}H-^{13}C HSQC (500 and 126 MHz, D_2O) spectrum of **L**·2Cl.

Figure S18. ^{1}H-^{13}C HMBC (500 and 126 MHz, D_2O) spectrum of **L**·2Cl.

1.5. Synthesis and characterization data of R·4PF$_6$.

A solution of **1**·2Br[S2] (140 mg, 0.4 mmol), **2b**·2Br (222 mg, 0.4 mmol) and TFA (10% molar) in 260 mL of water was heated at 60 ºC for 24 h. After cooling, excess of KPF$_6$ was added until no further precipitation was observed. The obtained solid was filtrated and washed with water (3 × 10 mL), yielding virtually pure **R**·4PF$_6$ (393 mg, 83 %) as a reddish powder. Mp = 312.1 – 313.0 ºC (decomposition).^{1}H NMR (500 MHz, CD$_3$CN) δ 10.83 (s, 2H), 8.55 (d, J = 6.9 Hz, 4H), 8.50 (broad s, 2H), 8.27 (d, J = 6.9 Hz, 4H), 8.20 (s, 2H), 7.79 (broad s, 4H), 7.62 (s, 4H), 7.55 (s, 4H), 7.25 (broad s, 2H), 5.73 (s, 4H), 5.49 (s, 4H) ppm. ^{13}C NMR (126 MHz, CD$_3$CN) δ 154.32 (C), 149.65 (C), 144.57 (CH), 144.13 (CH), 142.82 (CH), 140.43 (HC=N), 134.54 (C), 134.06 (C), 131.13 (CH), 130.73 (CH), 124.67 (CH), 110.05 (CH), 109.67 (CH), 63.08 (CH$_2$), 61.07 (CH$_2$) ppm. HR-ESI-MS: m/z calculated for [M-PF$_6$]$^+$ 1039.1983, found: 1039.1981. [M-2PF$_6$]$^{2+}$. 447.1168, found 447.1155. [M-3PF$_6$]$^{3+}$. 249.7563, found 249.7551. [M-H-2PF$_6$]$^+$. 893.2263, found: 893.2243. [M-H-3PF$_6$]$^{2+}$. 374.1308, found 374.1300. [M-H-4PF$_6$]$^{3+}$. 201.0989, found 201.0990. [M-2H-3PF$_6$]$^+$. 747.2543, found: 747.2541. [M-2H-4PF$_6$]$^{2+}$. 301.1448, found 301.1442. Analysis calculated for C$_{38}$H$_{36}$F$_{24}$N$_8$P$_4$: C, 38.53; H, 3.06; N, 9.46; Found: C, 38.65; H, 3.03; N, 9.39.

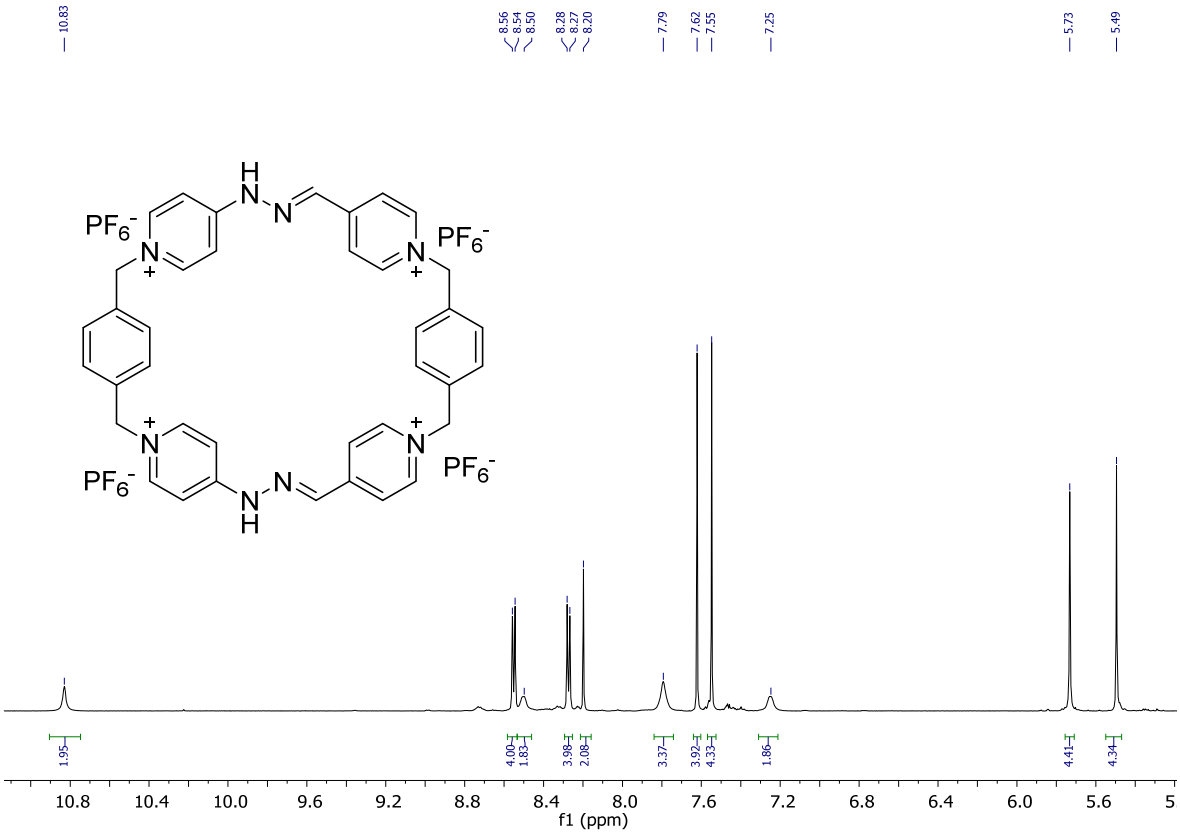

Figure S19. ^{1}H NMR (500 MHz, CD$_3$CN) spectrum of **R**·4PF$_6$.

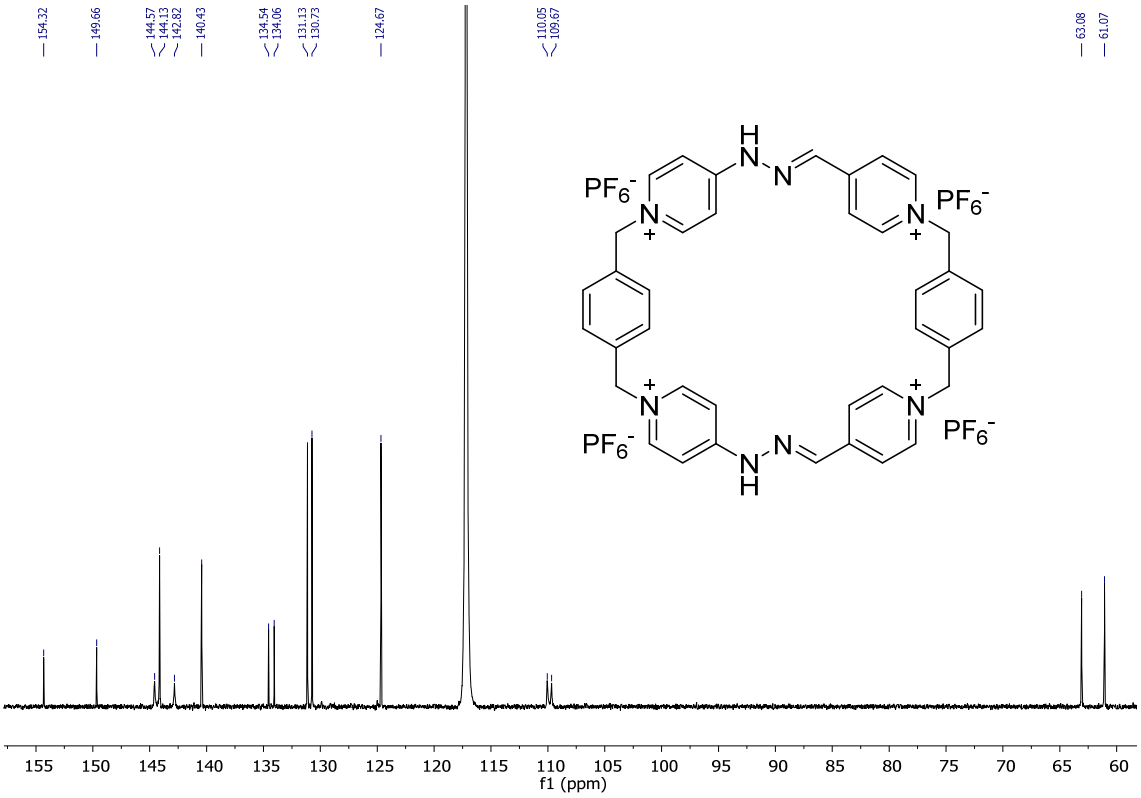

Figure S20. ^{13}C NMR (126 MHz, CD_3CN) spectrum of **R**·4PF_6.

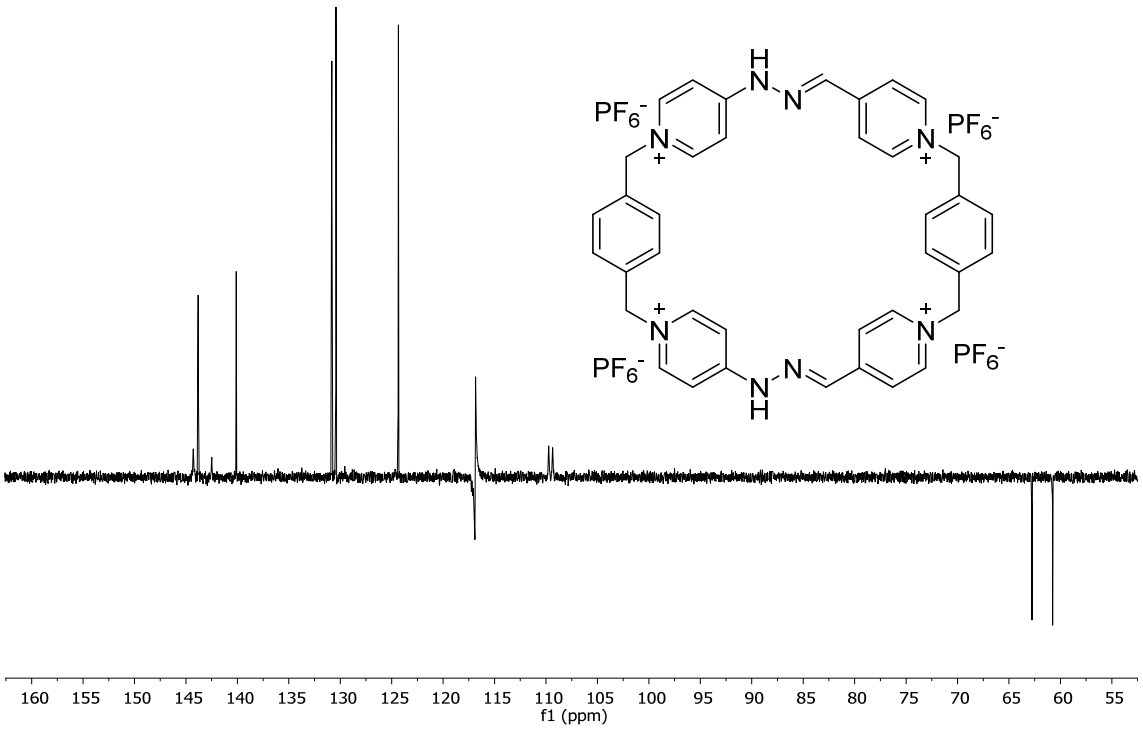

Figure S21. DEPT-135 (126 MHz, CD_3CN) spectrum of **R**·4PF_6.

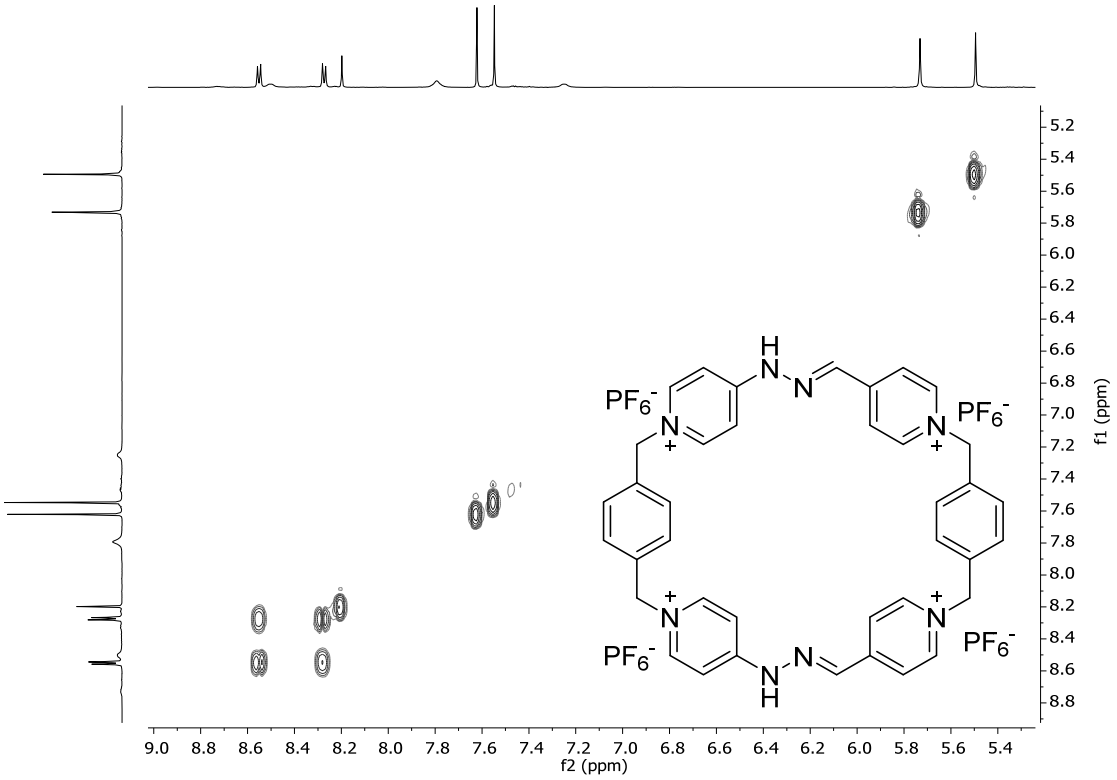

Figure S22. ^{1}H-^{1}H COSY (500 and 126 MHz, CD_3CN) spectrum of **R**·4PF_6.

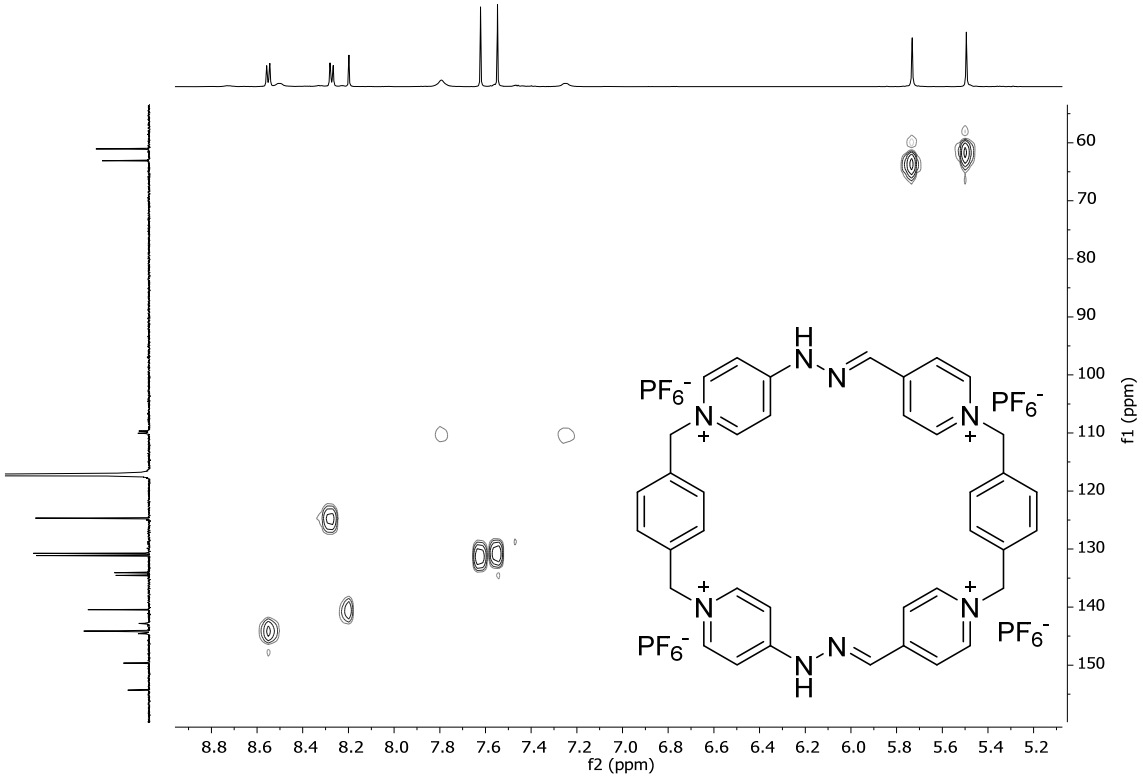

Figure S23. ^{1}H-^{13}C HSQC (500 and 126 MHz, CD_3CN) spectrum of **R**·4PF_6.

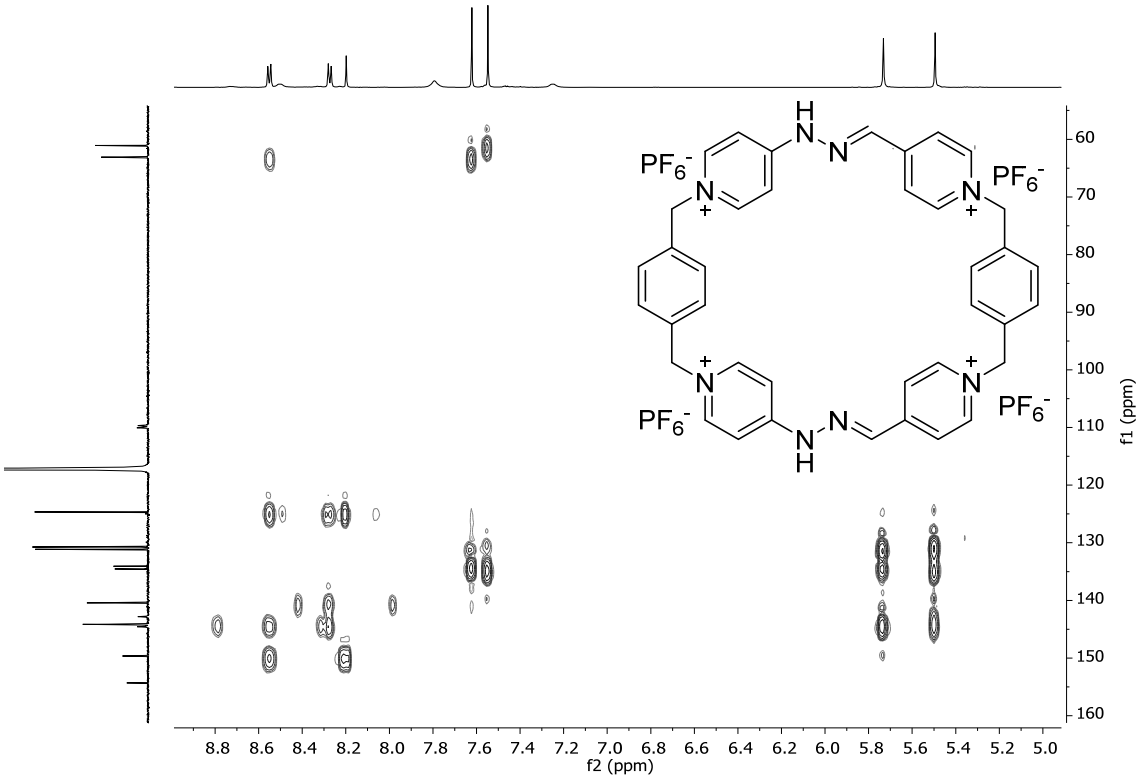

Figure S24. ^{1}H-^{13}C HMBC (500 and 126 MHz, CD_3CN) spectrum of **R**·4PF_6.

1.6. Synthesis and characterization data of R·4Cl.

An excess of tetrabutylammonium chloride (TBACl), was added to a solution of **R**·4PF_6 (393 mg, 0.33 mmol) in acetonitrile until no further precipitation was observed. The obtained solid was filtrated and washed with acetonitrile (3 × 10 mL) yielding **R**·4Cl (220 mg, 89 %) as a beige powder. Mp = 298.5 – 299.0 ºC.

1.6.1. R^{4+} (pD = 6):

^{1}H NMR (500 MHz, D_2O) *δ* 8.75 (d, *J* = 6.4 Hz, 4H), 8.59 (broad s, 2H), 8.26 (s, 2H), 8.24 (d, *J* = 6.6 Hz, 4H), 7.97 (broad s, 2H), 7.71 (broad s, 2H), 7.61 (s, 4H), 7.53 (s, 4H), 7.22 (broad s, 2H), 5.82 (s, 4H), 5.53 (s, 4H) ppm. ^{13}C NMR (126 MHz, D2O) *δ* 154.58 (C), 150.02 (C), 144.19 (CH), 143.34 (CH), 142.88 (CH), 140.69 (HC=N), 134.94 (C), 134.47 (C), 130.83 (CH), 130.43 (CH), 124.72 (CH), 109.99 (CH), 109.87 (CH), 63.46 (CH_2), 61.37 (CH_2) ppm.

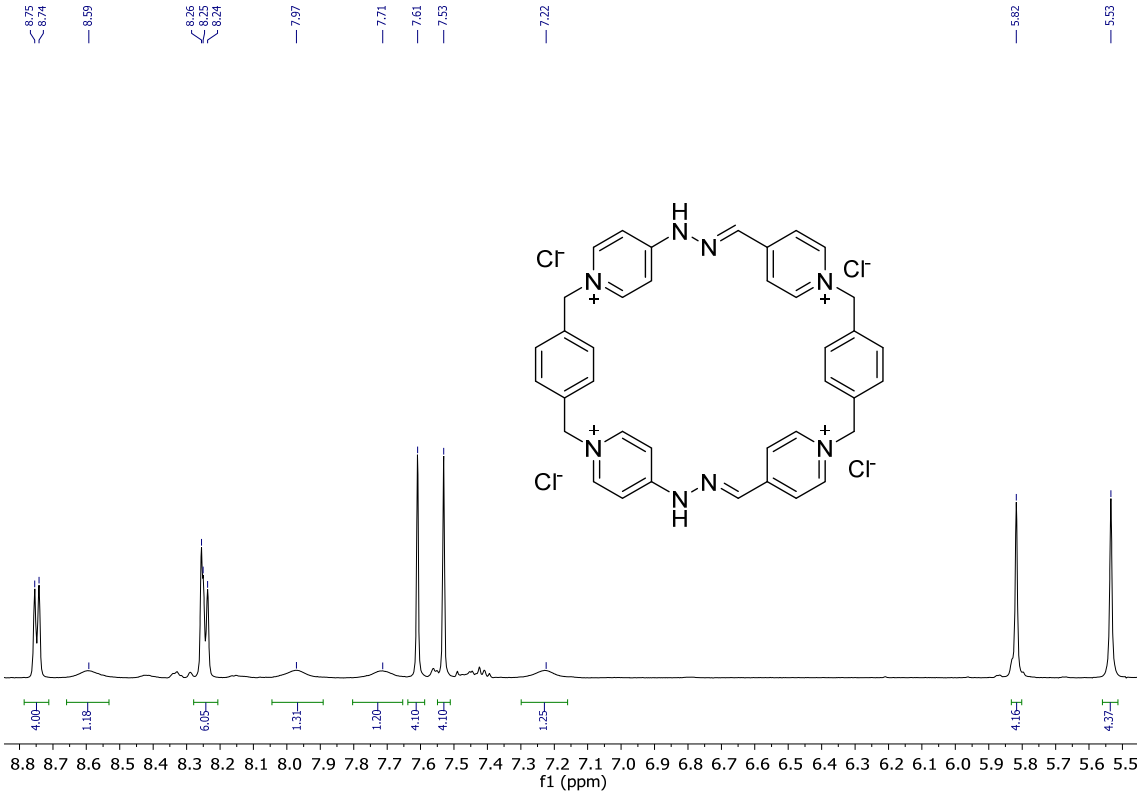

Figure S25. ^{1}H NMR (500 MHz, D_2O) spectrum of **R**·4Cl.

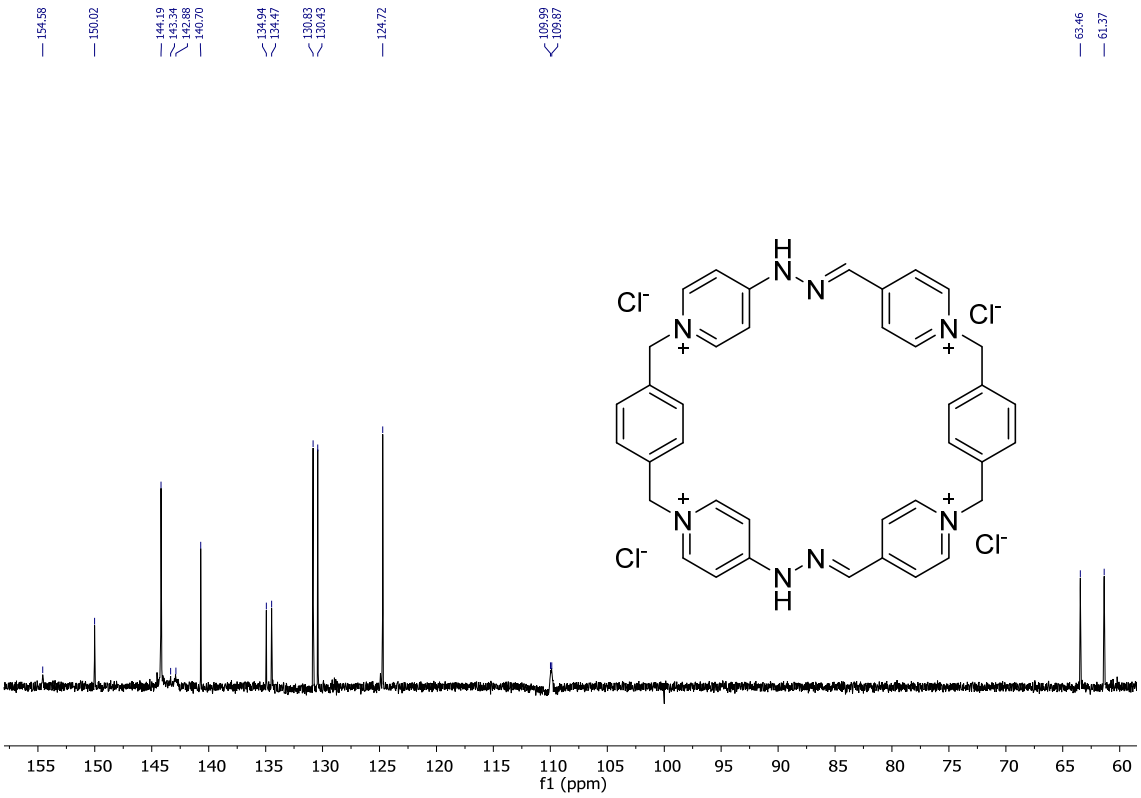

Figure S26. ^{13}C NMR (126 MHz, D_2O) spectrum of **R**·4Cl.

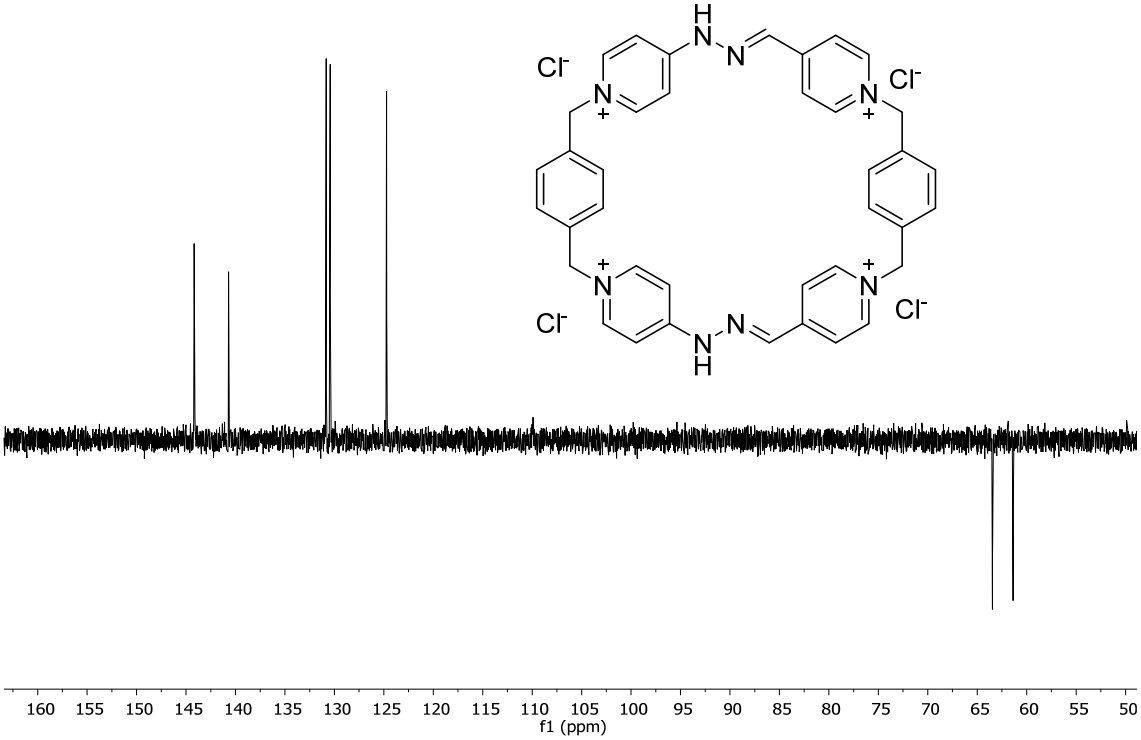

Figure S27. DEPT-135 (126 MHz, D_2O) spectrum of **R**·4Cl.

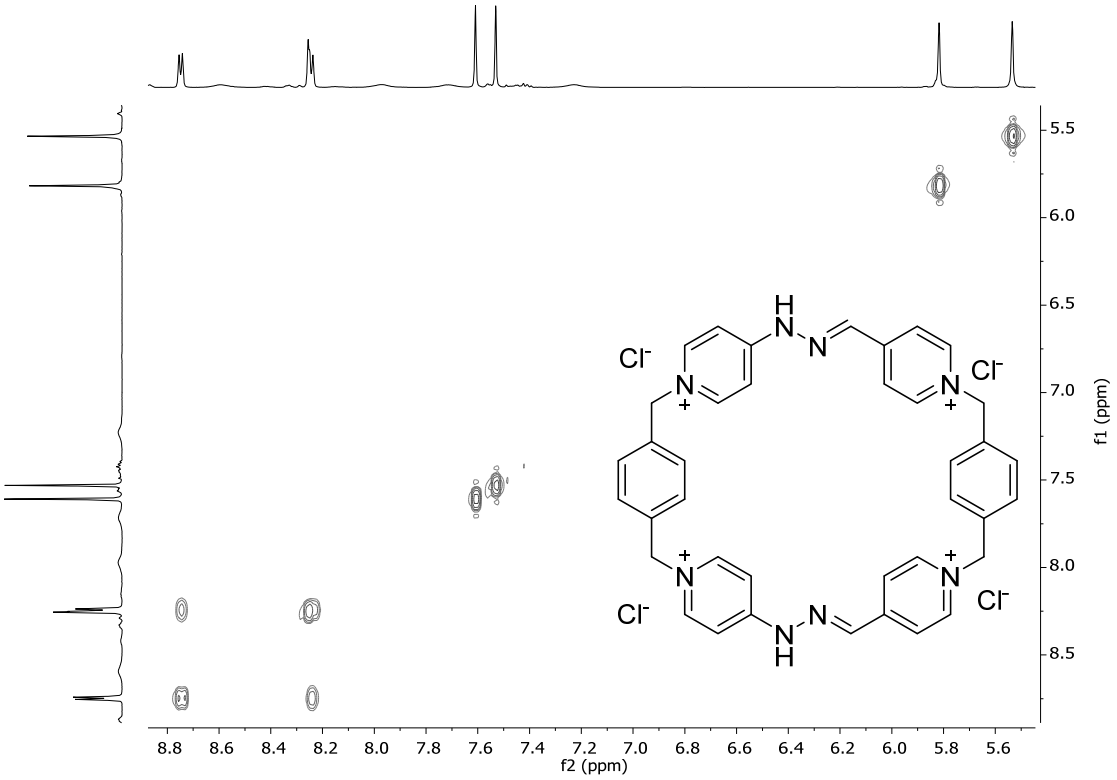

Figure S28. ^{1}H-^{1}H COSY (500 MHz, D_2O) spectrum of **R**·4Cl.

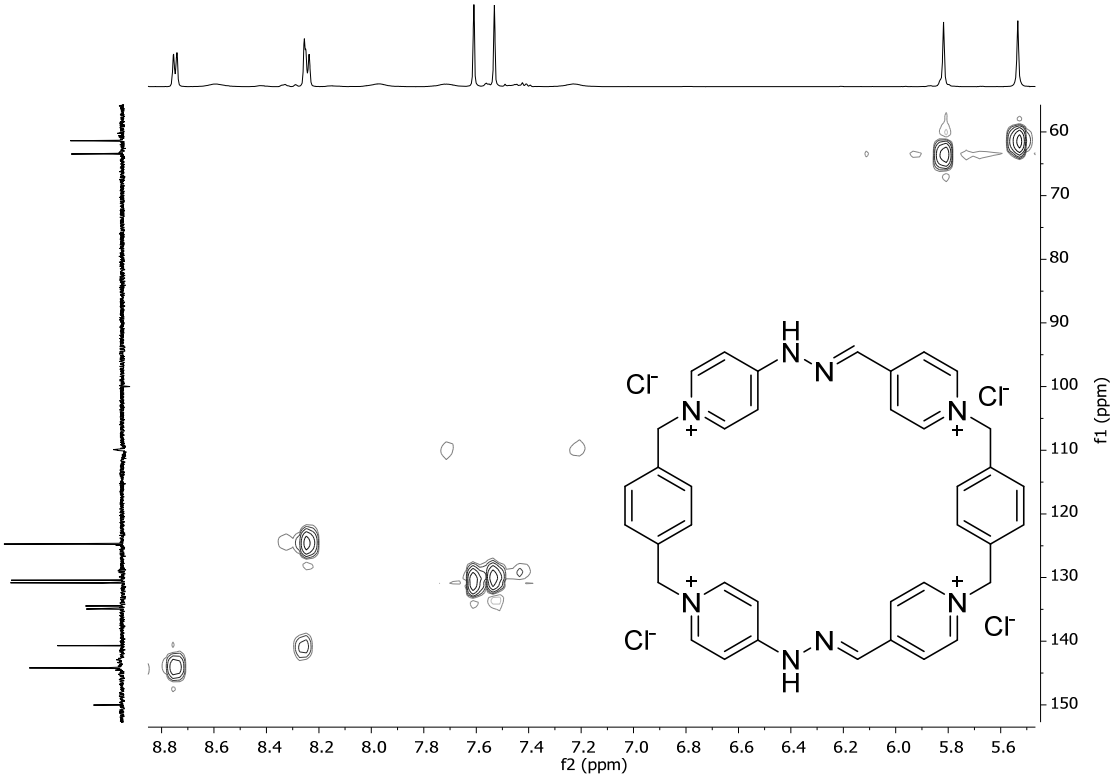

Figure S29. ^{1}H-^{13}C HSQC (500 and 126 MHz, D_2O) spectrum of **R**·4Cl.

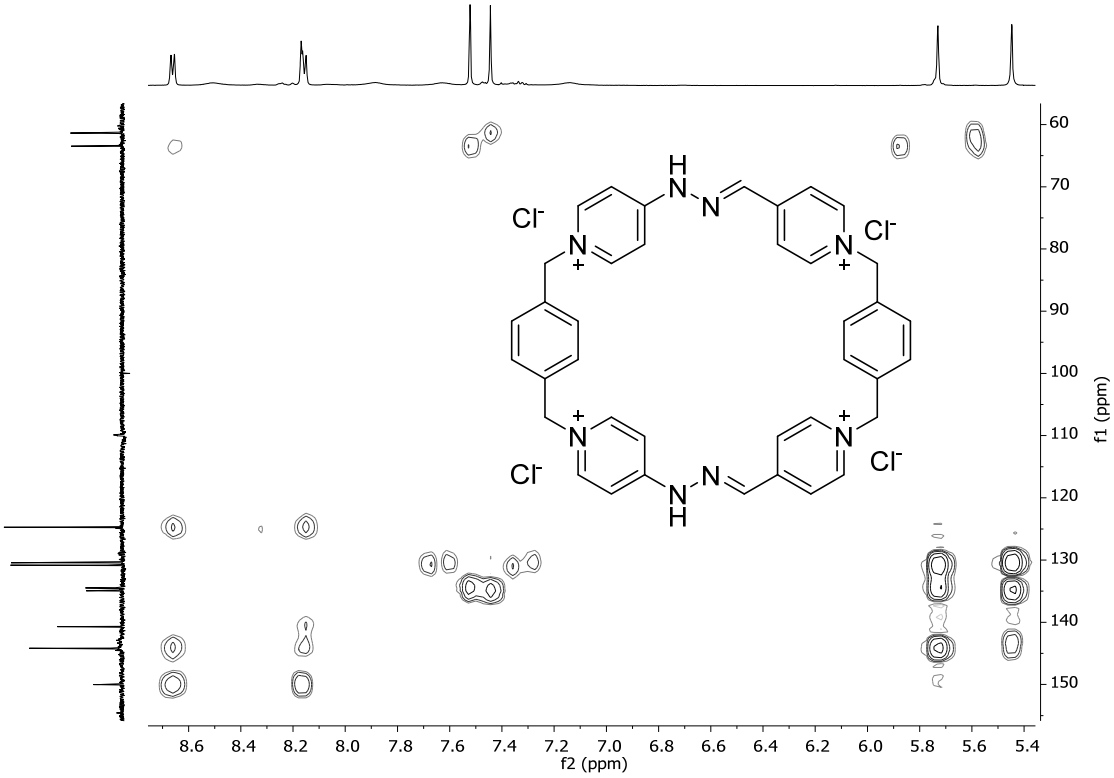

Figure S30. ^{1}H-^{13}C HMBC (500 and 126 MHz, D_2O) spectrum of **R**·4Cl.

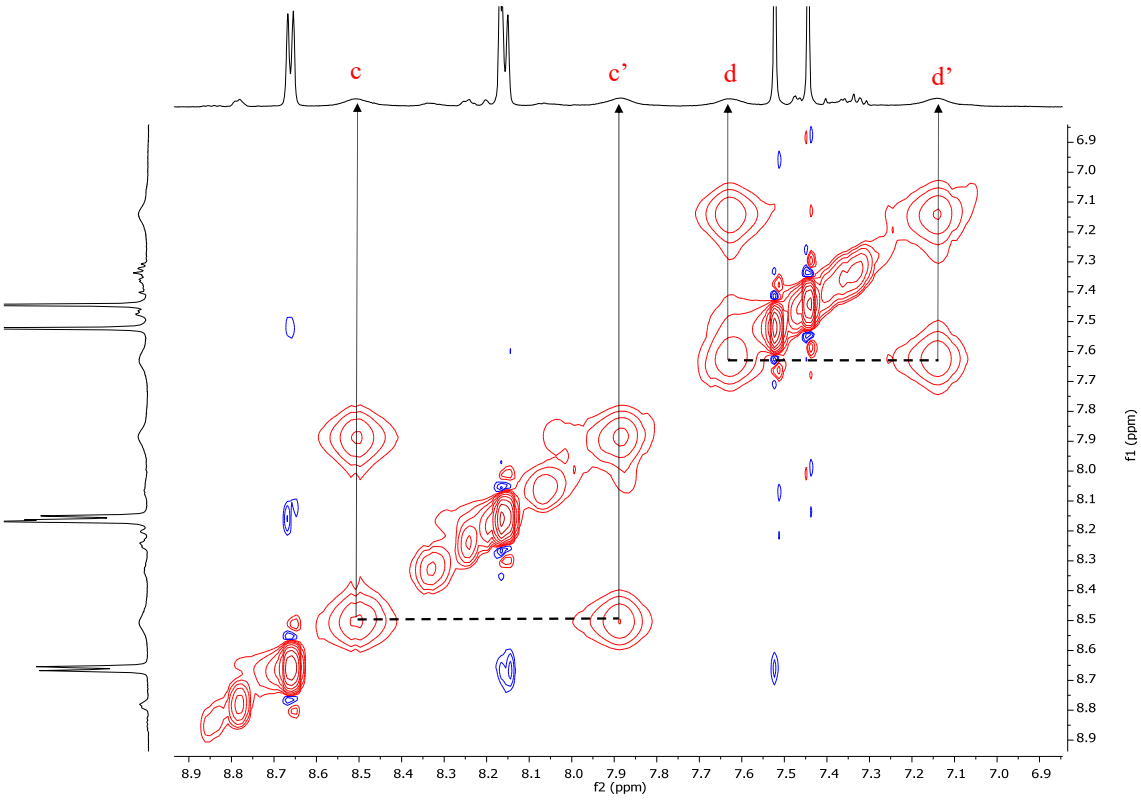

Figure S31. ^{1}H-^{1}H NOESY (500 MHz, D_2O) spectrum of **R**·4Cl. The EXSY correlations assigned to interconversions between H_c – $H_{c'}$ and H_d – $H_{d'}$ are highlighted with crossing lines.

R^{2+} (pD = 10):

^{1}H NMR (500 MHz, D_2O) *δ* 8.66 (d, *J* = 6.2 Hz, 4H), 8.35 (broad s, 2H), 8.21 (s, 2H), 8.16 (d, *J* = 6.0 Hz, 4H), 7.76 (broad s, 2H), 7.60 (s, 4H), 7.49 (s, 4H), 7.03 (broad s, 2H), 5.76 (s, 4H), 5.40 (s, 4H) ppm. ^{13}C NMR (126 MHz, D_2O) δ 160.22 (C), 150.85 (C), 143.74 (CH), 143.15 (CH), 141.68 (CH), 140.67 (HC=N), 135.33 (C), 134.66 (C), 130.69 (CH), 130.11 (CH), 124.11 (CH), 111.17 (CH), 109.57 (CH), 63.20 (CH_2), 60.77 (CH_2) ppm.

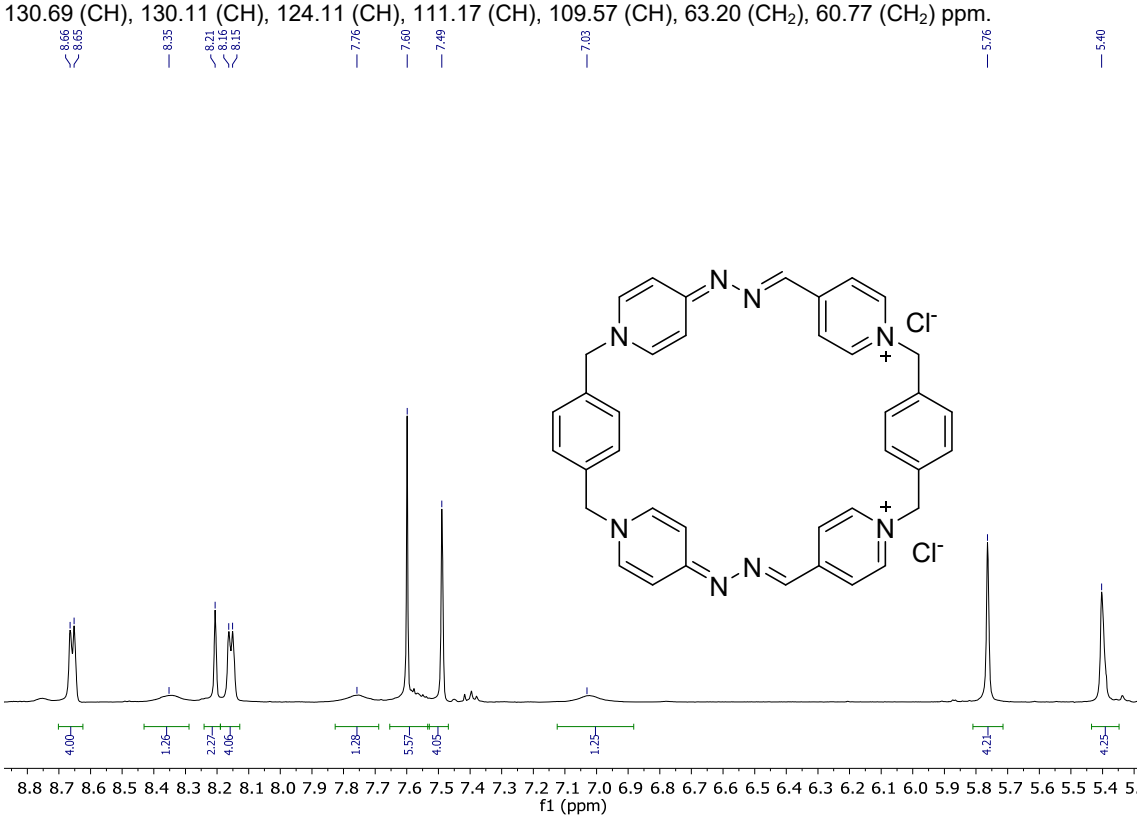

Figure S32. ^{1}H NMR (500 MHz, D_2O) spectrum of **R**·2Cl.

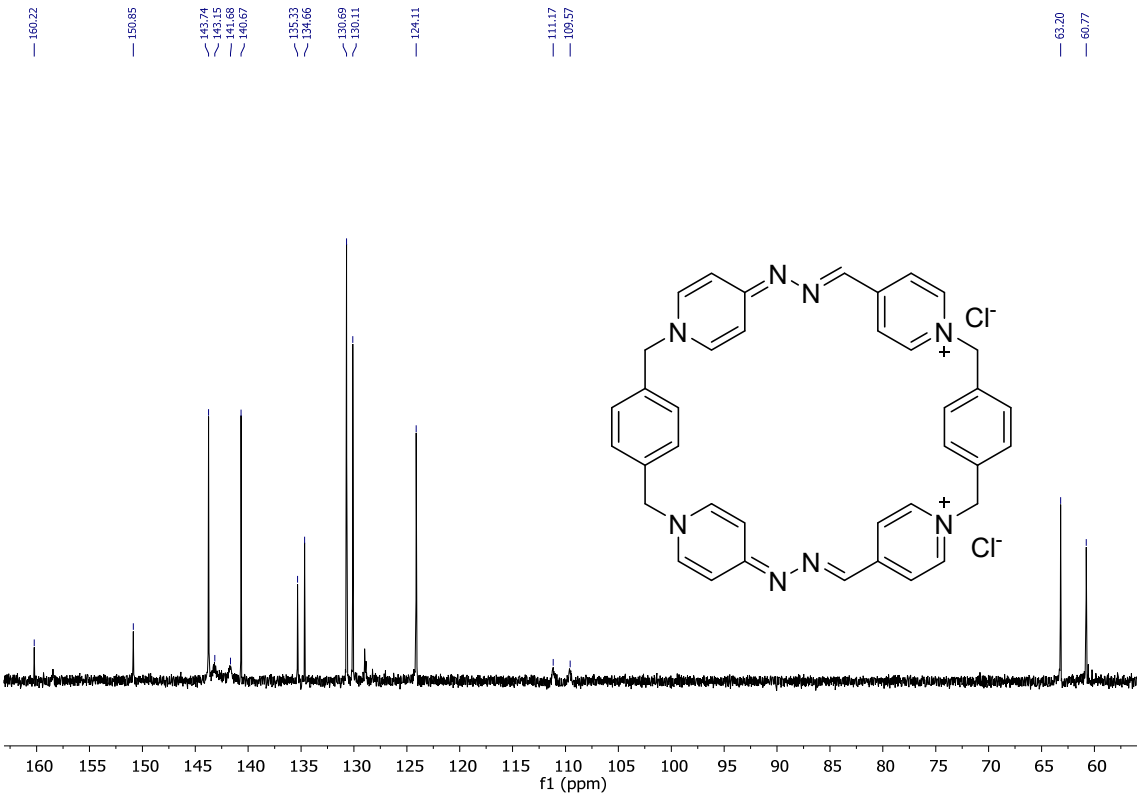

Figure S33. ^{13}C NMR (126 MHz, D_2O) spectrum of **R**·2Cl.

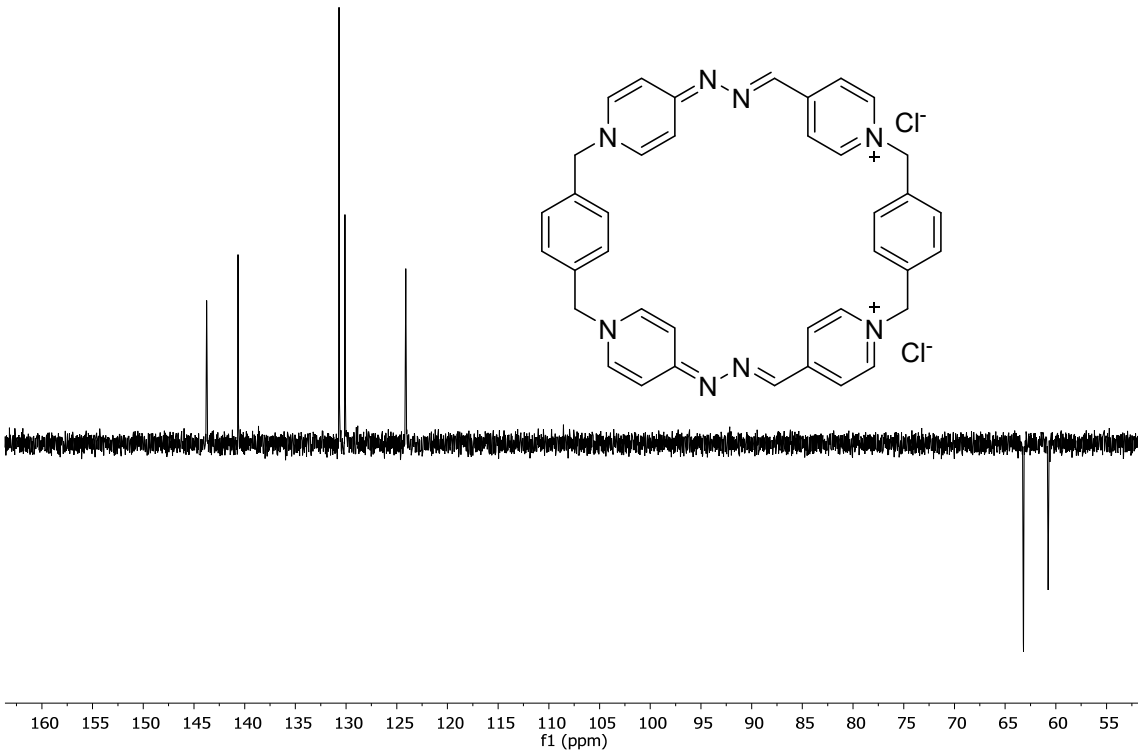

Figure S34. DEPT-135 (126 MHz, D_2O) spectrum of **R**·2Cl.

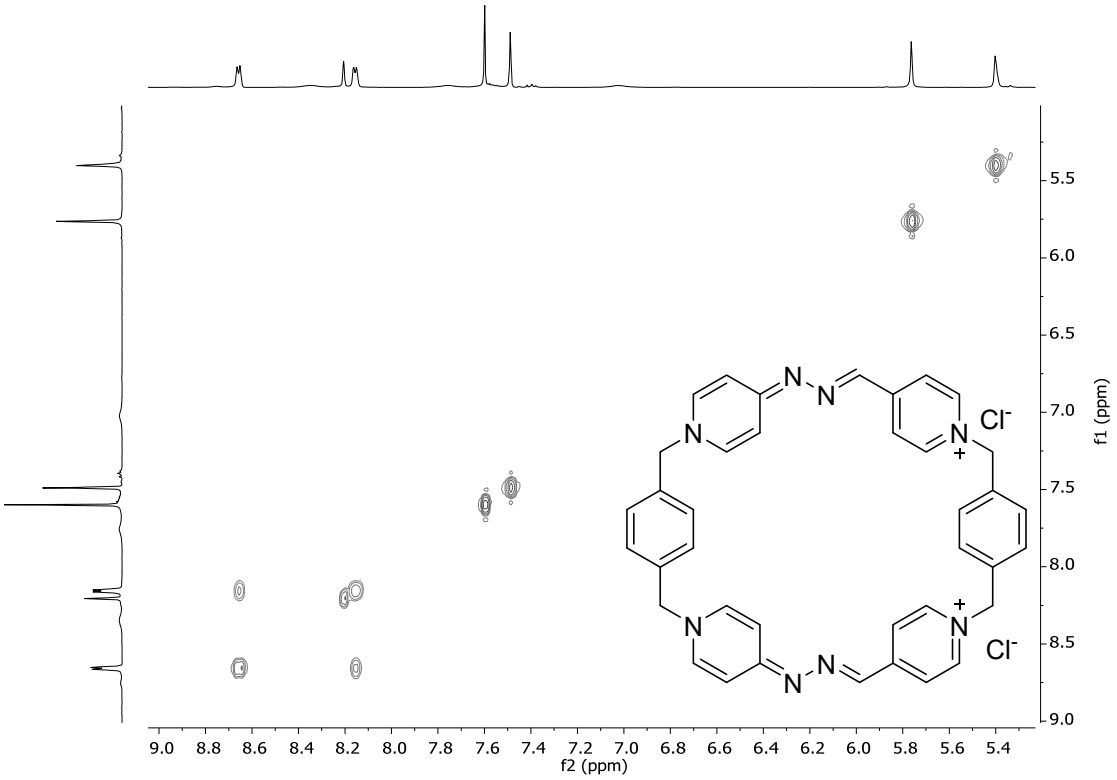

Figure S35. ^{1}H-^{1}H COSY (500 MHz, D_2O) spectrum of **R**·2Cl.

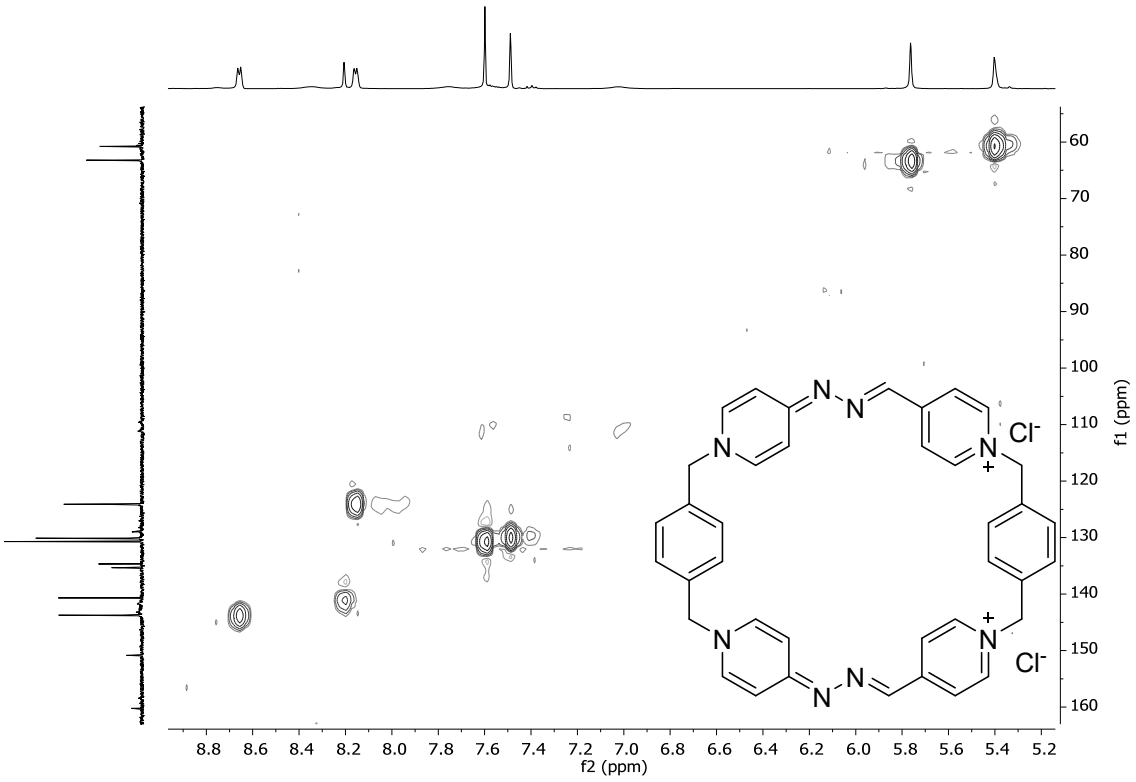

Figure S36. ^{1}H-^{13}C HSQC (500 and 126 MHz, D_2O) spectrum of **R**·2Cl.

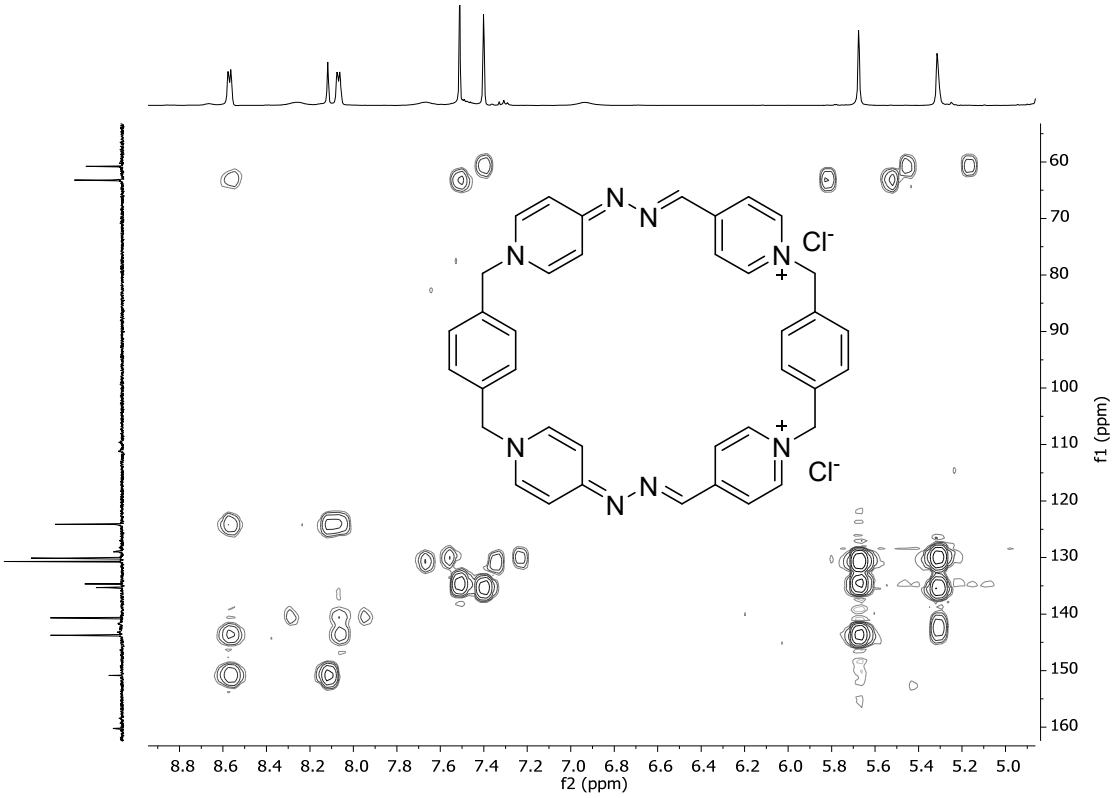

Figure S37. ^{1}H-^{13}C HMBC (500 and 126 MHz, D_2O) spectrum of **R**·2Cl.

1.7. General synthetic procedure and NMR characterization for inclusion complexes.

Equimolar 1.5 mM solutions of **R**·4Cl and the corresponding guest were prepared in D_2O at room temperature, and the corresponding NMR recorded immediately after.

1.7.1. NMR characterization of R·4Cl⊂2,7-DHN (2,7-DHN = 2,7-Dihydroxynaphthalene).

^{1}H NMR (500 MHz, D_2O) δ 8.74 (d, J = 6.7 Hz, 4H), 8.34 (d, J = 7.0 Hz, 2H), 8.28 (d, J = 7.3 Hz, 2H), 7.74 (s, 4H), 7.70 (s, 4H), 7.57 (d, J = 6.7 Hz, 4H), 7.25 (s, 2H), 6.93 (d, J = 5.0 Hz, 2H), 6.64 (d, J = 4.7 Hz, 2H), 6.60 (d, J = 8.7 Hz, 2H), 6.24 (s, 2H), 5.64 (s, 4H), 5.37 (s, 4H), 5.29 (d, J = 8.5 Hz, 2H) ppm. ^{13}C NMR (126 MHz, D_2O) δ 153.55 (C), 148.95 (C), 143.21 (CH), 142.74 (CH), 142.52 (CH), 138.90 (HC=N), 136.98 (C), 136.38 (C), 135.59 (C), 130.17 (CH), 129.81 (CH), 129.08 (CH), 124.66 (CH), 122.53 (C), 114.63 (CH), 110.22 (CH), 109.75 (CH), 106.91 (CH), 64.31 (CH_2), 62.21 (CH_2) ppm.

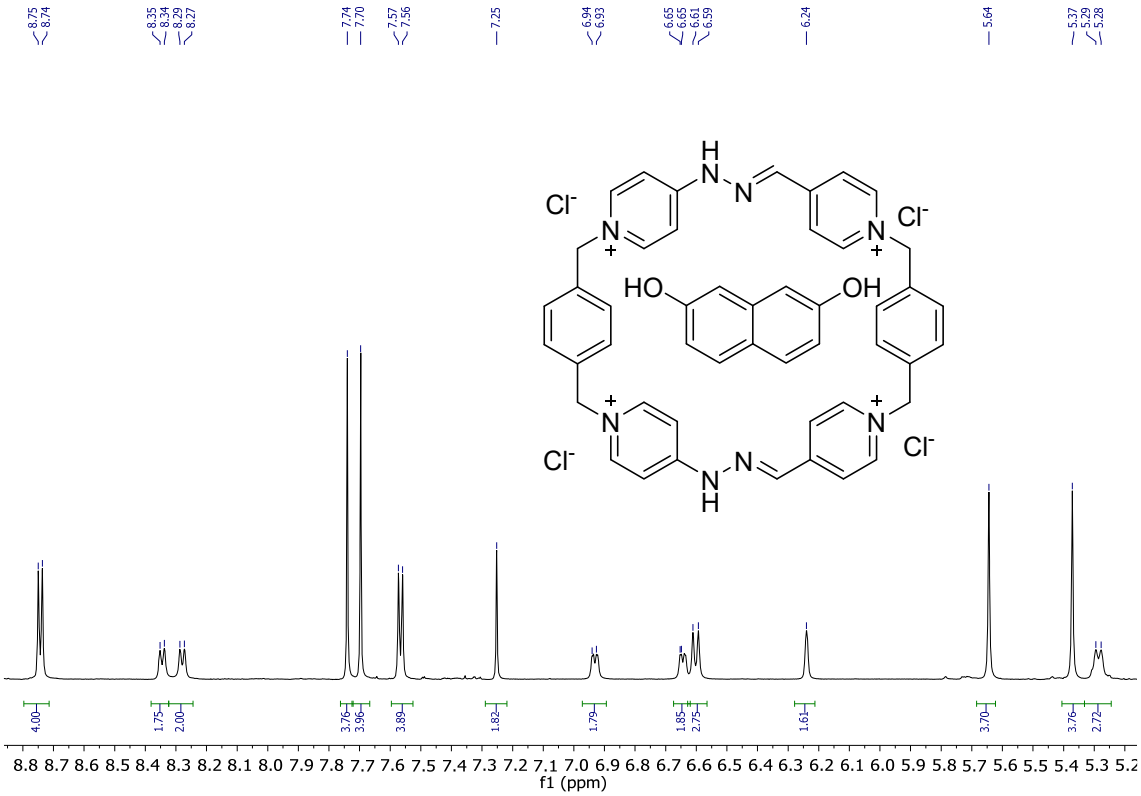

Figure S38. ^{1}H NMR (500 MHz, D_2O) spectrum of **R**·4Cl⊂2,7-DHN.

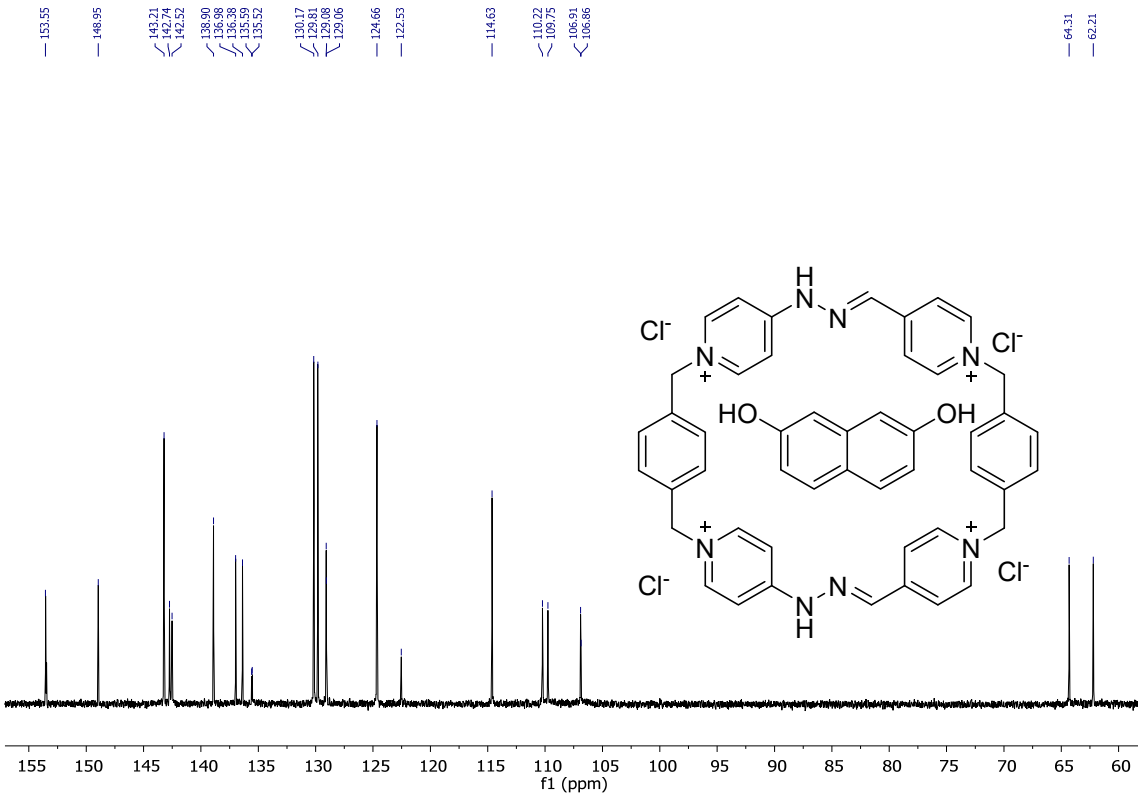

Figure S39. ^{13}C NMR (126 MHz, D_2O) spectrum of **R**·4Cl⊂2,7-DHN.

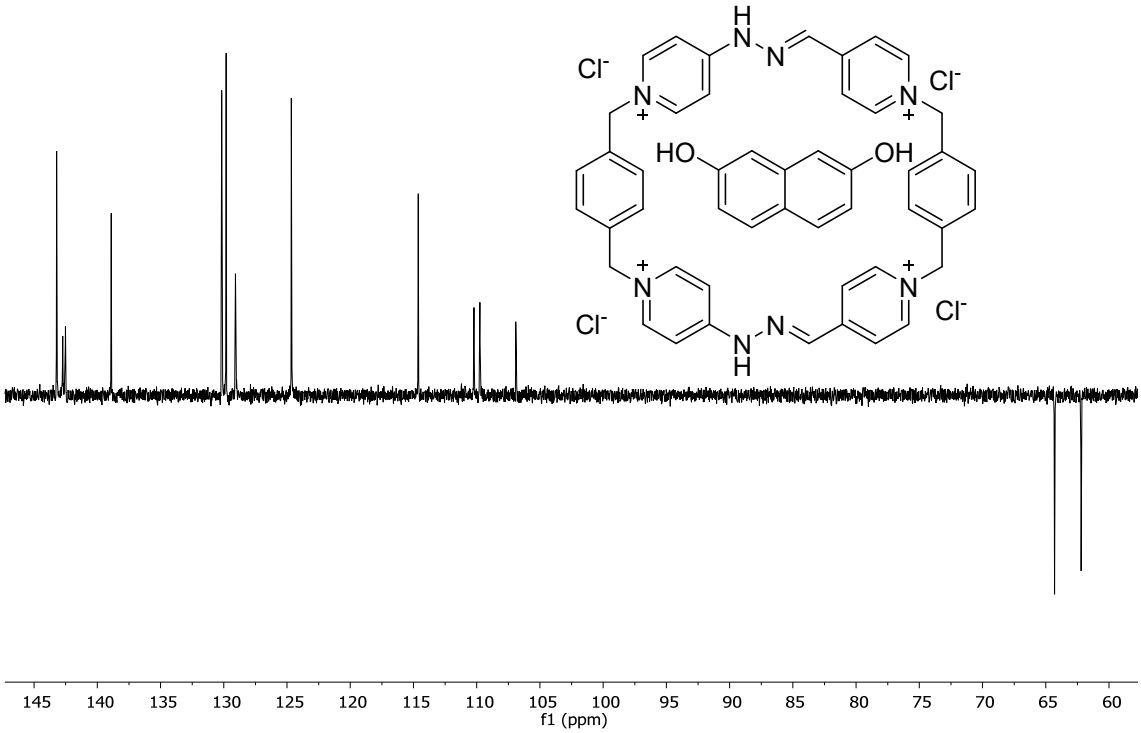

Figure S40. DEPT-135 (126 MHz, D_2O) spectrum of **R**·4Cl⊂2,7-DHN.

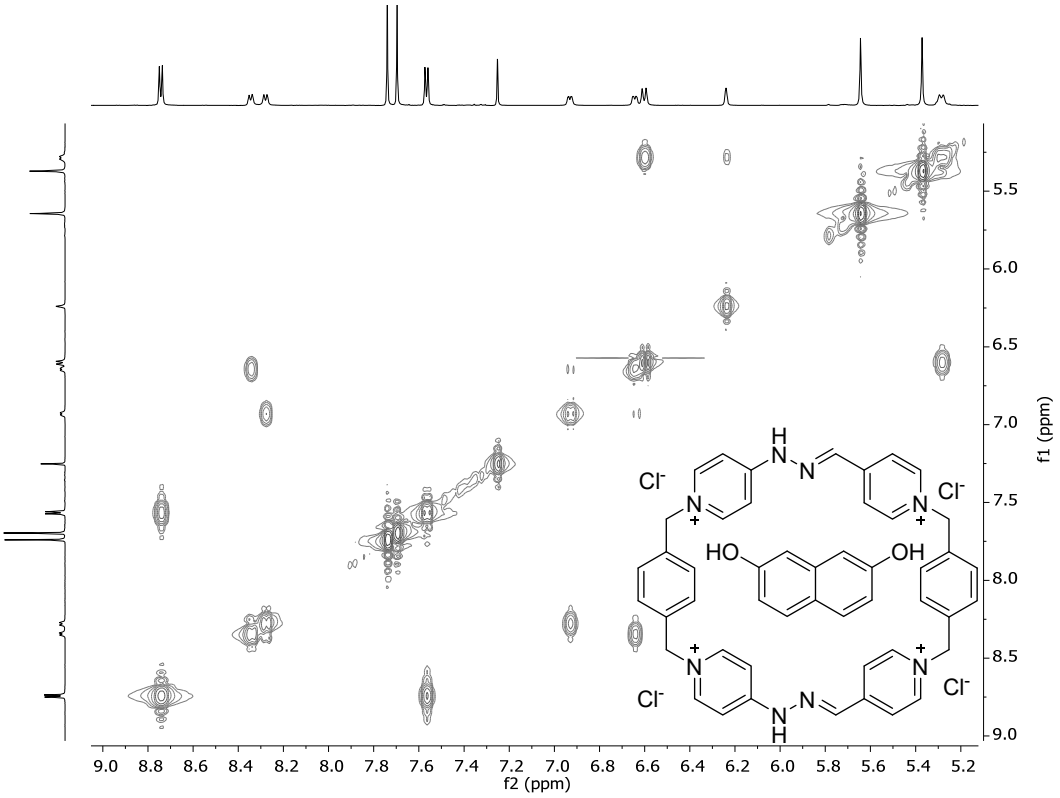

Figure S41. ^{1}H-^{1}H COSY (500 MHz, D_2O) spectrum of **R**·4Cl⊂2,7-DHN.

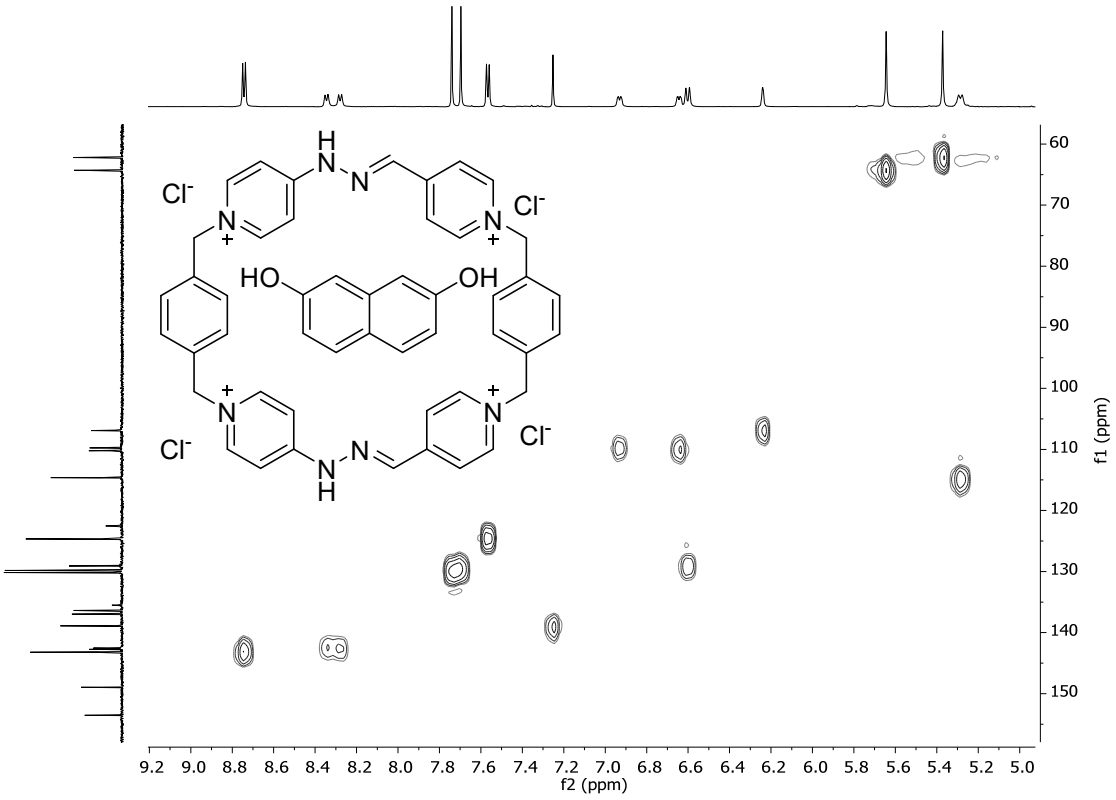

Figure S42. ^{1}H-^{13}C HSQC (500 and 126 MHz, D_2O) spectrum of **R**·4Cl⊂2,7-DHN.

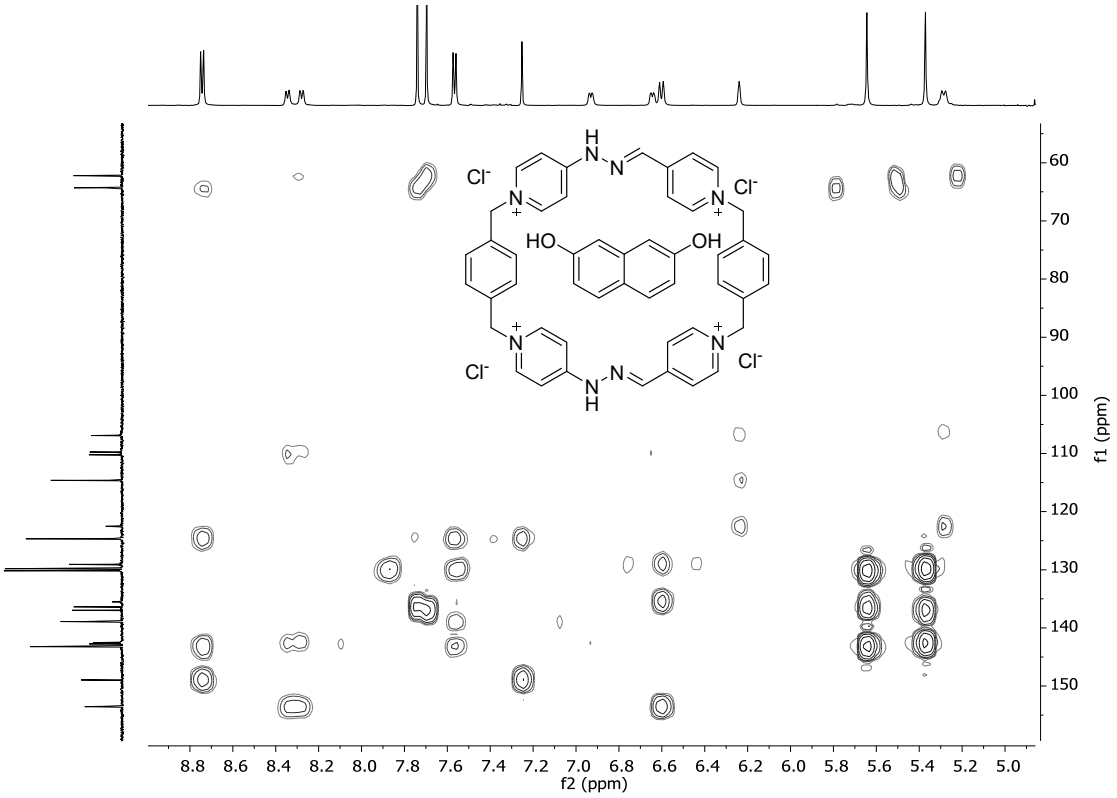

Figure S43. ^{1}H-^{13}C HMBC (500 and 126 MHz, D_2O) spectrum of **R**·4Cl⊂2,7-DHN.

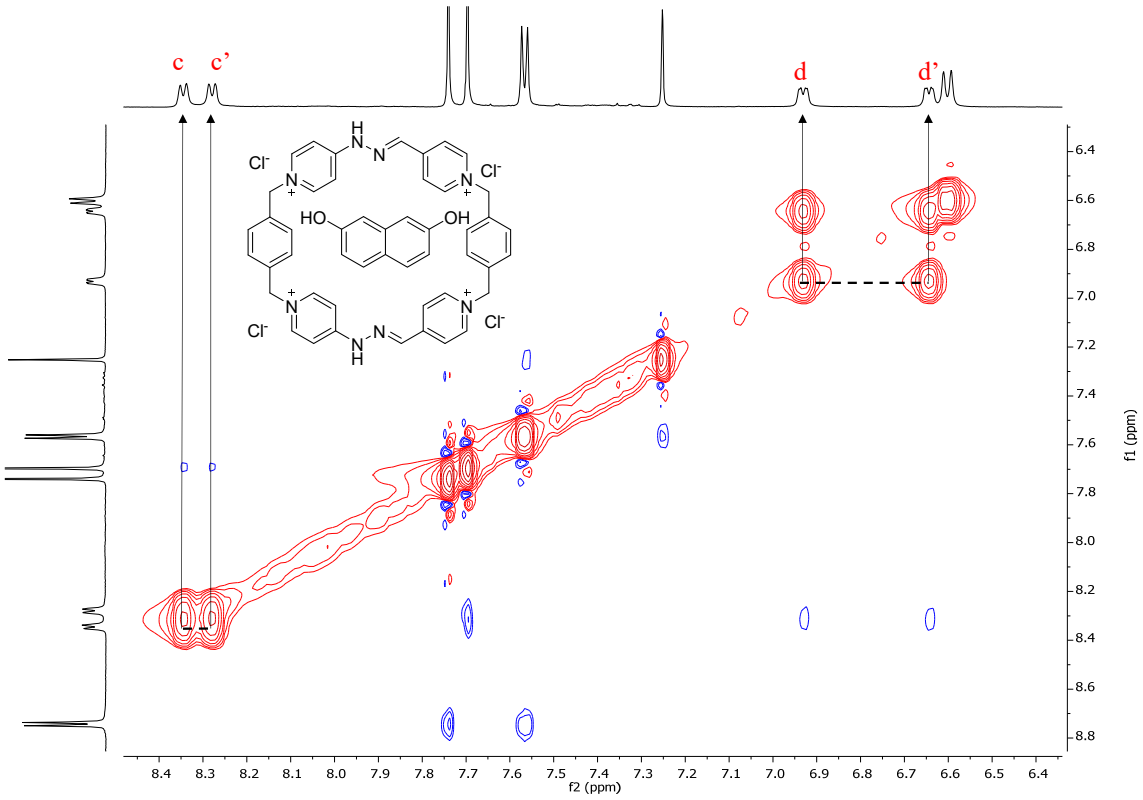

Figure S44. ^{1}H-^{1}H NOESY (500 MHz, D_2O) spectrum of **R**·4Cl⊂2,7-DHN. The EXSY correlations assigned to interconversions between Hc – Hc' and Hd – Hd' are highlighted with crossing lines.

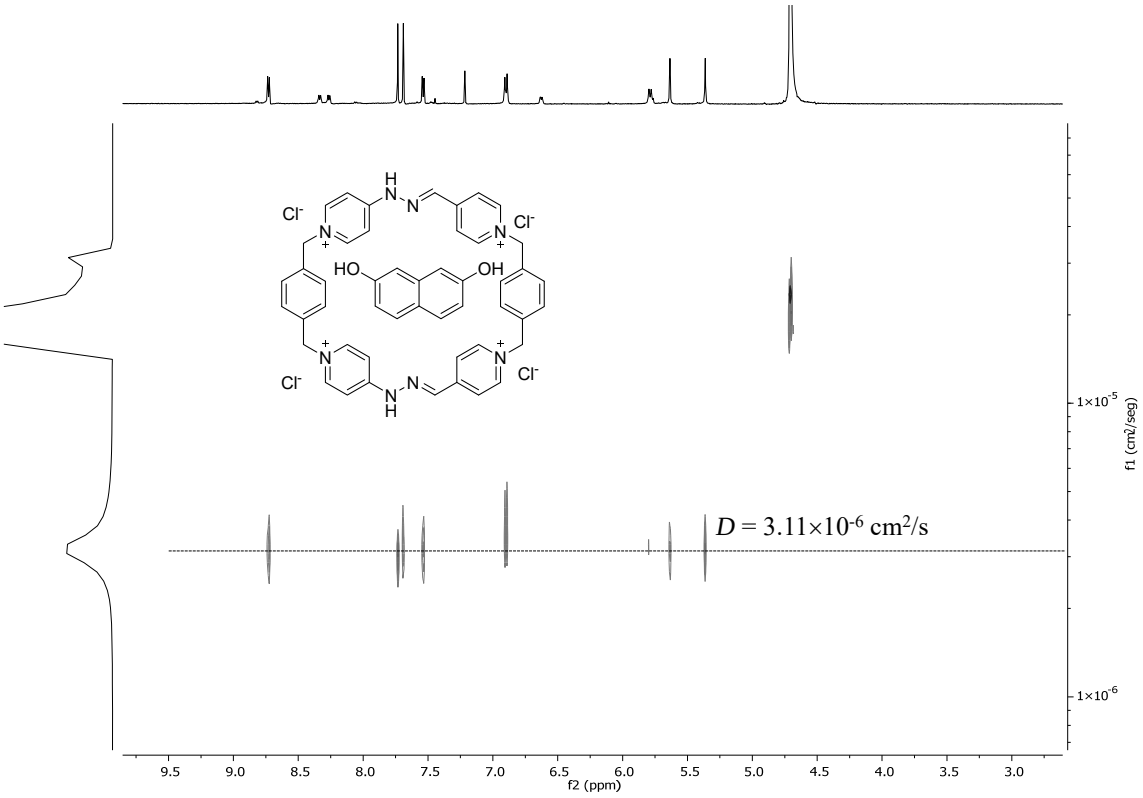

Figure S45. DOSY NMR (500 MHz, D_2O) spectrum of **R**·4Cl⊂2,7-DHN.

1.7.2. NMR characterization of R·4Cl⊂1,5-DHN (1,5-DHN = 1,5-dihydroxynaphthalene).

^{1}H NMR (500 MHz, D_2O) δ 8.76 (d, *J* = 6.7 Hz, 4H), 8.45 (d, *J* = 6.7 Hz, 2H), 8.20 (d, *J* = 6.9 Hz, 2H), 7.78 (s, 4H), 7.69 (s, 4H), 7.55 (d, *J* = 6.7 Hz, 4H), 7.35 (s, 2H), 6.79 (dd, *J* = 12.4, 7.1 Hz, 4H), 6.37 (d, *J* = 8.3 Hz, 2H), 5.68 (s, 4H), 5.48 (d, *J* = 7.3 Hz, 2H), 5.40 (s, 4H), 5.11 (t, *J* = 7.4 Hz, 2H) ppm. ^{13}C NMR (126 MHz, D_2O) δ 153.67 (C), 150.74 (C), 149.14 (C), 143.40 (CH), 142.94 (CH), 142.84 (CH), 139.12 (HC=N), 136.76 (C), 136.46 (C), 130.21 (CH), 129.78 (CH), 125.08 (C), 124.73 (CH), 123.88 (CH), 112.75 (CH), 110.32 (CH), 109.83 (CH), 108.21 (CH), 64.11 (CH_2), 62.05 (CH_2) ppm.

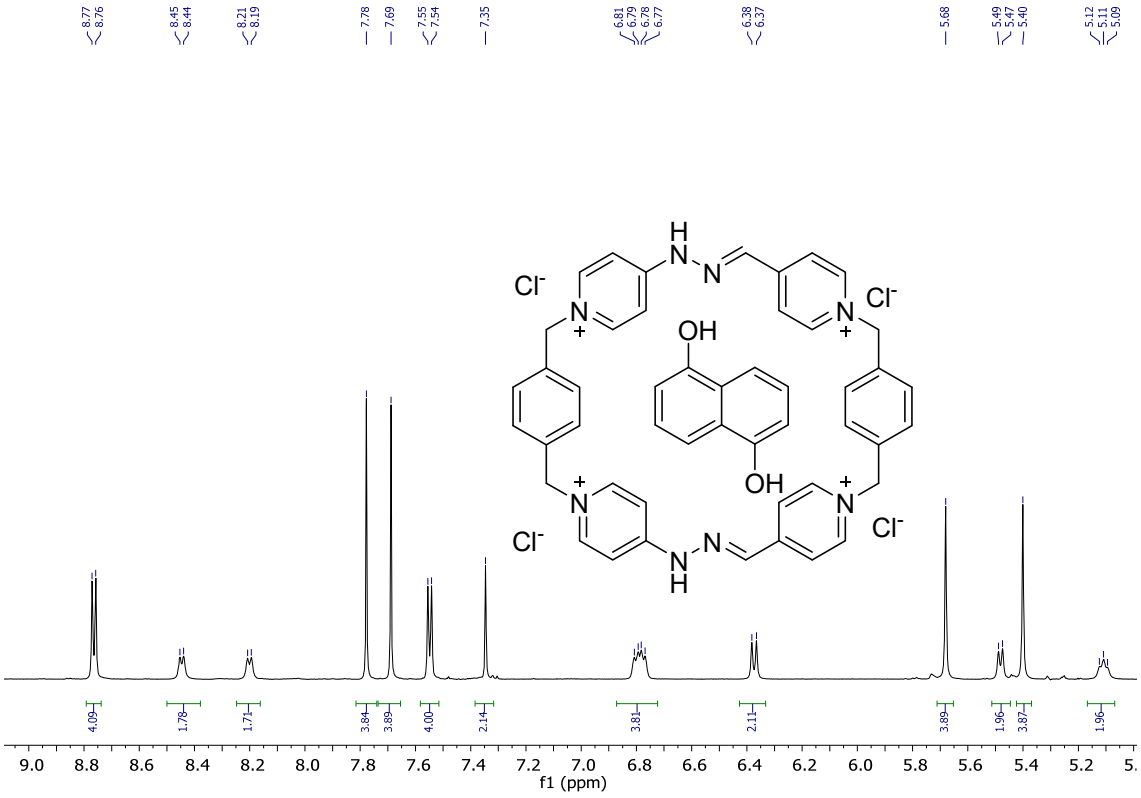

Figure S46. ^{1}H NMR (500 MHz, D_2O) spectrum of **R**·4Cl⊂1,5-DHN.

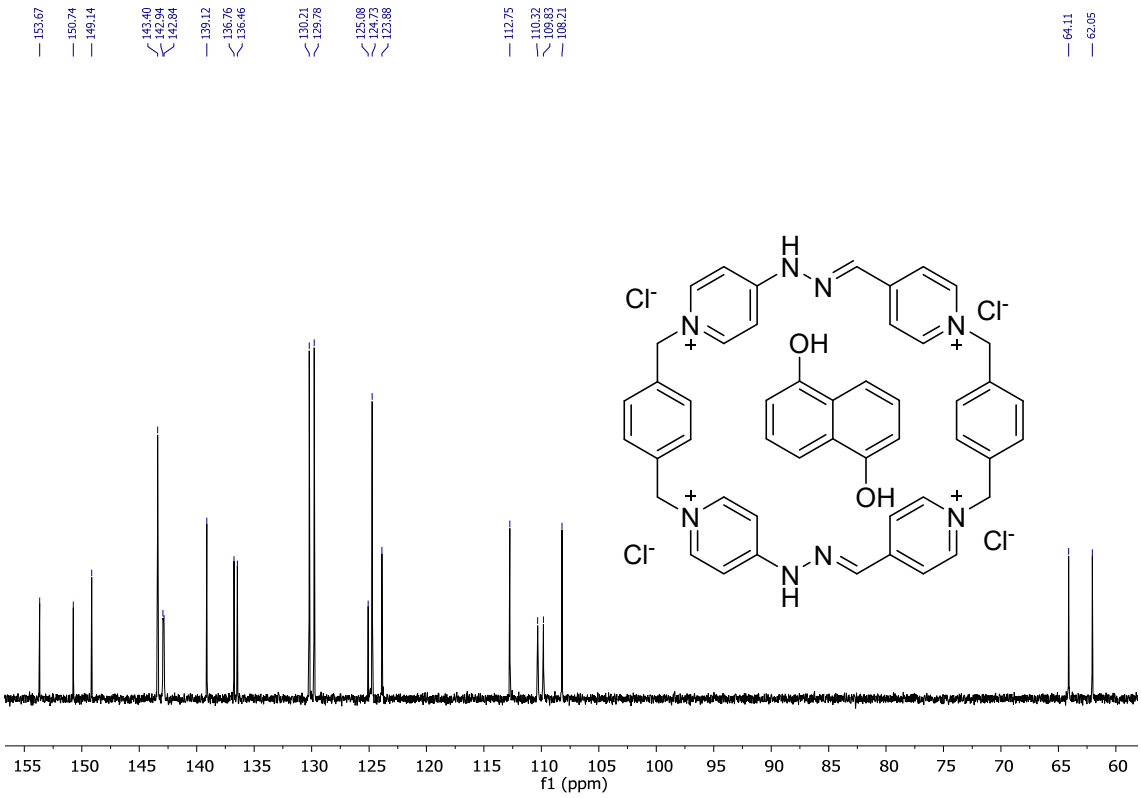

Figure S47. ^{13}C NMR (126 MHz, D_2O) spectrum of **R**·4Cl⊂1,5-DHN.

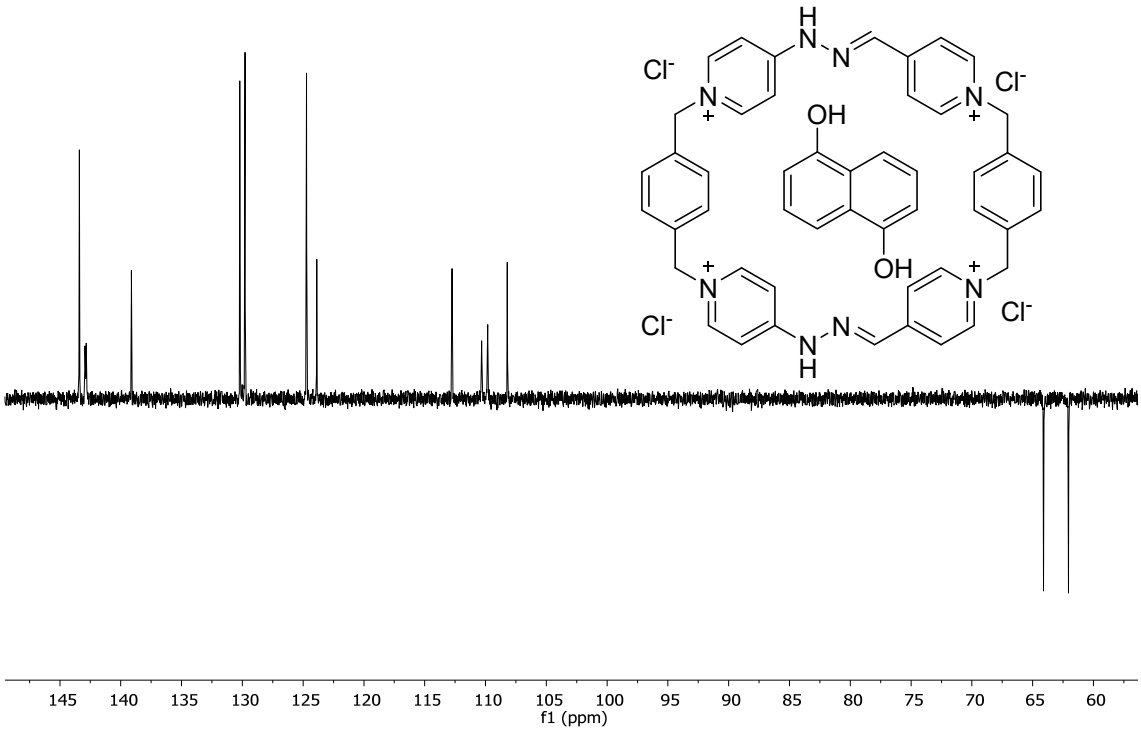

Figure S48. DEPT-135 (126 MHz, D_2O) spectrum of **R**·4Cl⊂1,5-DHN.

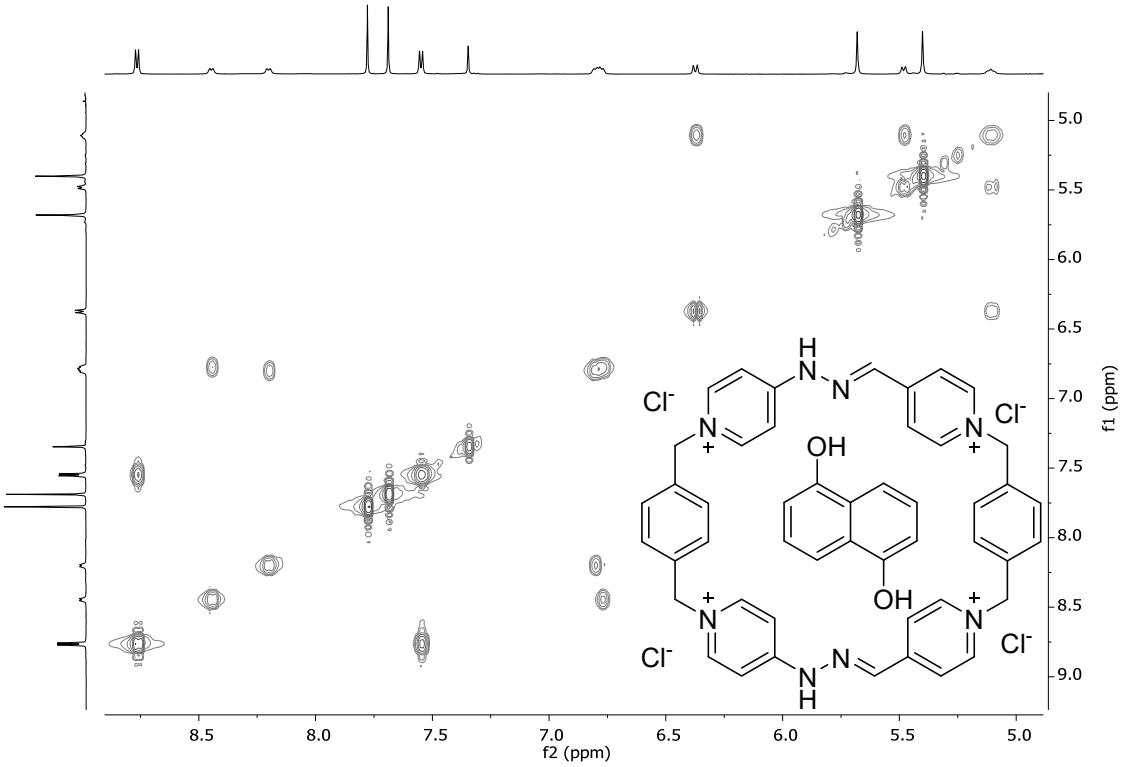

Figure S49. ^{1}H-^{1}H COSY (500 MHz, D_2O) spectrum of **R**·4Cl⊂1,5-DHN.

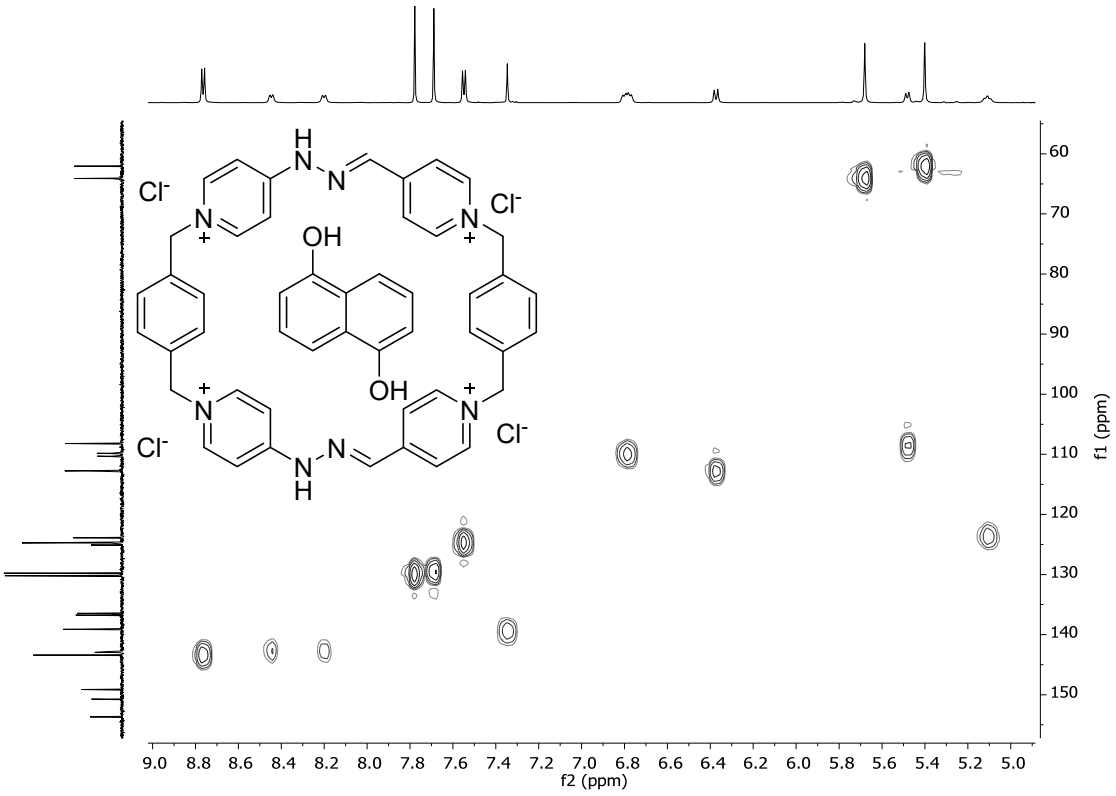

Figure S50. ^{1}H-^{13}C HSQC (500 and 126 MHz, D_2O) spectrum of **R**·4Cl⊂1,5-DHN.

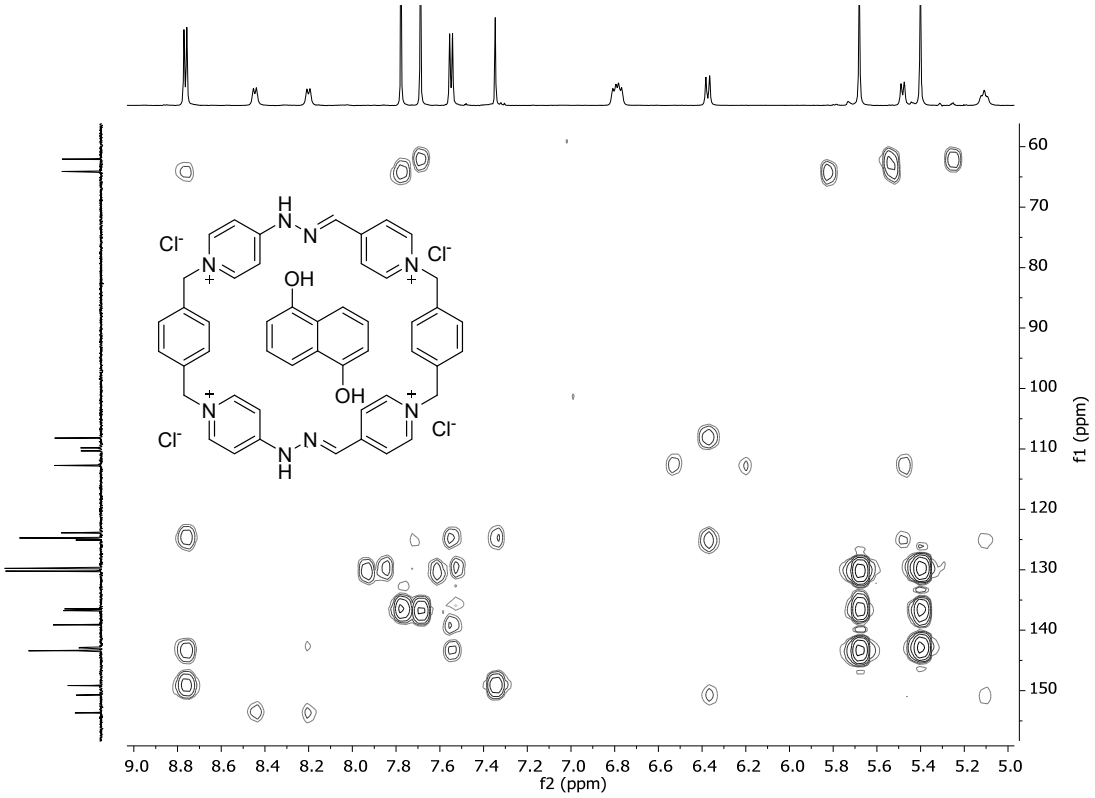

Figure S51. ^{1}H-^{13}C HMBC (500 and 126 MHz, D_2O) spectrum of **R**·4Cl⊂1,5-DHN.

1.7.3. NMR characterization of R·4Cl⊂1,5-DHNc (1,5-DHNc = 2,2'-(((naphthalene-1,5-diylbis(oxy))bis(ethane-2,1-diyl))bis(oxy))bis(ethan-1-ol).

^{1}H NMR (500 MHz, D_2O) δ 8.79 (d, J = 6.7 Hz, 4H), 8.49 (d, J = 6.5 Hz, 2H), 8.21 (d, J = 6.6 Hz, 2H), 7.81 (s, 4H), 7.72 (s, 2H), 7.53 (d, J = 6.6 Hz, 4H), 7.34 (s, 2H), 6.84 – 6.75 (m, 4H), 6.64 (broad s, 2H), 5.79 (broad s, 2H), 5.70 (s, 4H), 5.50 (broad s, 2H), 5.42 (s, 4H), 3.95 (d, J = 4.0 Hz, 5H), 3.93 – 3.86 (m, 5H), 3.76 (d, J = 5.2 Hz, 5H), 3.73 (d, J = 5.4 Hz, 5H) ppm. ^{13}C NMR (126 MHz, D_2O) δ 153.66 (C), 153.28 (C), 149.14 (C), 143.49 (CH), 143.03 (CH), 142.97 (CH), 139.12 (HC=N), 137.00 (C), 136.66 (C), 130.18 (CH), 129.74 (CH), 125.60 (C), 124.79 (CH), 124.39 (CH), 113.75 (CH), 110.38 (CH), 109.94 (CH), 105.54 (CH), 72.22 (CH_2), 69.27 (CH_2), 67.88 (CH_2), 64.09 (CH_2), 62.03 (CH_2), 60.49 (CH_2).

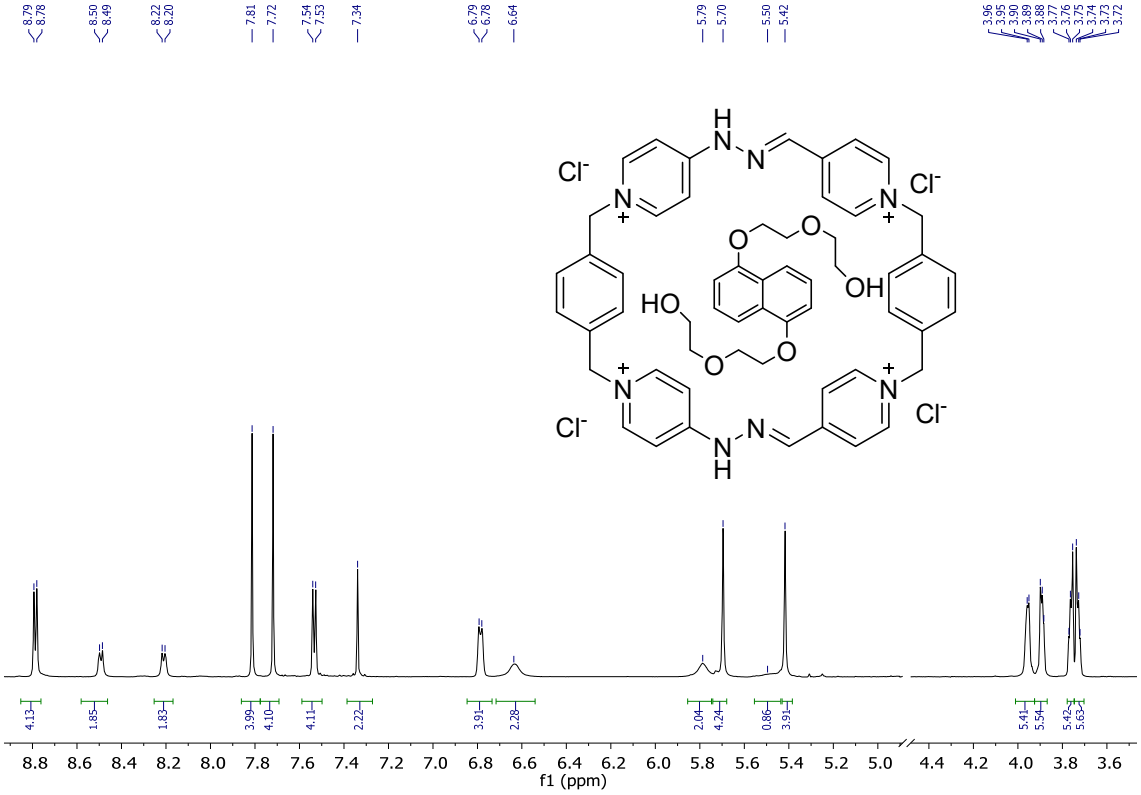

Figure S52. ^{1}H NMR (500 MHz, D_2O) spectrum of **R**·4Cl⊂1,5-DHNc.

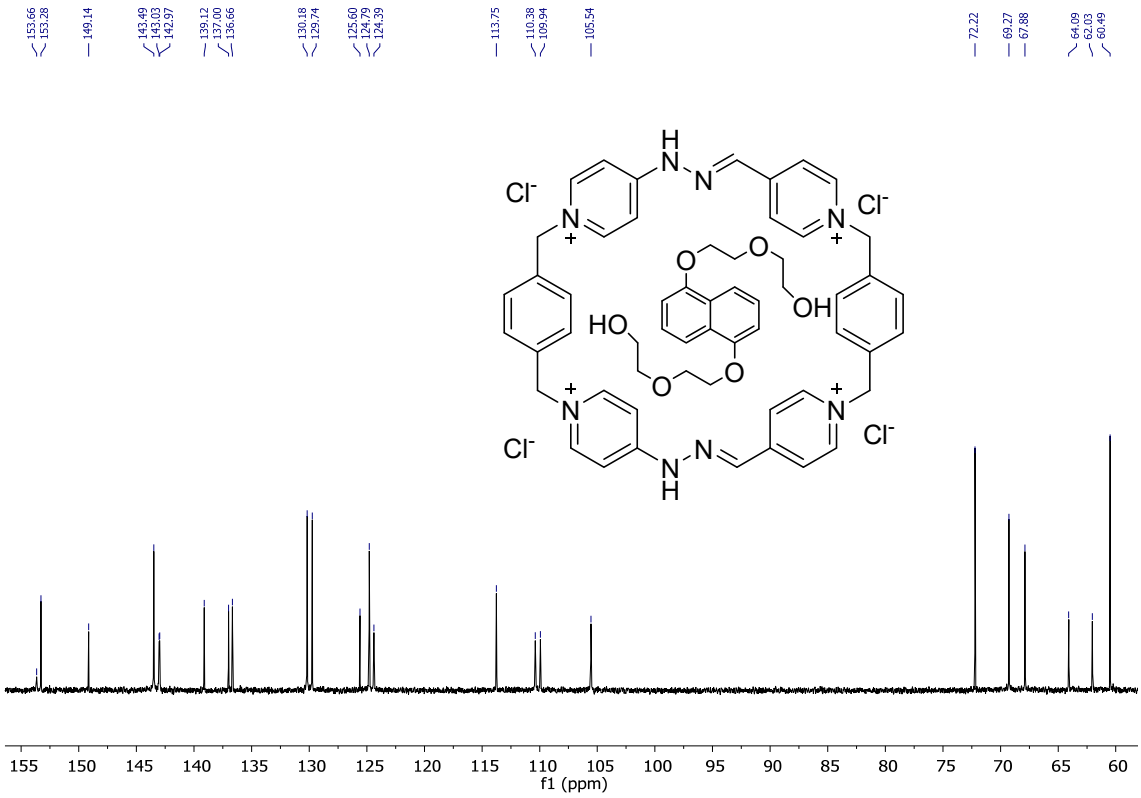

Figure S53. ^{13}C NMR (126 MHz, D_2O) spectrum of **R**·4Cl⊂1,5-DHNc.

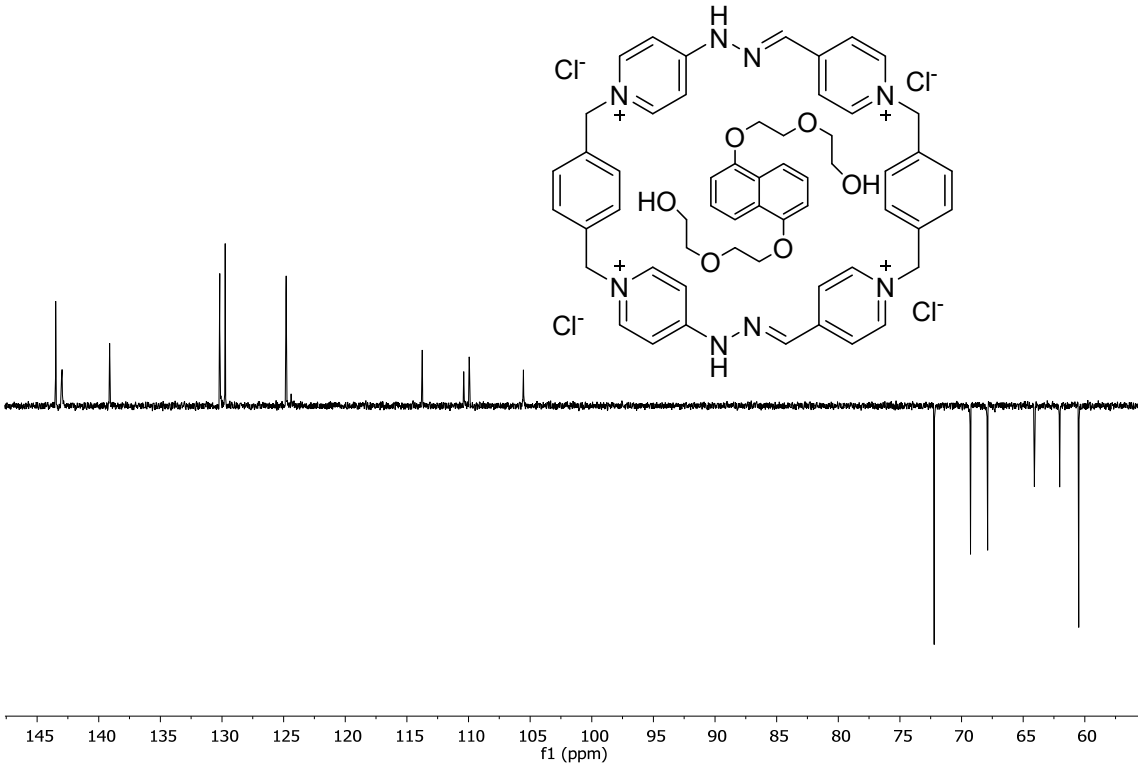

Figure S54. DEPT-135 (126 MHz, D_2O) spectrum of **R**·4Cl⊂1,5-DHNc.

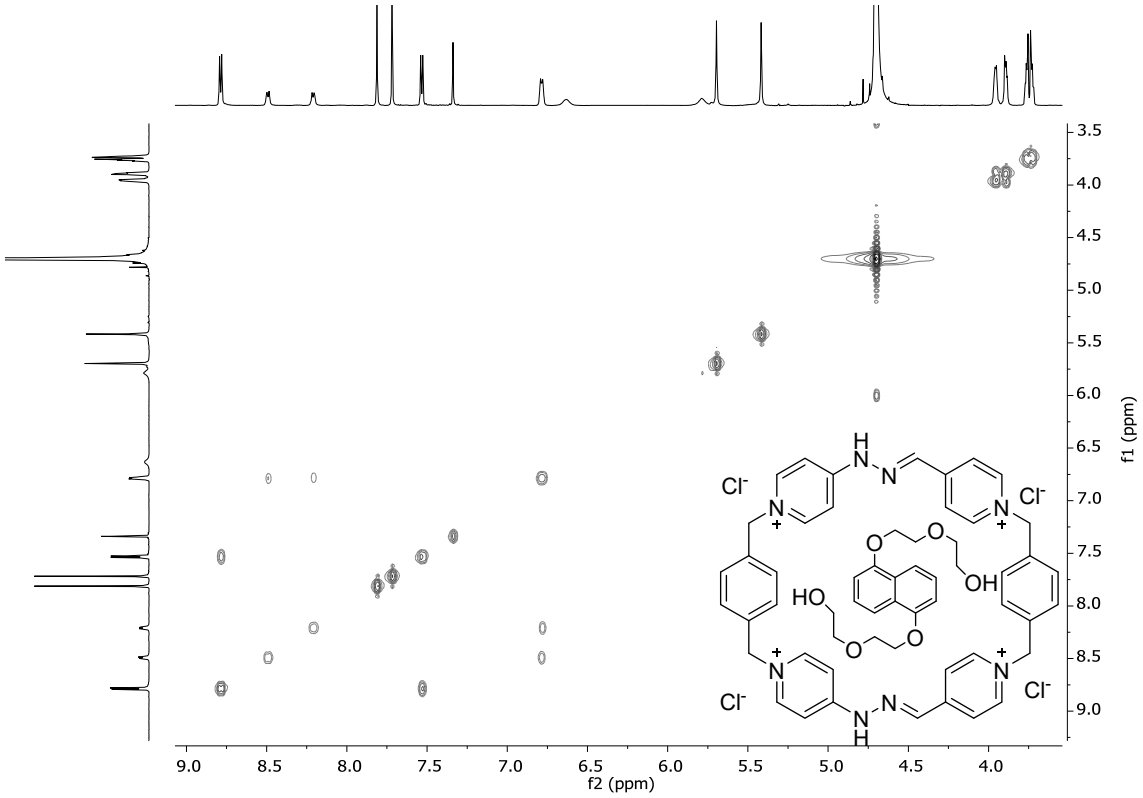

Figure S55. ^{1}H-^{1}H COSY (500 MHz, D_2O) spectrum of **R**·4Cl⊂1,5-DHNc.

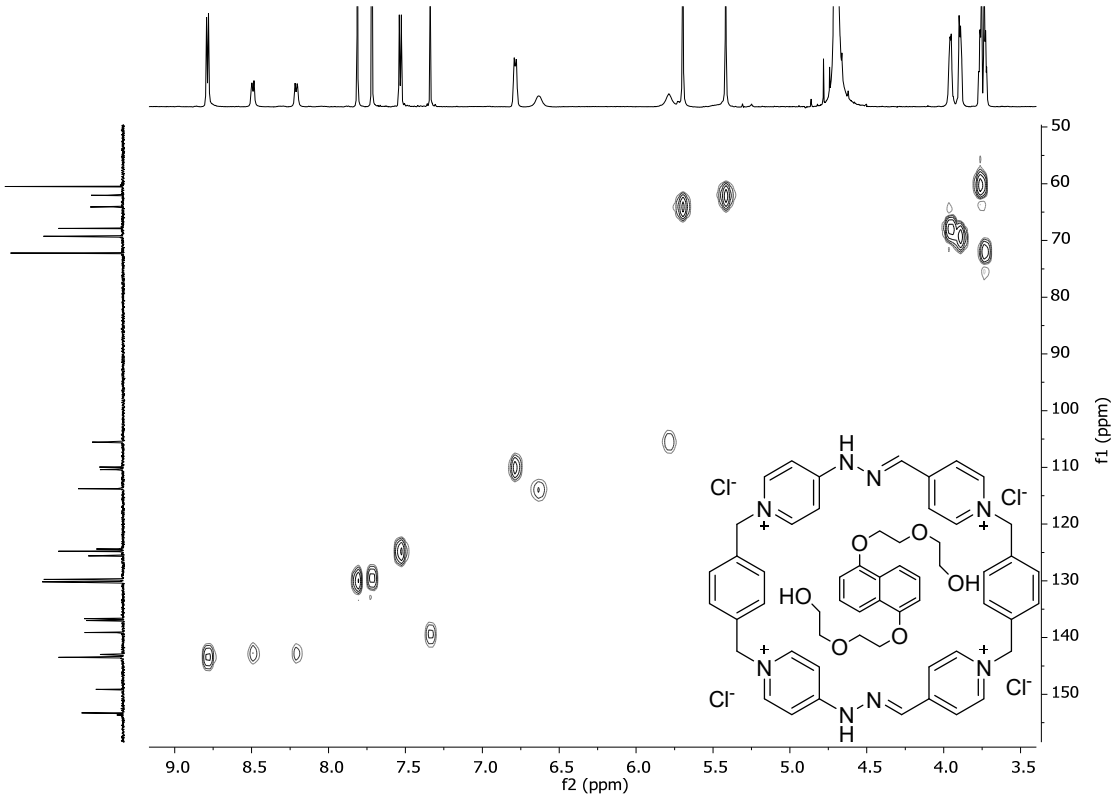

Figure S56. ^{1}H-^{13}C HSQC (500 and 126 MHz, D_2O) spectrum of **R**·4Cl⊂1,5-DHNc.

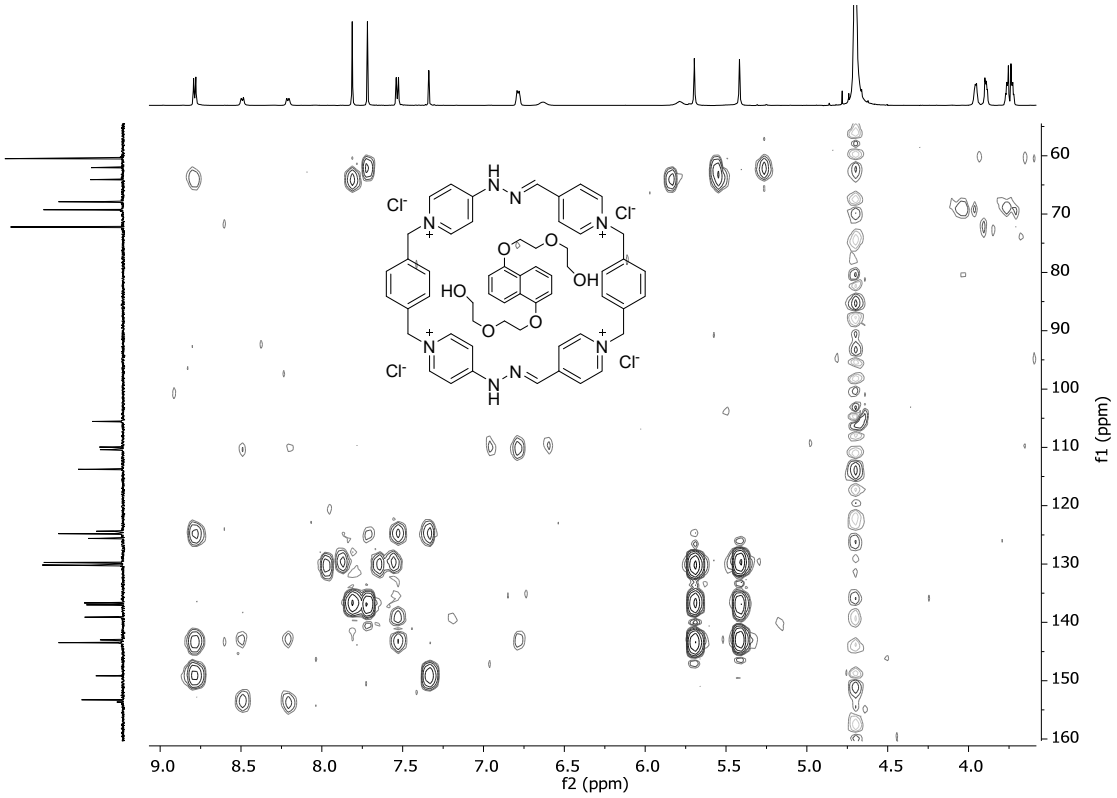

Figure S57. ^{1}H-^{13}C HMBC (500 and 126 MHz, D_2O) spectrum of **R**·4Cl⊂1,5-DHNc.

1.7.4. NMR characterization of R·4Cl⊂CAR (CAR = carbazole).

^{1}H NMR (500 MHz, D_2O) δ 8.71 (d, J = 6. 8 Hz, 4H), 8.34 (broad s, 2H), 8.19 (broad s, 2H), 7.79 (s, 4H), 7.71 (s, 4H), 7.60 (broad s, 4H), 7.14 (d, J = 7.8 Hz, 2H), 7.11 (broad s, 2H), 6.58 (broad s, 2H), 5.69 (s, 4H), 5.58 (t, J = 7.4 Hz, 2H), 5.40 (s, 4H), 5.30 (d, J = 8.1 Hz, 2H), 4.90 (t, J = 7.6 Hz, 2H) ppm. ^{13}C NMR (126 MHz, D_2O) δ 148.80 (C), 143.30 (CH), 142.63 (CH), 139.19 (C), 138.39 (C), 130.56 (CH), 130.11 (CH), 125.51 (CH), 124.74 (CH), 121.83 (C), 118.61 (CH), 117.92 (CH), 110.53 (CH), 109.60 (CH), 109.03 (CH), 64.08 (CH_2), 61.99 (CH_2) ppm.

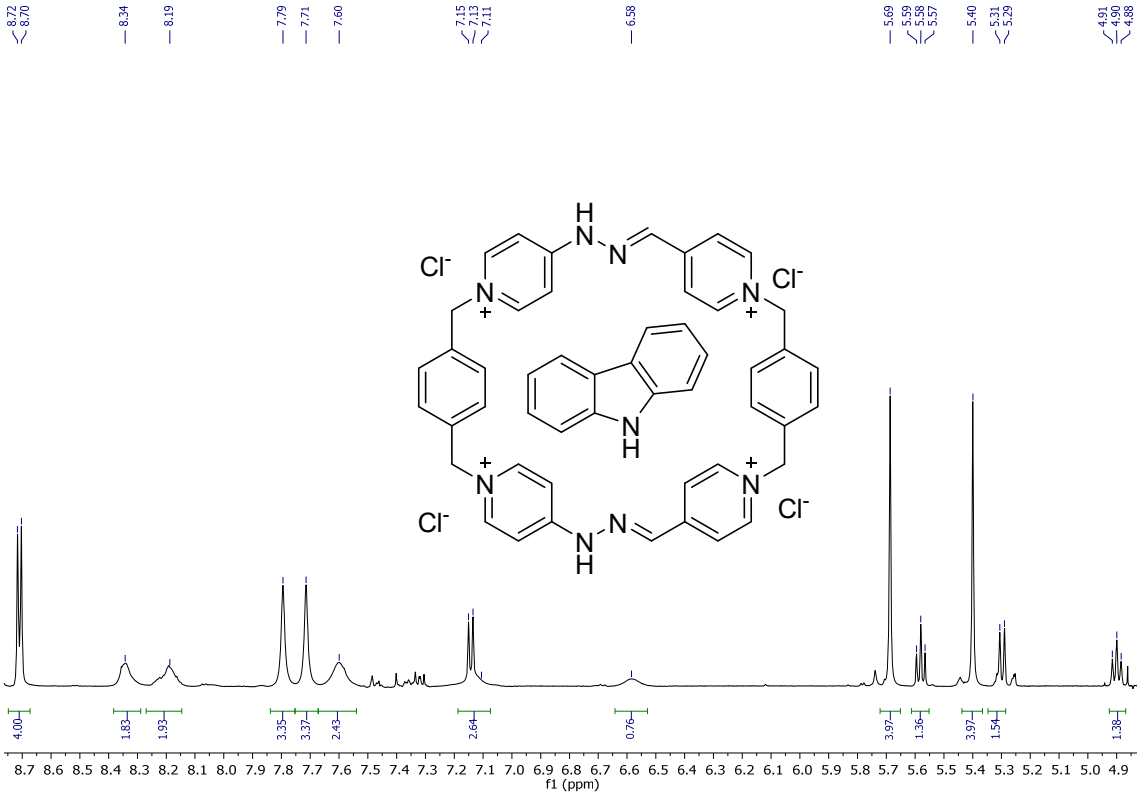

Figure S58. ^{1}H NMR (500 MHz, D_2O) spectrum of **R**·4Cl⊂CAR.

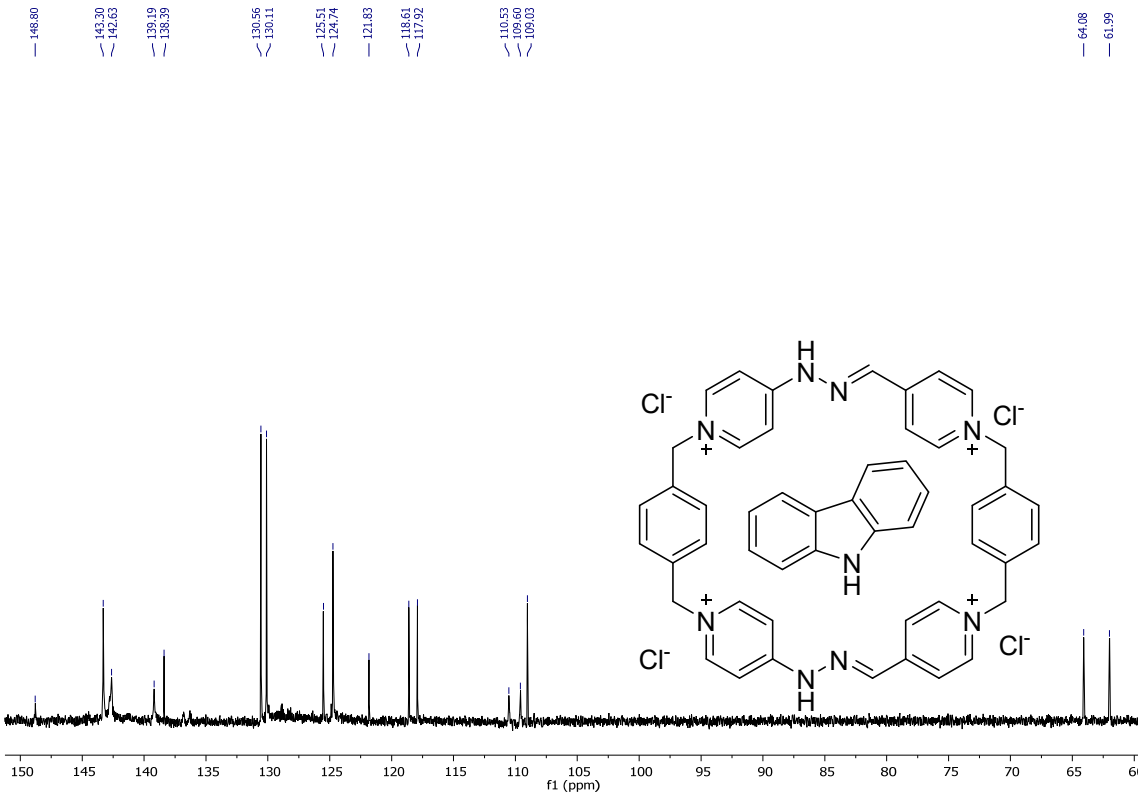

Figure S59. ^{13}C NMR (126 MHz, D_2O) spectrum of **R**·4Cl⊂CAR.

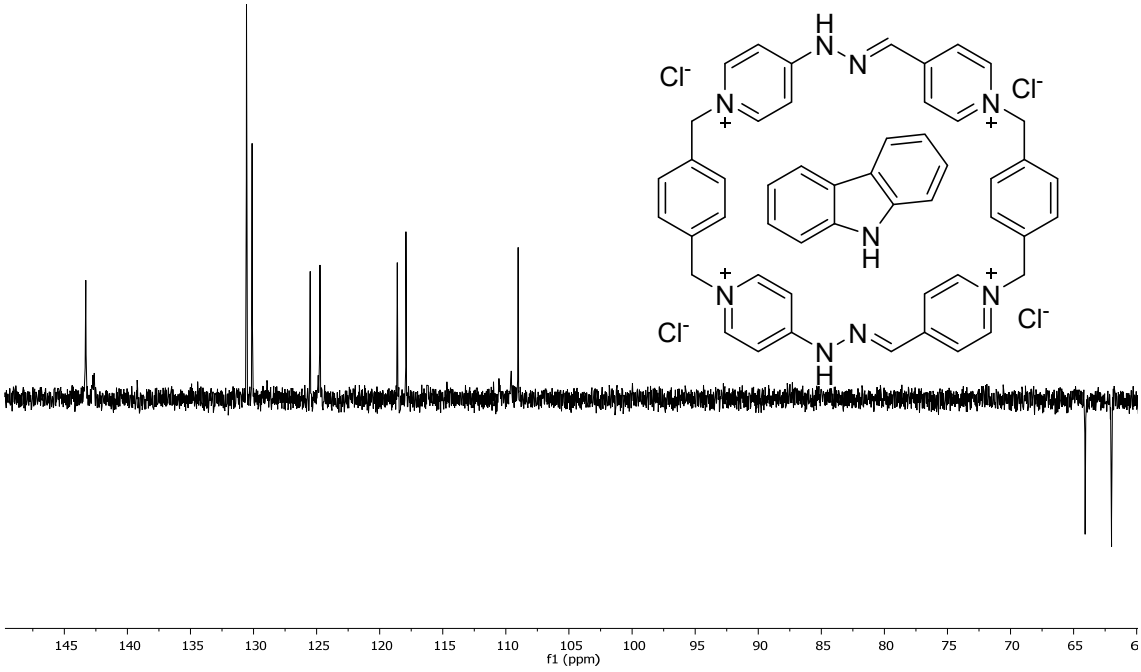

Figure S60. DEPT-135 (126 MHz, D_2O) spectrum of **R**·4Cl⊂CAR.

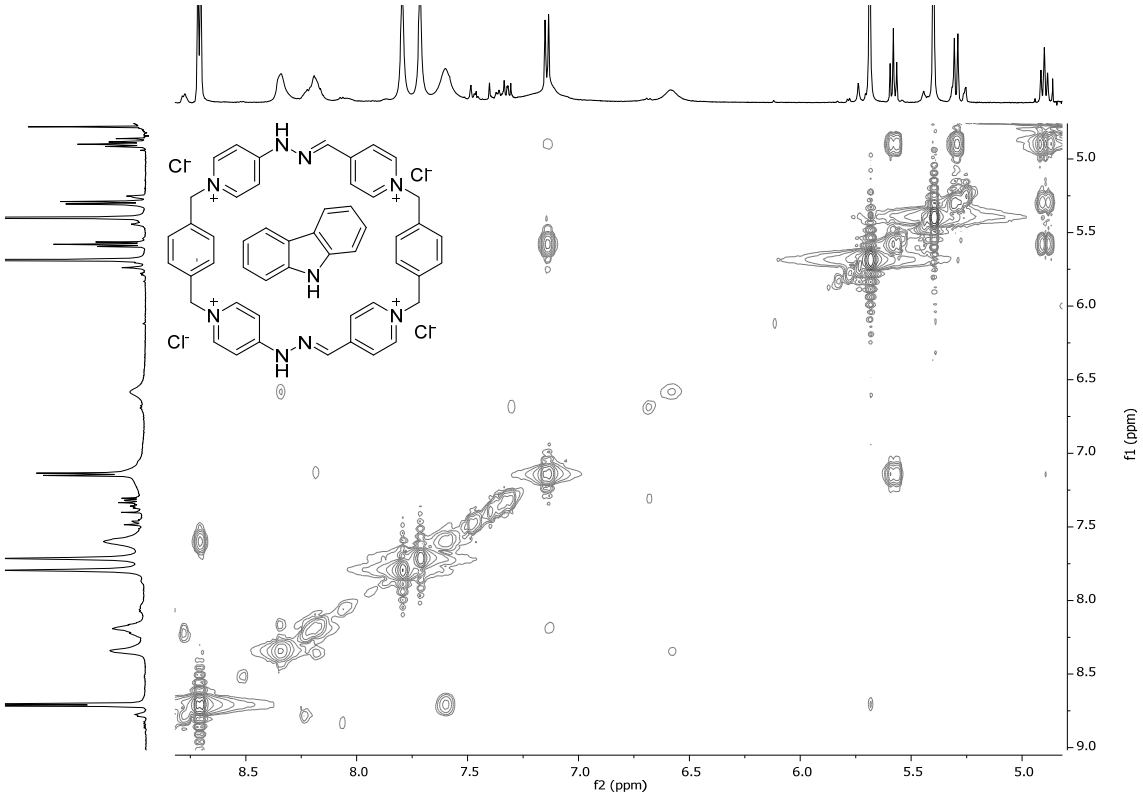

Figure S61. ^{1}H-^{1}H COSY (500 MHz, D_2O) spectrum of **R**·4Cl⊂CAR.

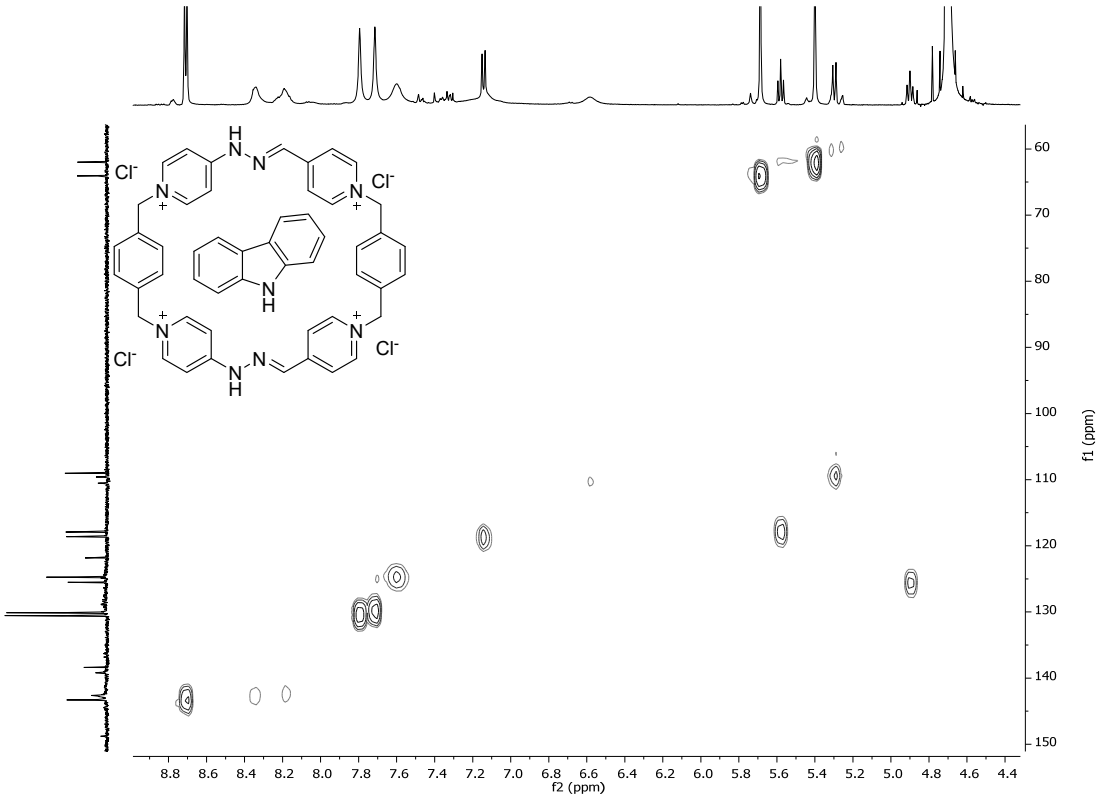

Figure S62. ^{1}H-^{13}C HSQC (500 and 126 MHz, D_2O) spectrum of **R**·4Cl⊂CAR.

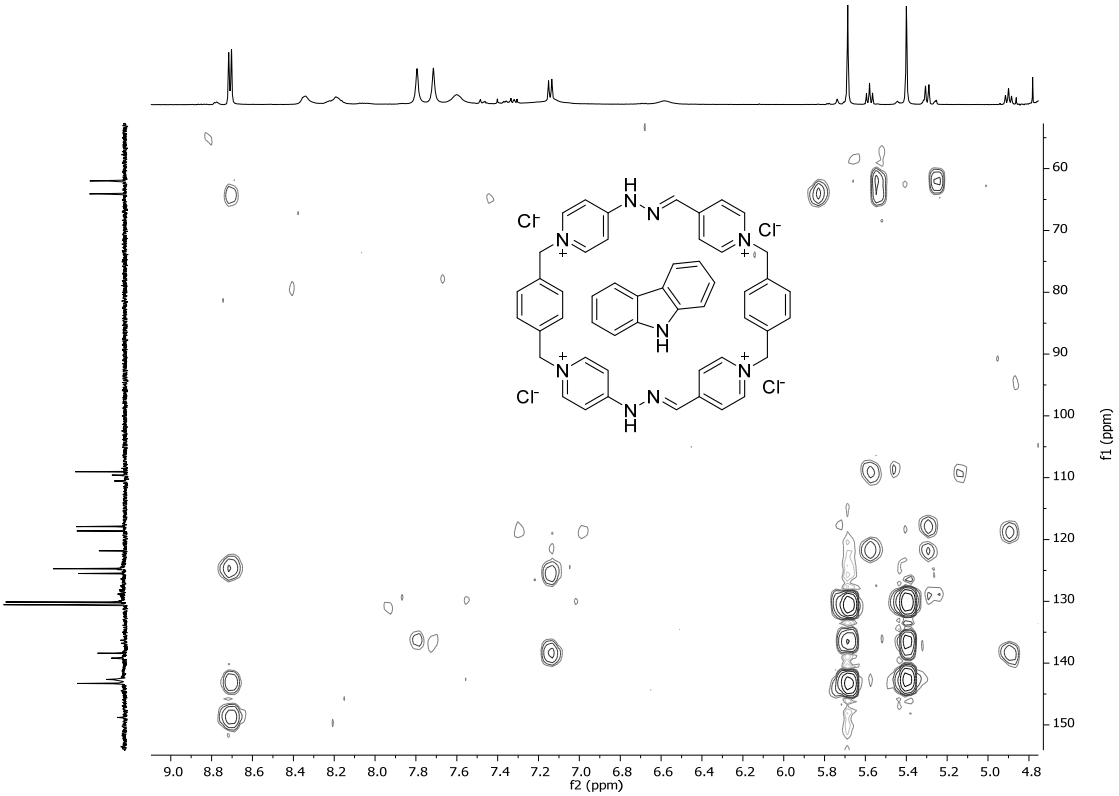

Figure S63. ^{1}H-^{13}C HMBC (500 and 126 MHz, D_2O) spectrum of **R**·4Cl⊂CAR.

1.7.5. NMR characterization of R·4Cl⊂Pyr (Pyr = pyrene).

^{1}H NMR (500 MHz, D_2O) δ 8.75 (d, *J* = 5.8 Hz, 4H), 8.37 (s, 2H), 8.26 (s, 2H), 8.03 (s, 4H), 7.96 (s, 4H), 7.09 (s, 4H), 6.82 (s, 3H), 6.56 (d, *J* = 7.6 Hz, 4H), 6.40 (t, *J* = 7.5 Hz, 2H), 6.25 (d, *J* = 26.1 Hz, 4H), 5.72 (s, 4H), 5.44 (s, 4H) ppm. ^{13}C NMR (126 MHz, D_2O) δ 143.24 (CH), 142.81 (CH), 142.39 (C), 138.02 (CH), 130.68 (CH), 130.27 (CH), 129.51 (C), 126.60 (CH), 125.76 (CH), 124.68 (CH), 124.17 (CH), 123.25 (C), 110.41 (CH), 109.52 (CH), 64.29 (CH_2), 62.25 (CH_2) ppm.

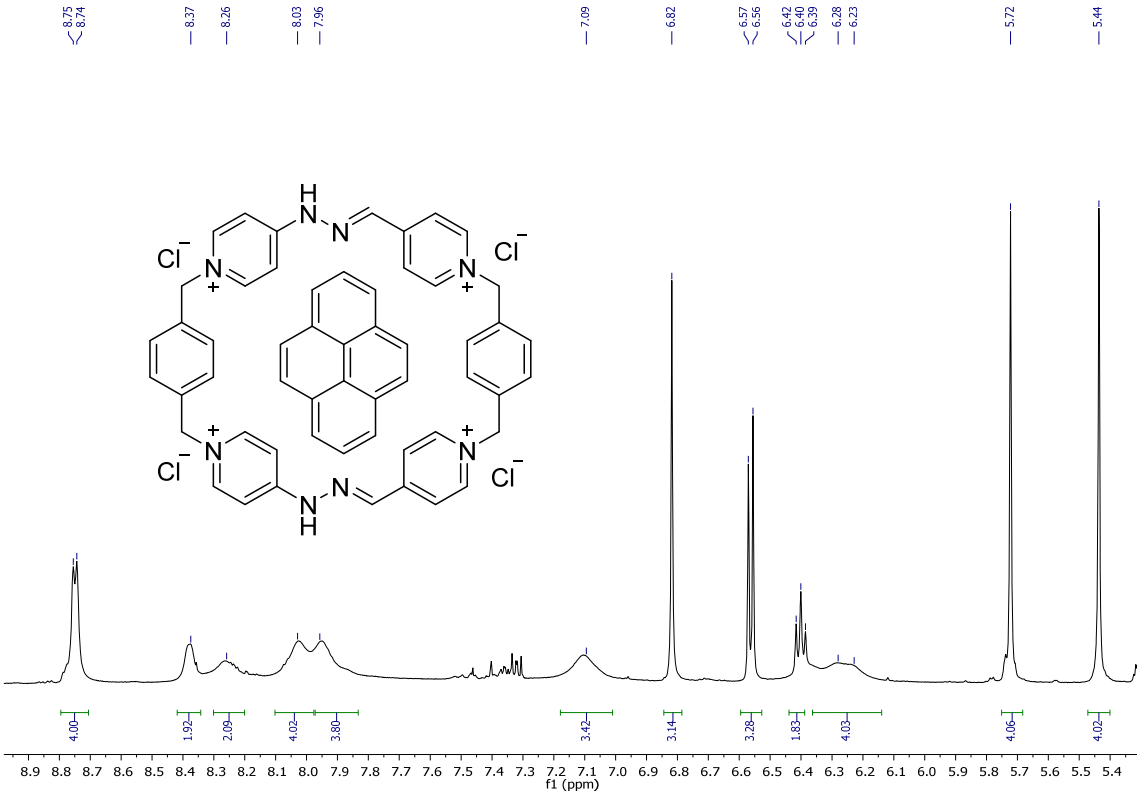

Figure S64. ^{1}H NMR (500 MHz, D_2O) spectrum of **R**·4Cl⊂Pyr.

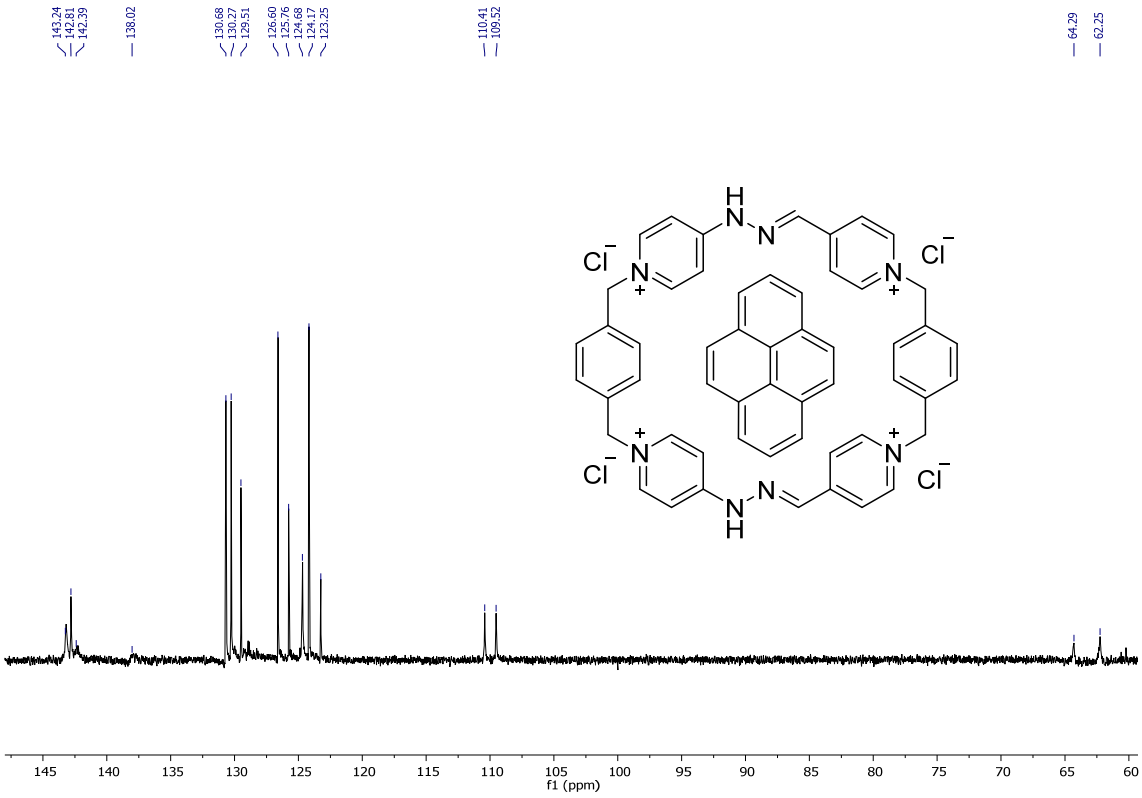

Figure S65. ^{13}C NMR (126 MHz, D_2O) spectrum of **R**·4Cl⊂Pyr.

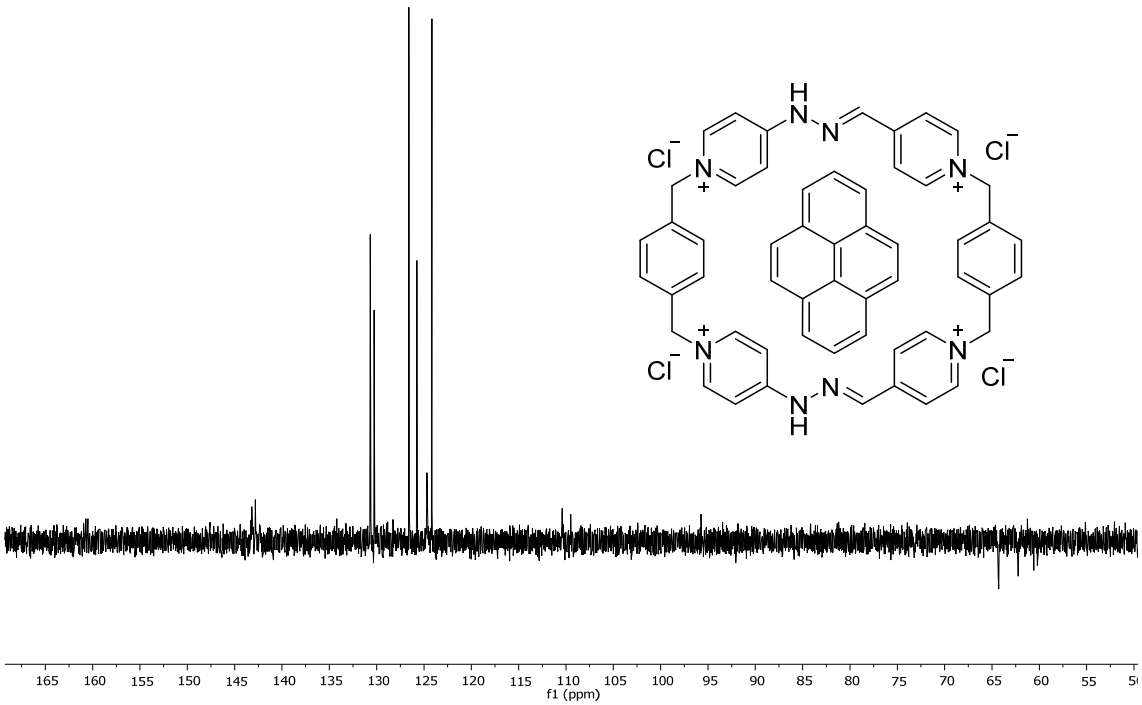

Figure S66. DEPT-135 (126 MHz, D_2O) spectrum of **R**·4Cl⊂Pyr.

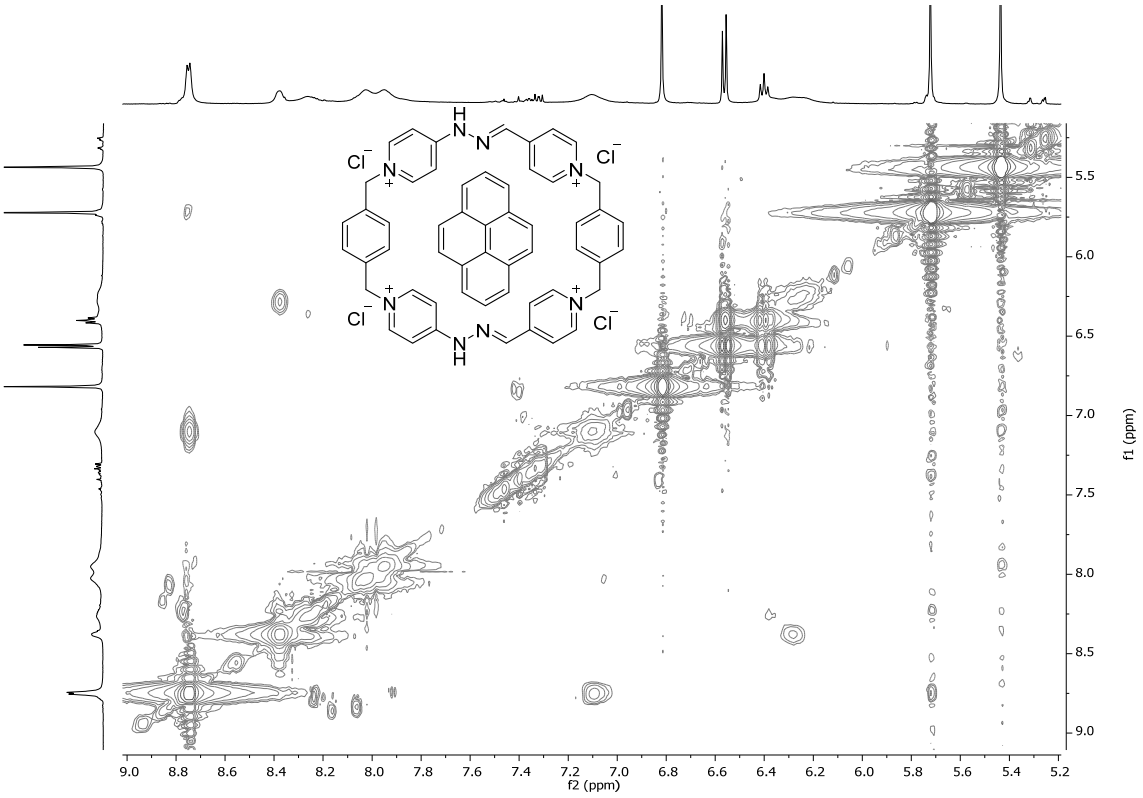

Figure S67. ^{1}H-^{1}H COSY (500 MHz, D_2O) spectrum of **R**·4Cl⊂Pyr.

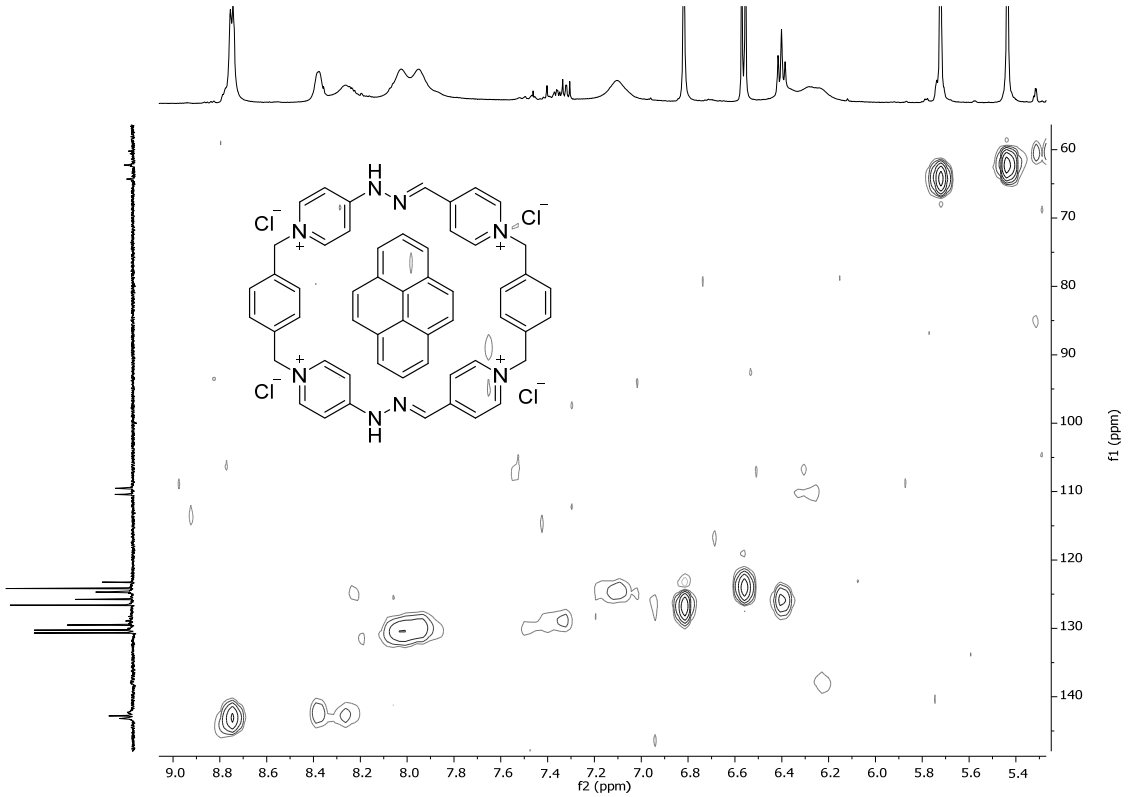

Figure S68. ^{1}H-^{13}C HSQC (500 and 126 MHz, D_2O) spectrum of **R**·4Cl⊂Pyr.

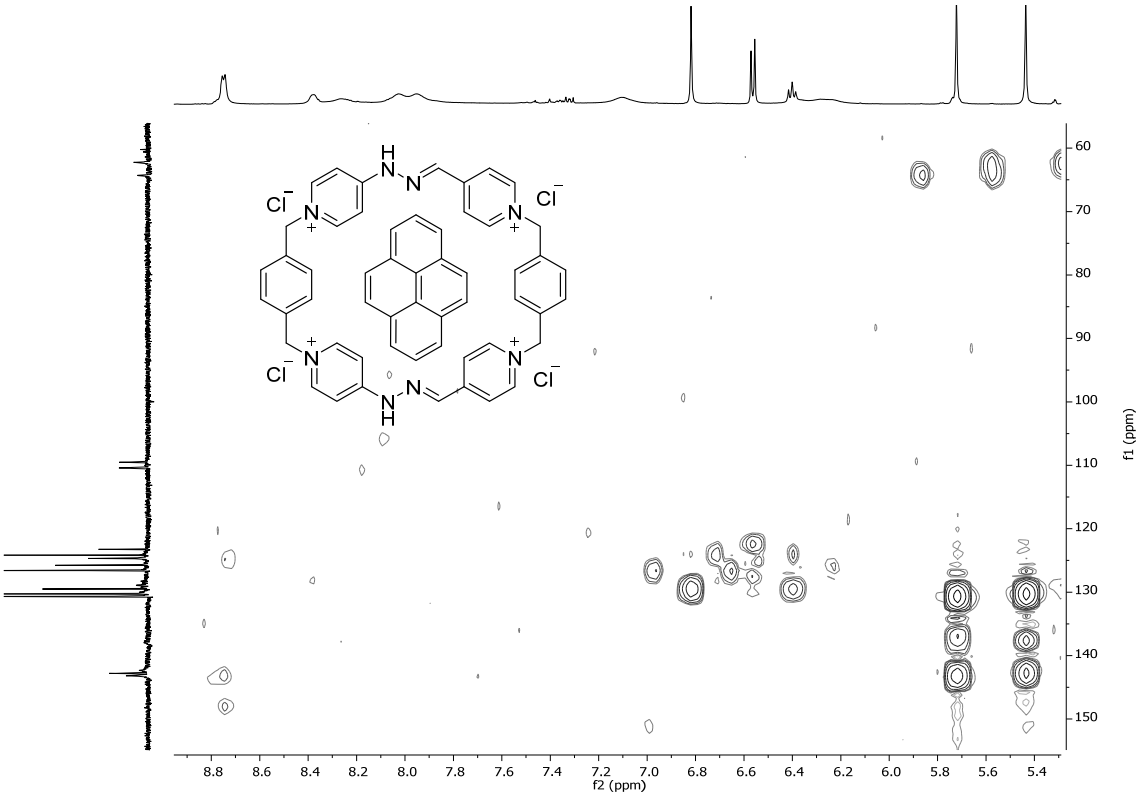

Figure S69. ^{1}H-^{13}C HMBC (500 and 126 MHz, D_2O) spectrum of **R**·4Cl⊂Pyr.

1.8. Inclusion complex of R^{4+} and R^{2+} in CD_3CN with 1,5-DHNc.

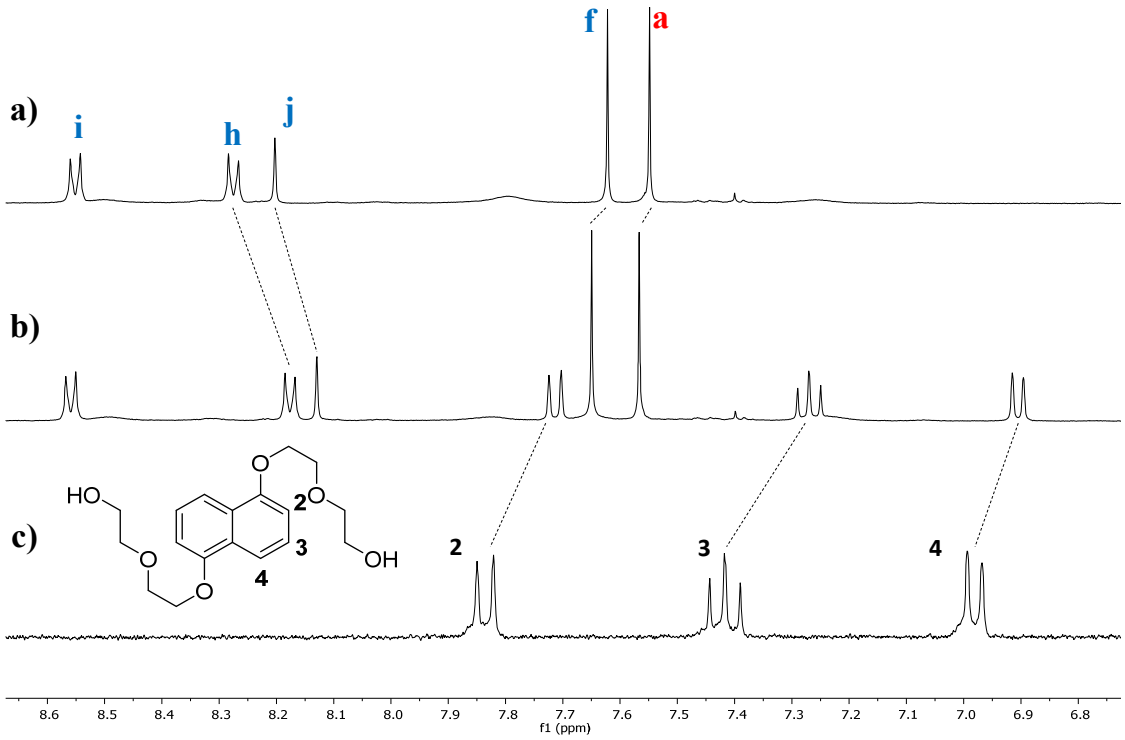

Figure S70. ^{1}H NMR (300 MHz, CD_3CN) of: a) solution of **R**·4PF_6 at 1.5 mM with 1 equivalent of TFA-d, b) same mixture of a) with 1 equivalent of 1,5-DHNc, c) solution of 1,5-DHN.

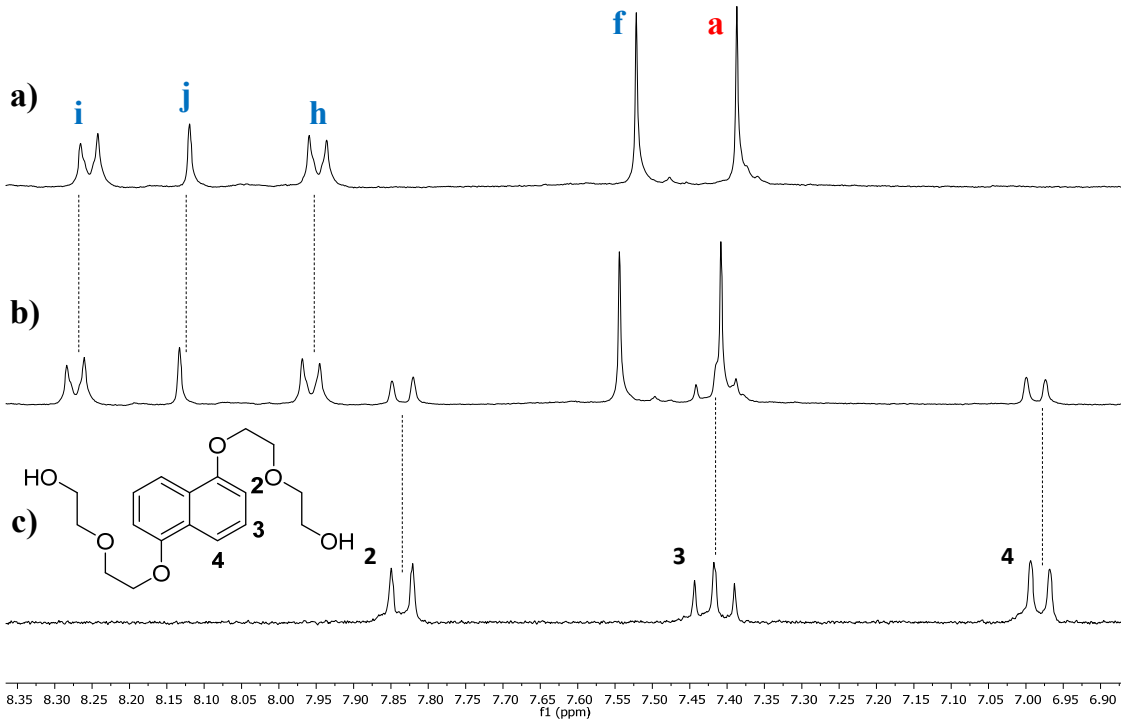

Figure S71. ^{1}H NMR (300 MHz, CD_3CN) of: a) solution of **R**·4PF_6 at 1.5 mM with 1 equivalent of Et_3N, b) same mixture of a) with 1 equivalent of 1,5-DHNc, c) solution of 1,5-DHN.

1.9. Inclusion complex of R^{4+} and R^{2+} in CD_3CN with Pyr.

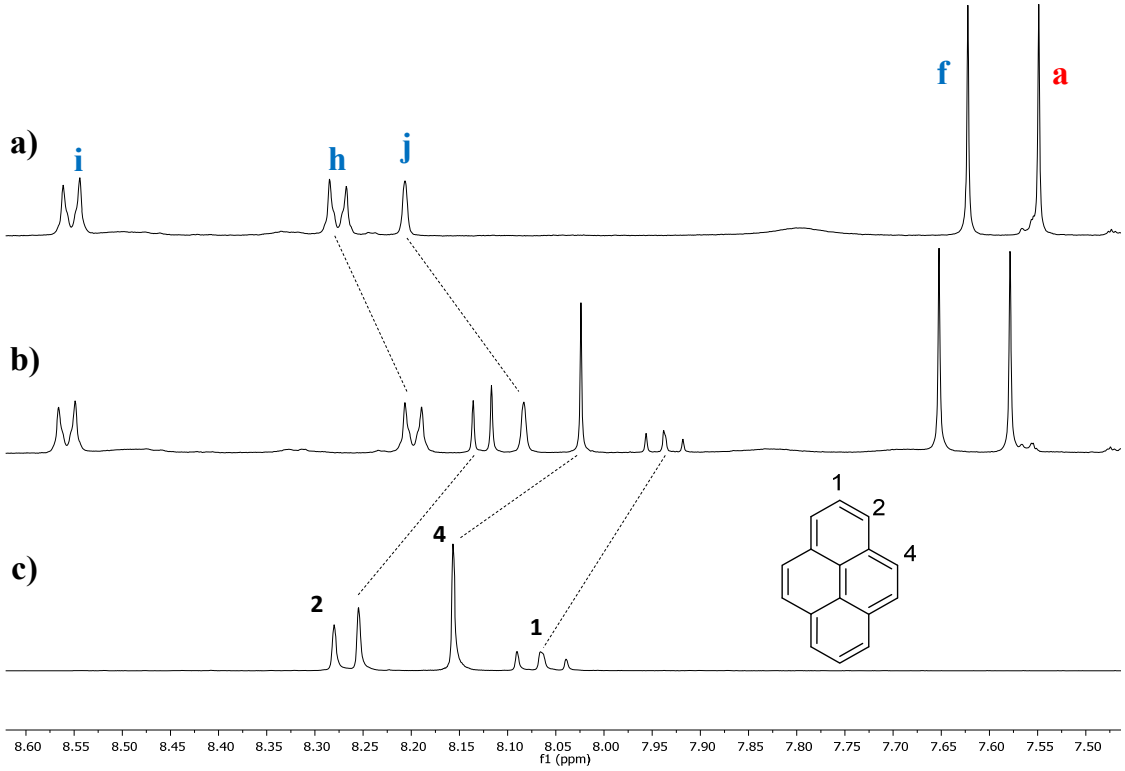

Figure S72. ^{1}H NMR (300 MHz, CD_3CN) of: a) solution of **R**·4PF_6 at 1.5 mM with 1 equivalent of TFA-d, b) same mixture of a) with 1 equivalent of Pyr, c) solution of Pyr.

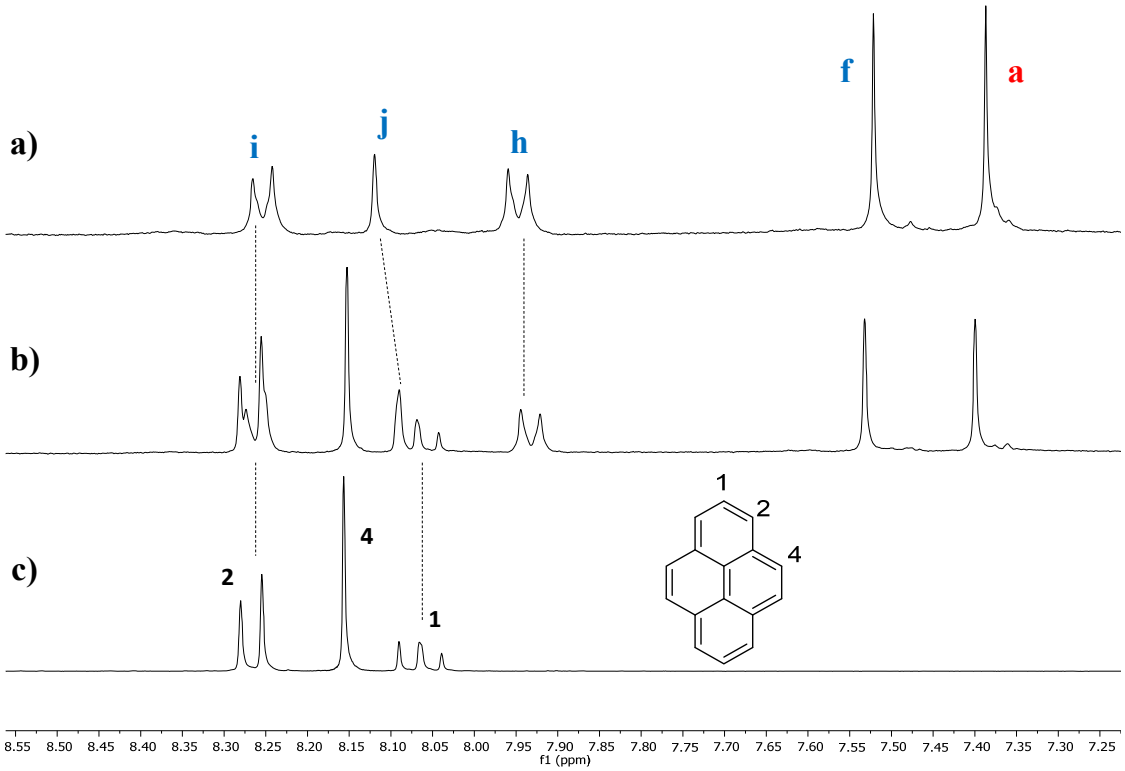

Figure S73. ^{1}H NMR (300 MHz, CD_3CN) of: a) solution of **R**·4PF_6 at 1.5 mM with 1 equivalent of Et_3N, b) same mixture of a) with 1 equivalent of Pyr, c) solution of Pyr.

1.10. Inclusion complex of R^{4+} in CD_3CN with 2,7-DHN.

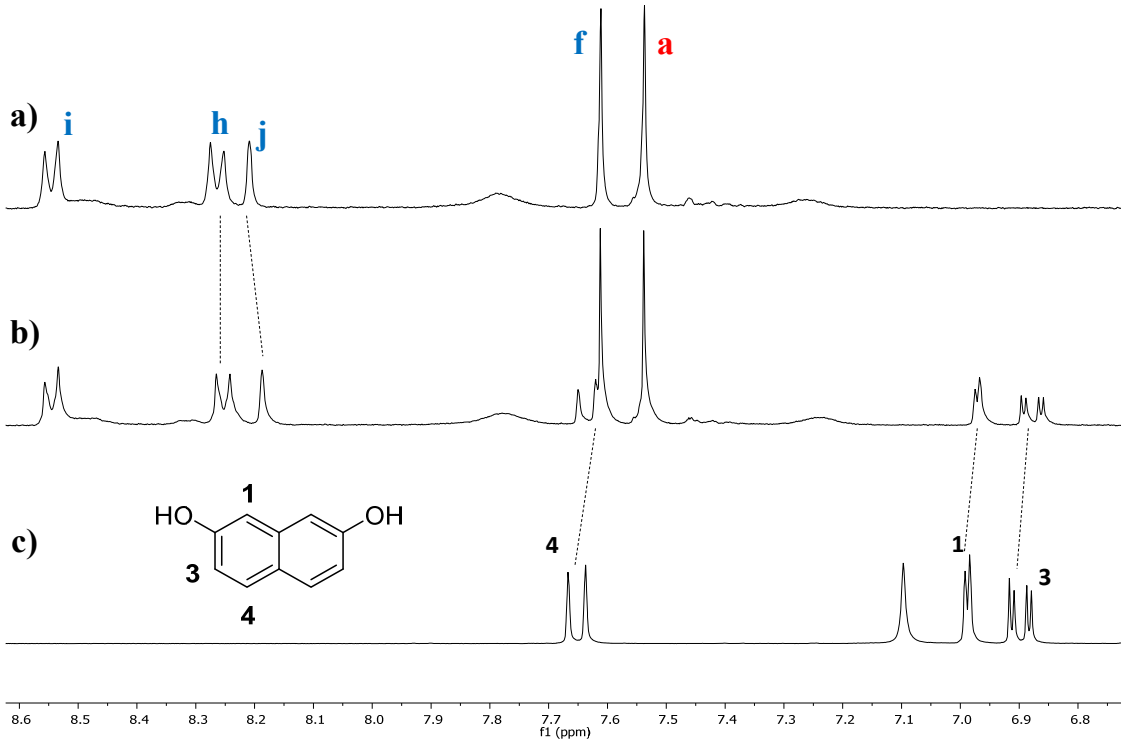

Figure S74. ^{1}H NMR (300 MHz, CD_3CN) of: a) solution of **R**·4PF_6 at 1.5 mM with 1 equivalent of TFA-d, b) same mixture of a) with 1 equivalent of 2,7-DHN, c) solution of 2,7-DHN.

1.11. Inclusion complex of R^{4+} in CD_3CN with 1,5-DHN.

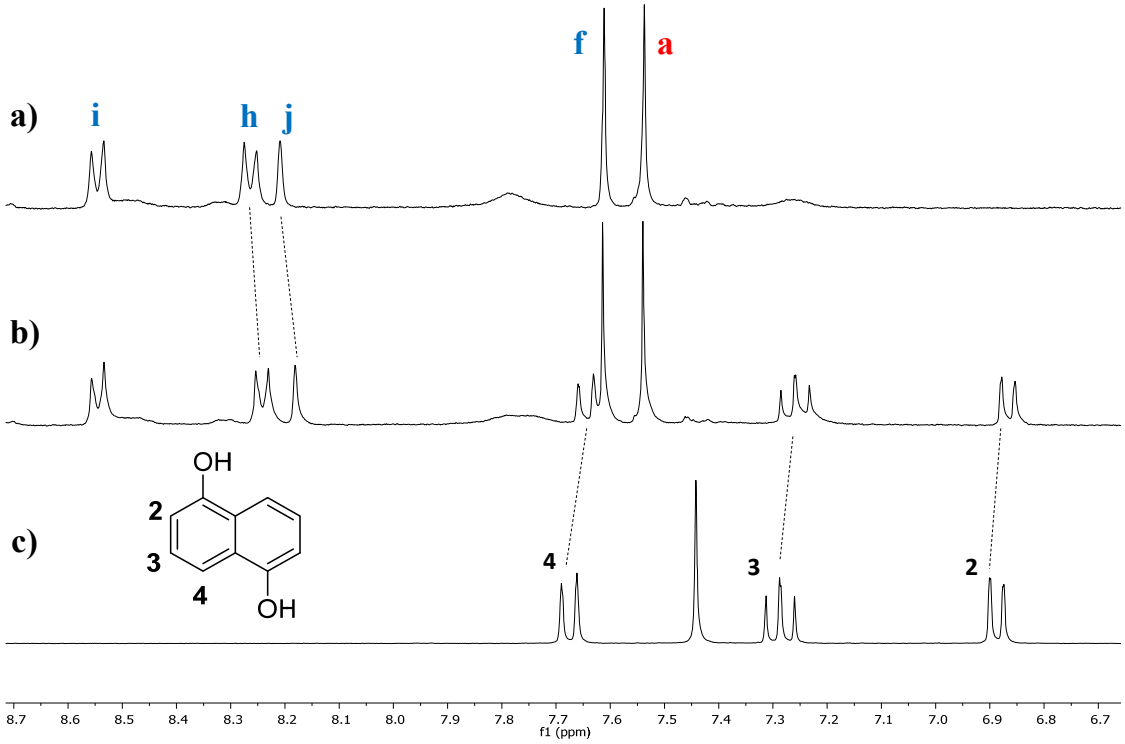

Figure S75. ^{1}H NMR (300 MHz, CD_3CN) of: a) solution of **R**·4PF_6 at 1.5 mM with 1 equivalent of TFA-d, b) same mixture of a) with 1 equivalent of 1,5-DHN, c) solution of 1,5-DHN.

1.12. Inclusion complex of R^{4+} in CD_3CN with CAR.

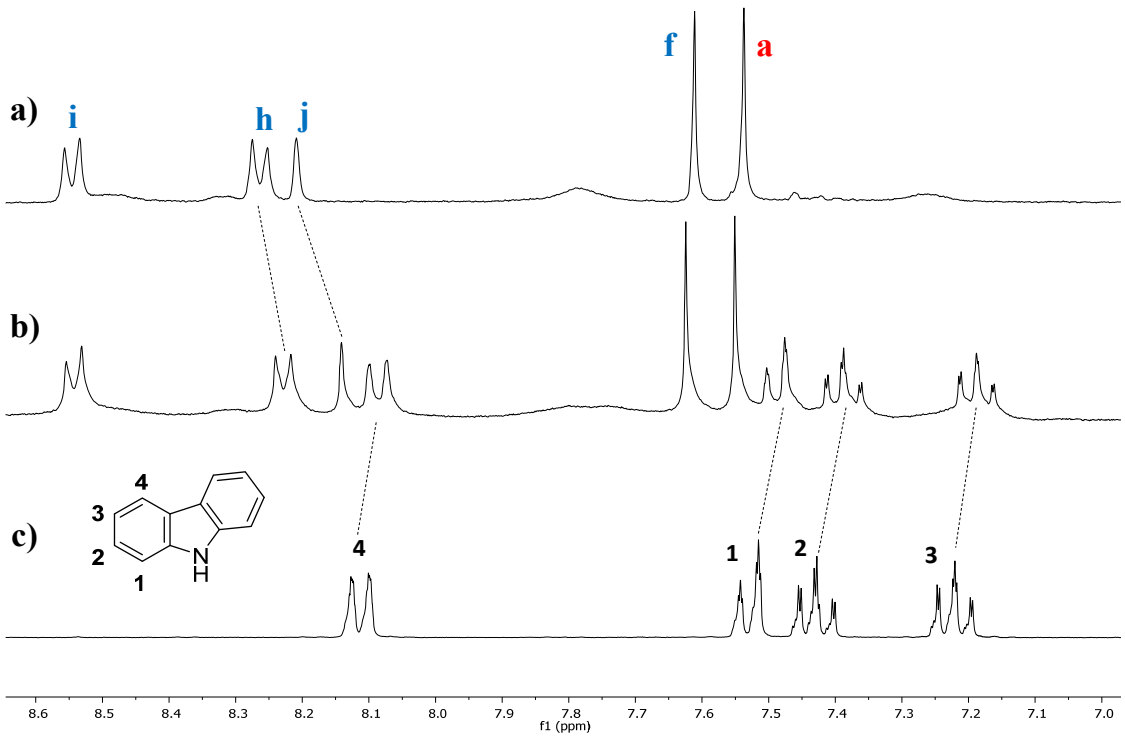

Figure S76. ^{1}H NMR (300 MHz, CD_3CN) of: a) solution of **R**·4PF_6 at 1.5 mM with 1 equivalent of TFA-d, b) same mixture of a) with 1 equivalent of carbazole, c) solution of carbazole.

2. Determination of K_a value for inclusion complex R·4Cl⊂1,5-DHN at pD = 6.

To carry out the titration, mixtures of **R**·4Cl and 1,5-DHN of different proportions were prepared from appropriate stocks solutions in Na_2DPO_4/NaD_2PO_4 buffer at pD = 6.

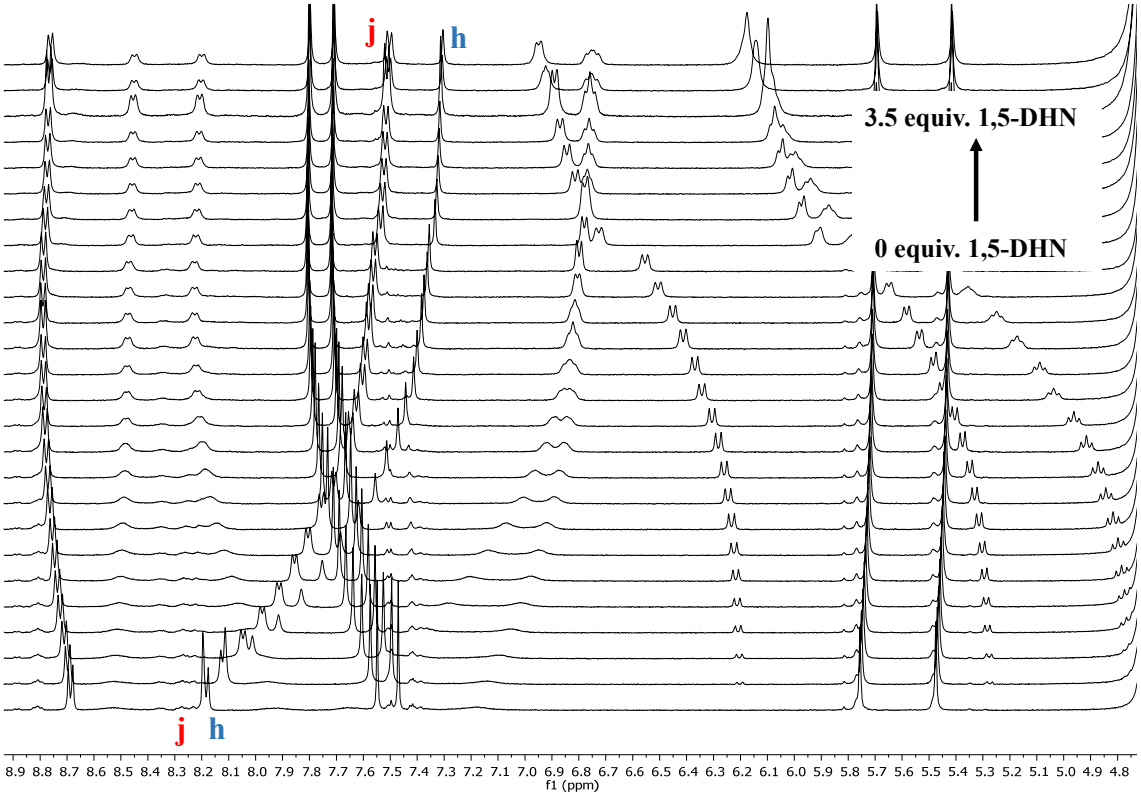

Figure S77. ^{1}H NMR (500 MHz, D_2O) spectra of **R**·4Cl (1.4 mM) upon titration with 1,5-DHN (10 mM). The chemical shift of signals Hj and Hh were used for the fitting.

The mechanism proposed for the fitting process equilibria, and introduced on the software *Dynafit* was the following: **R^{4+} + 1,5-DHN ⟺ R^{4+}⊂1,5-DHN**

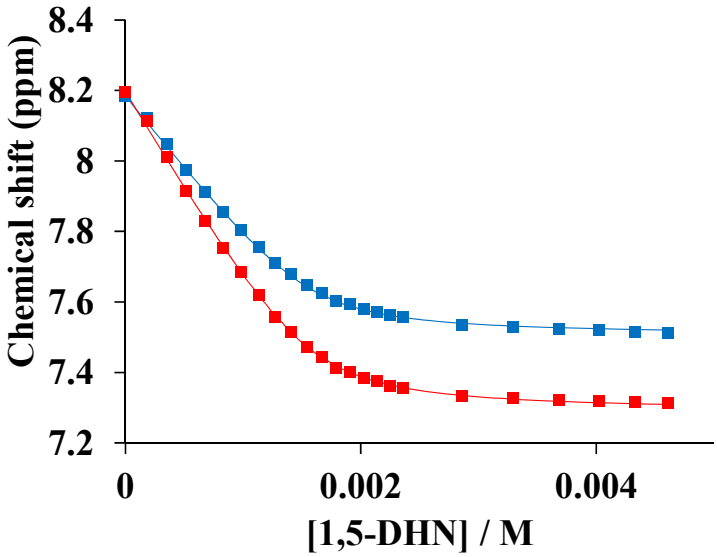

Figure S78. Fitting of experimental data (squares) for signals Hj and Hh.

Concentration **1,5-DHN** (molL^{-1})	Chemical shift (j)	Residual (j)	Chemical shift (h)	Residual (h)
0	8.1842	0	8.1965	0
1.79E-04	8.121	0.01011	8.1126	0.01409
3.51E-04	8.0468	0.00543	8.012	0.00642
5.17E-04	7.9755	3.10E-05	7.9149	-0.00259
6.78E-04	7.9123	-8.00E-04	7.8303	-0.00382
8.33E-04	7.8556	5.21E-04	7.7525	-0.00406
9.84E-04	7.8051	0.00387	7.6847	1.14E-04
0.00113	7.7556	0.00265	7.6182	-0.00185
0.00127	7.7097	-6.01E-04	7.5558	-0.00724
0.00141	7.6786	0.00443	7.5136	-0.00114
0.00154	7.647	0.00254	7.4715	-0.00353
0.00167	7.6257	0.00503	7.4429	-3.26E-04
0.00179	7.6031	7.82E-04	7.4133	-0.0054
0.00191	7.593	0.00494	7.4002	5.53E-04
0.00203	7.5803	0.00324	7.3841	-8.44E-04
0.00214	7.5728	0.00438	7.3747	0.00131
0.00225	7.5629	0.00129	7.363	-0.00128
0.00236	7.5565	4.47E-04	7.3555	-0.00136
0.00286	7.5355	-0.00412	7.3339	-9.85E-04
0.00329	7.5283	-0.0034	7.327	0.00269
0.00368	7.5234	-0.00373	7.3221	0.0039
0.00402	7.5195	-0.00466	7.3187	0.00448
0.00433	7.5162	-0.00588	7.316	0.00456
0.00461	7.5128	-0.00774	7.3129	0.00351

Table S1. Experimental data for the titration at pD = 6.

3. Determination of K_a value for inclusion complex R·4Cl⊂2,7-DHN at pD = 6.

To carry out the titration, mixtures of **R**·4Cl and 1,5-DHNc of different proportions were prepared from appropriate stocks solutions in Na_2DPO_4/NaD_2PO_4 buffer at pD = 6.

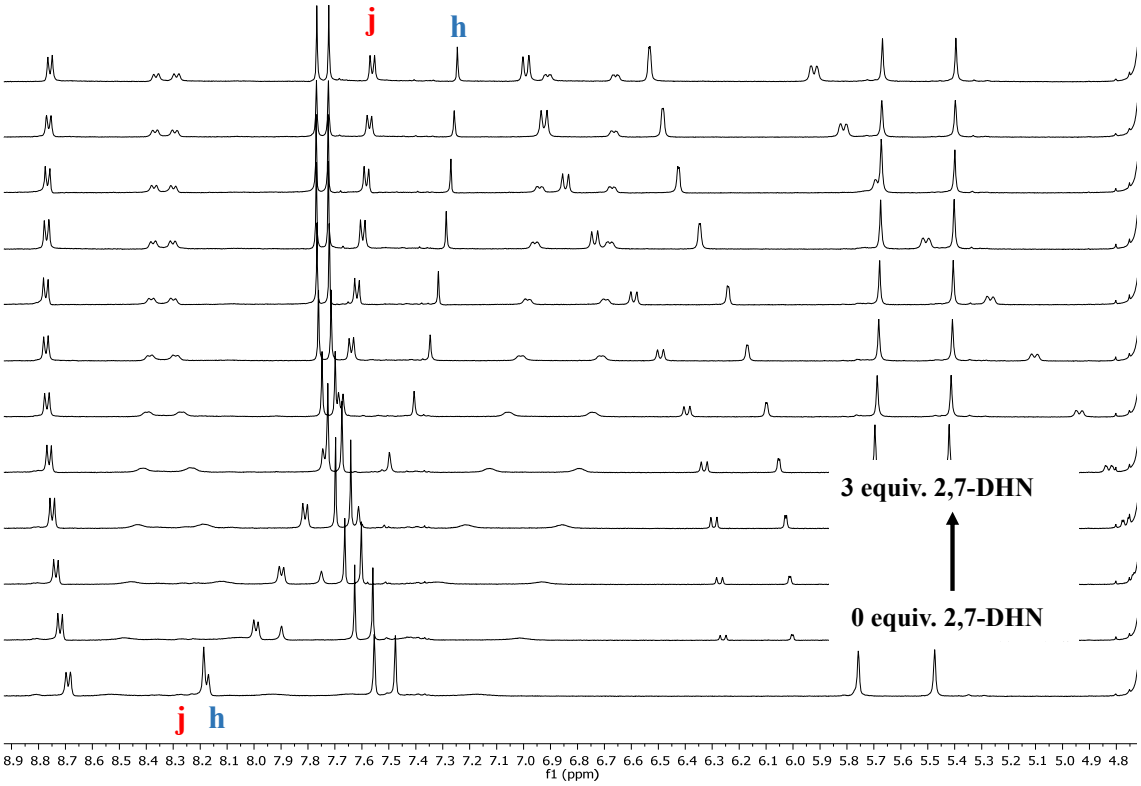

Figure S79. ^{1}H NMR (500 MHz, D_2O) spectra of **R**·4Cl (1 mM) upon titration with 2,7-DHN (10 mM). The chemical shift of signals Hj and Hh were used for the fitting.

The mechanism proposed for the fitting process equilibria, and introduced on the software *Dynafit* was the following: **R^{4+} + 2,7-DHN ⟺ R^{4+}⊂2,7-DHN**

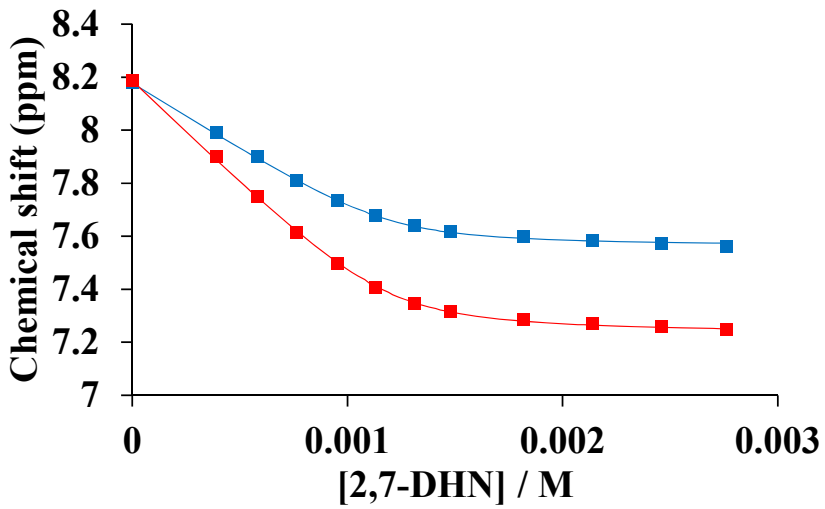

Figure S80. Fitting of experimental data (squares) for signals Hj and Hh.

. Concentration **2,7-DHN** (molL^{-1})	Chemical shift (j)	Residual (j)	Chemical shift (h)	Residual (h)
0	8.1776	0	8.1863	0
3.92E-04	7.9929	0.00877	7.898	0.01117
5.82E-04	7.8983	0.00456	7.75	0.00309
7.62E-04	7.8106	-0.00183	7.6126	-0.00845
9.52E-04	7.7358	5.14E-04	7.4973	-0.00434
0.00113	7.6783	0.00164	7.4062	-0.00469
0.00131	7.6392	0.00177	7.3468	-0.00336
0.00148	7.618	0.00398	7.3158	0.00187
0.00182	7.5967	0.00505	7.287	0.00771
0.00214	7.5831	0.00116	7.2698	0.00553
0.00246	7.5719	-0.00483	7.2572	9.92E-04
0.00276	7.5614	-0.01211	7.2457	-0.00552

Table S2. Experimental data for the titration at pD = 6.

4. Determination of K_a value for inclusion complex R·4Cl⊂1,5-DHNc at pD = 6.

To carry out the titration, mixtures of **R**·4Cl and 1,5-DHNc of different proportions were prepared from appropriate stocks solutions in Na_2DPO_4/NaD_2PO_4 buffer at pD = 6.

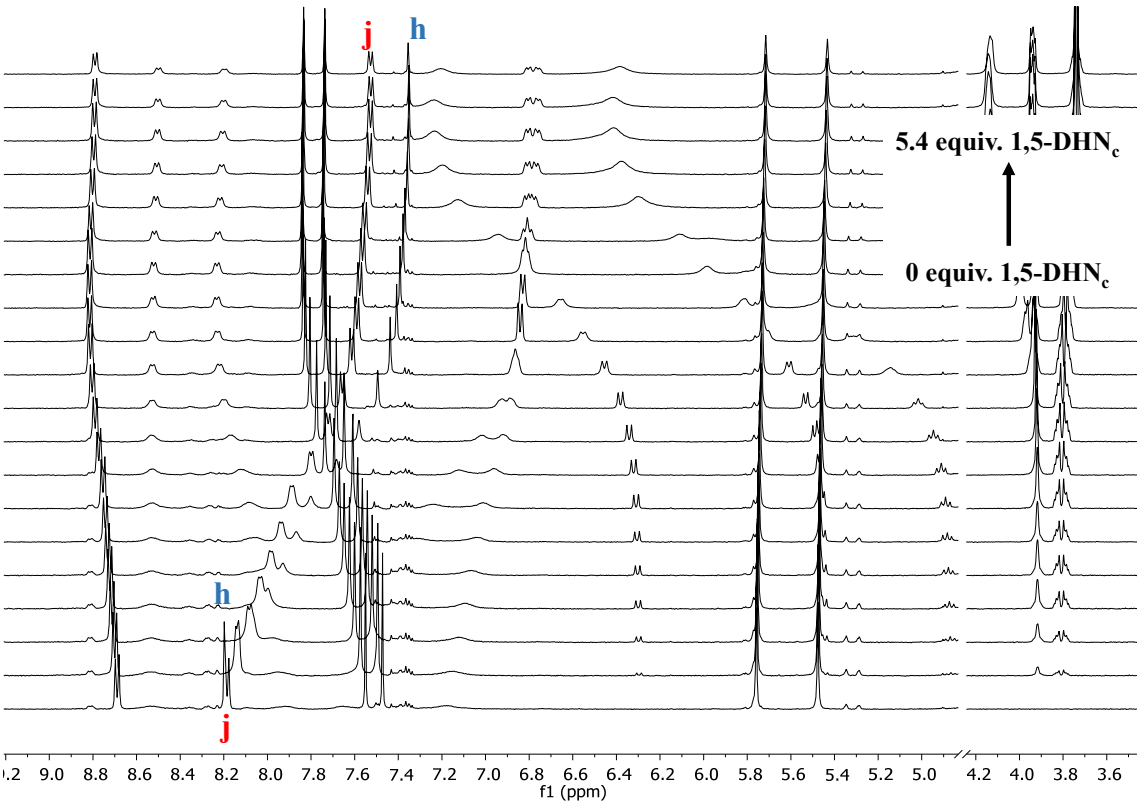

Figure S81. ^{1}H NMR (500 MHz, D_2O) spectra of **R**·4Cl (1.47 mM) upon titration with 1,5-DHNc (10 mM). The chemical shift of signals Hj and Hh were used for the fitting.

The mechanism proposed for the fitting process equilibria, and introduced on the software *Dynafit* was the following: **R^{4+} + 1,5-DHNc ⟺ R^{4+}⊂1,5-DHNc**

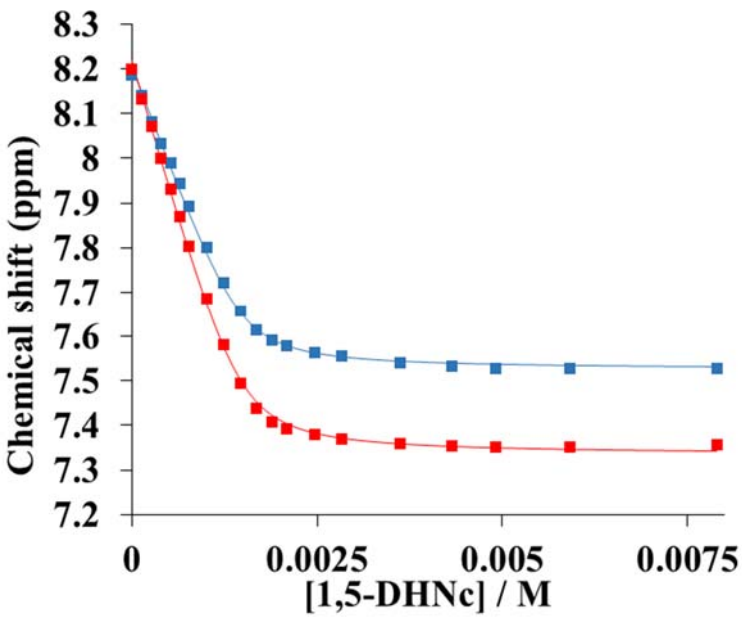

Figure S82. Fitting of experimental data (squares) for signals Hj and Hh.

Concentration **1,5-DHNc** ($molL^{-1}$)	Chemical shift (j)	Residual (j)	Chemical shift (h)	Residual (h)
0.000000	8.1853	-0.02099	8.1985	-0.02039
0.000136	8.1388	-0.00766	8.1322	-0.00896
0.000269	8.0814	-0.00708	8.0701	0.00427
0.000399	8.0333	0.00083	7.9996	0.00653
0.000527	7.9882	0.01004	7.9303	0.00777
0.000652	7.9431	0.01689	7.8688	0.01376
0.000775	7.8929	0.01642	7.8025	0.01206
0.001015	7.8001	0.01466	7.6846	0.01244
0.001245	7.7219	0.01181	7.5805	0.00621
0.001468	7.6571	0.00340	7.4946	-0.00643
0.001682	7.6133	-0.00334	7.4371	-0.01579
0.001890	7.5904	-0.00301	7.4079	-0.01481
0.002090	7.5775	-0.00135	7.3925	-0.01129
0.002470	7.5639	0.00138	7.3783	-0.00428
0.002827	7.5547	0.00077	7.3699	-0.00152
0.003626	7.5401	-0.00388	7.3587	0.00020
0.004316	7.5325	-0.00711	7.3538	0.00098
0.004918	7.5277	-0.00946	7.3510	0.00136
0.005916	7.5262	-0.00832	7.3516	0.00539
0.007895	7.5277	-0.00398	7.3550	0.01249

Table S3. Experimental data for the titration at pD = 6.

5. Determination of K_a value for inclusion complex R·2Cl⊂1,5-DHNc at pD = 10

To carry out the titration, mixtures of **R**·2Cl and 1,5-DHNc of different proportion were prepared from appropriate stocks solutions in $Na_2CO_3/NaHCO_3$ buffer at pD = 10.

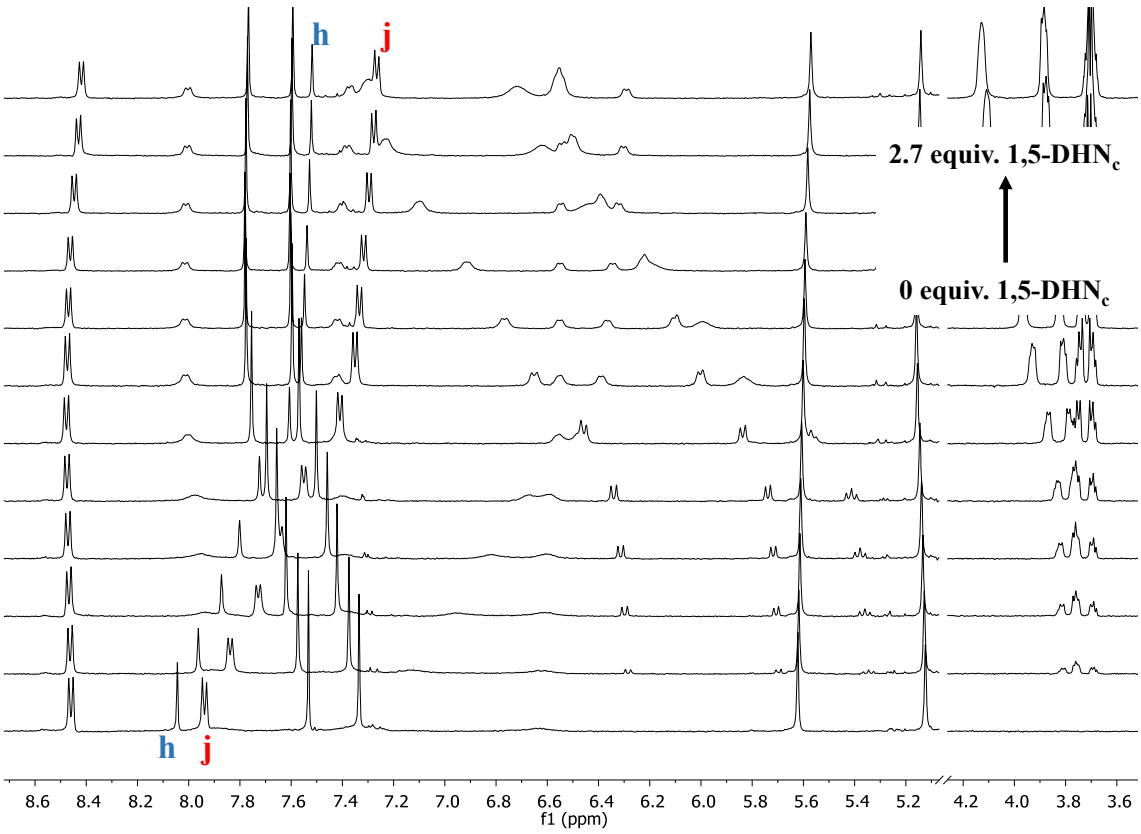

Figure S83. ^{1}H NMR (500 MHz, D_2O) spectra of **R**·2Cl (1.46 mM) upon titration with 1,5-DHNc (10 mM). The chemical shift of the signals Hj and Hh were used for the fitting.

The mechanism proposed for the fitting process equilibria, and introduced on the software *Dynafit* was the following: **R^{2+} + 1,5-DHNc ⟺ R^{2+}⊂1,5-DHNc**

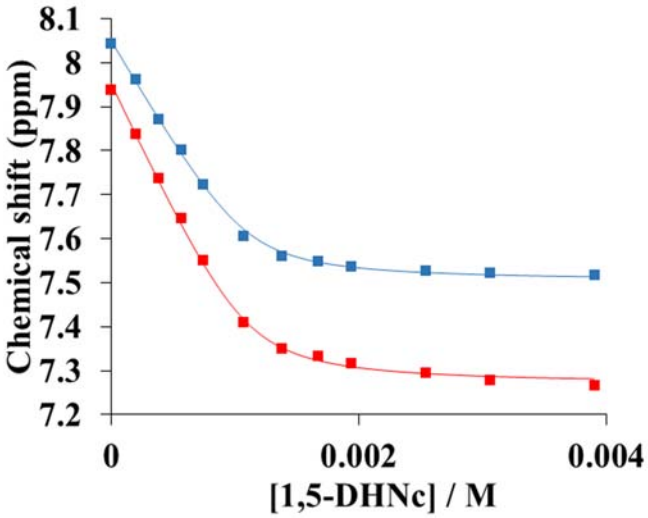

Figure S84. Fitting of the experimental data (squares) of signals Hj and Hh.

Concentration **1,5-DHNc** (molL^{-1})	Chemical shift (j)	Residual (j)	Chemical shift (h)	Residual (h)
0.000000	7.9383	-0.01404	8.0444	-0.00498
0.000196	7.8384	0.00077	7.9628	0.00505
0.000385	7.7366	0.00650	7.8724	0.00053
0.000566	7.6458	0.01389	7.8014	0.00797
0.000740	7.5507	0.00574	7.7237	-0.00028
0.001071	7.4101	-0.00624	7.6071	-0.01414
0.001379	7.3509	-0.00107	7.5601	-0.00973
0.001667	7.3335	0.01010	7.5477	0.00069
0.001935	7.3169	0.00775	7.5378	0.00217
0.002537	7.2957	0.00214	7.5280	0.00483
0.003056	7.2774	-0.00970	7.5213	0.00328
0.003902	7.2656	-0.01584	7.5181	0.00461

Table S4. Experimental data for the titration at pD = 10.

6. Determination of K_a value for inclusion complex R·4PF$_6$⊂2,7-DHN in acetonitrile.

To carry out the titration, mixtures of **R**·4PF$_6$ and 2,7-DHN of different proportion were prepared from appropriate stocks solutions with 2 equivalents of TFA to keep acidic solution.

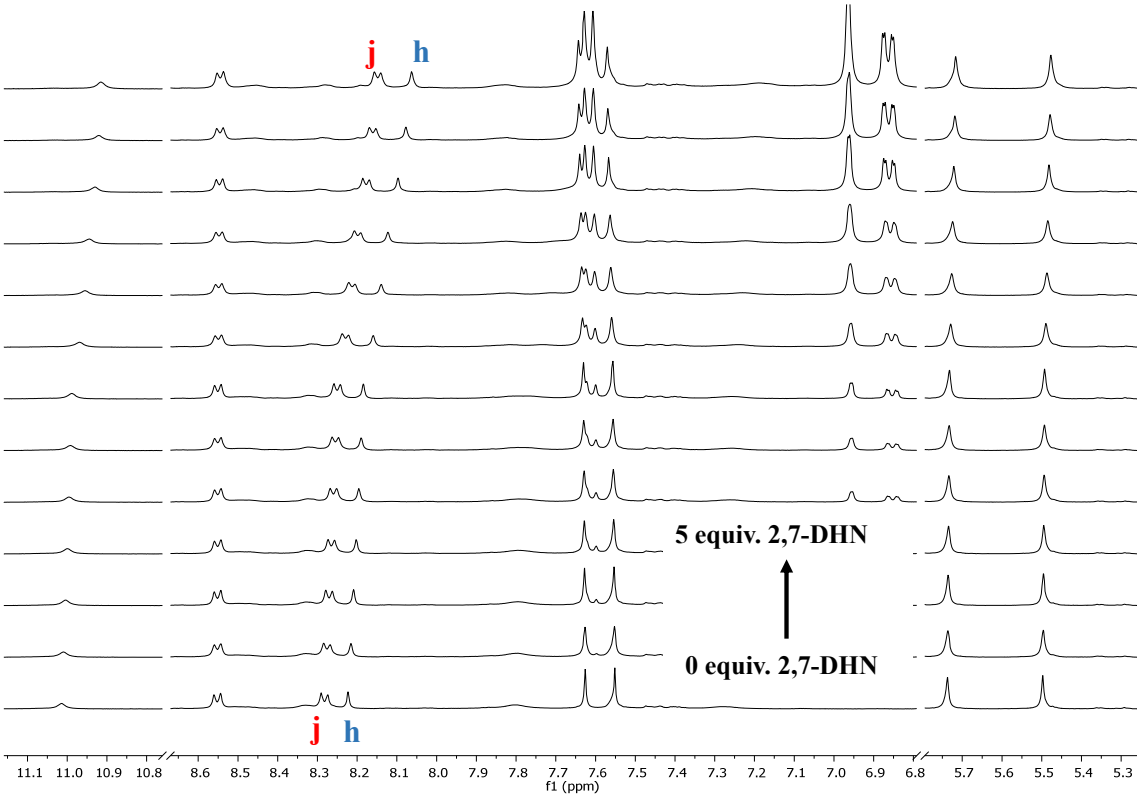

Figure S85. ^{1}H NMR (500 MHz, D$_2$O) spectra of **R**·4PF$_6$ (10 mM) upon titration with 2,7-DHN (100 mM). The chemical shift of the signals Hj and Hh were used for the fitting.

The mechanism proposed for the fitting process equilibria, and introduced on the software *Dynafit* was the following: **R^{2+} + 2,7-DHN ⟺ R^{2+}⊂2,7-DHN**.

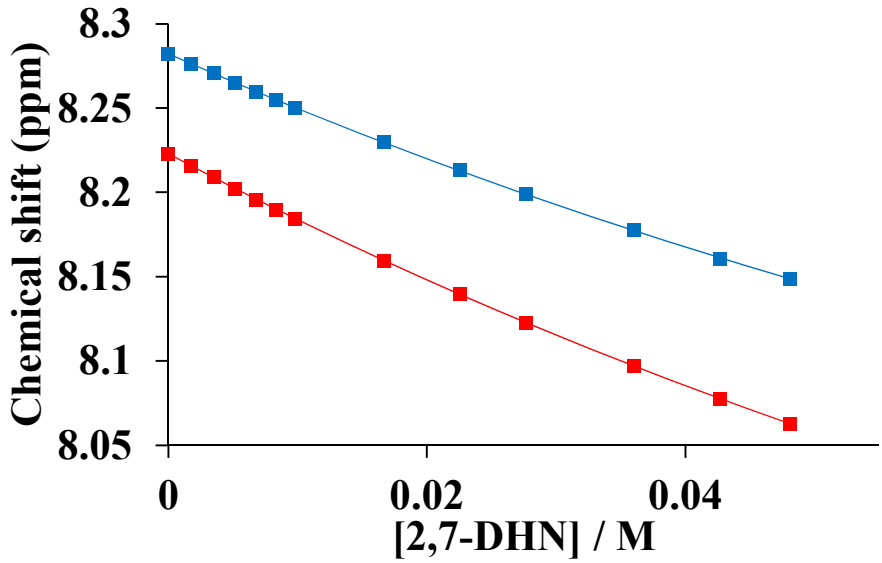

Figure S86. Fitting of the experimental data (squares) of signals Hj and Hh.

Concentration **2,7-DHN** (molL^{-1})	Chemical shift (j)	Residual (j)	Chemical shift (h)	Residual (h)
0	8.2823	0	8.2229	0
0.00179	8.2761	-1.40E-04	8.2157	6.80E-05
0.00351	8.2707	1.88E-04	8.2091	3.38E-04
0.00517	8.2651	2.99E-05	8.2023	6.47E-05
0.00678	8.2597	-1.71E-04	8.1957	-3.00E-04
0.00833	8.2548	-1.38E-04	8.1898	-2.84E-04
0.00984	8.2504	2.01E-04	8.1844	1.95E-08
0.01666	8.2298	2.19E-04	8.1596	-7.13E-05
0.02253	8.2131	2.96E-04	8.1395	-5.06E-05
0.02763	8.1989	-4.65E-06	8.1226	-2.80E-04
0.03605	8.1775	2.73E-04	8.0971	2.18E-04
0.04271	8.1608	-3.16E-04	8.0774	-1.58E-04
0.04811	8.1485	-1.71E-04	8.0629	2.68E-04

Table S5. Experimental data for the titration.

7. Determination of K_a value for inclusion complex R·4PF$_6$⊂1,5-DHNc in acetonitrile.

To carry out the titration, mixtures of **R**·4PF$_6$ and 1,5-DHNc of different proportion were prepared from appropriate stocks solutions with 2 equivalents of TFA to keep acidic solution.

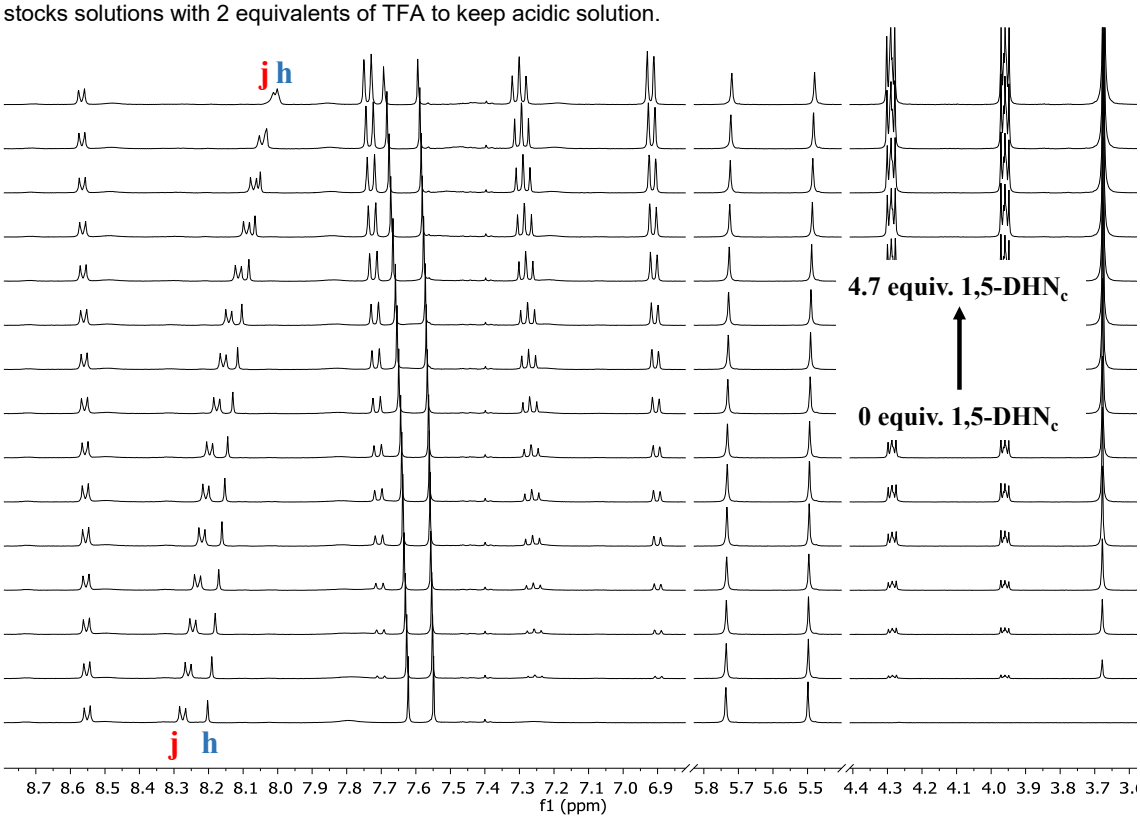

Figure S87. ^{1}H NMR (500 MHz, D$_2$O) spectra of **R**·4PF$_6$ (2 mM) upon titration with 1,5-DHNc (20 mM). The chemical shift of the signals Hj and Hh were used for the fitting.

The mechanism proposed for the fitting process equilibria, and introduced on the software *Dynafit* was the following: **R^{2+} + 1,5-DHNc ⟺ R^{2+}⊂1,5-DHNc**.

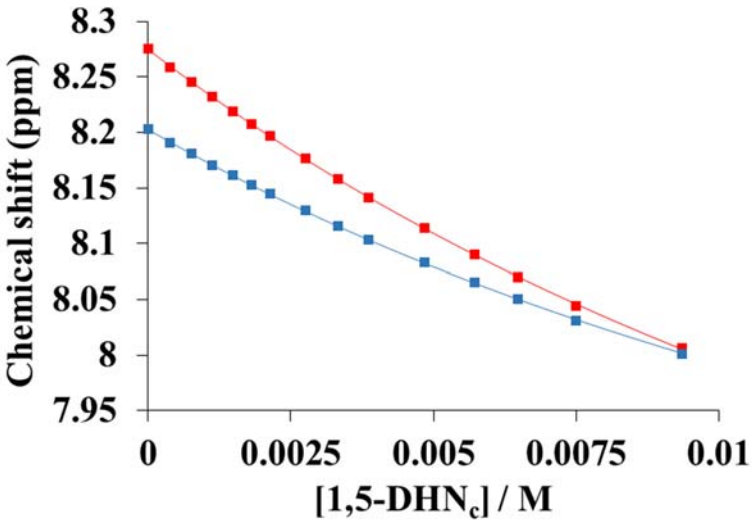

Figure S88. Fitting of the experimental data (squares) of signal Hj and Hh.

Concentration **1,5-DHNc** (molL^{-1})	Chemical shift (j)	Residual (j)	Chemical shift (h)	Residual (h)
0.00000	8.2751	0.00000	8.2028	0.00000
0.00039	8.2592	-0.00049	8.1908	-0.00052
0.00077	8.2458	0.00047	8.1808	0.00019
0.00113	8.2319	0.00000	8.1706	0.00000
0.00148	8.2194	0.00009	8.1614	0.00018
0.00182	8.2080	0.00050	8.1529	0.00048
0.00214	8.1969	0.00050	8.1447	0.00056
0.00276	8.1764	0.00034	8.1295	0.00051
0.00333	8.1577	-0.00020	8.1156	0.00015
0.00387	8.1415	-0.00008	8.1037	0.00041
0.00485	8.1138	0.00033	8.0832	0.00086
0.00571	8.0902	0.00008	8.0655	0.00057
0.00649	8.0698	-0.00062	8.0503	0.00005
0.00750	8.0442	-0.00185	8.0311	-0.00099
0.00936	8.0067	0.00148	8.0008	-0.00086

Table S6. Experimental data for the titration.

8. Determination of K_a value for inclusion complex R·4PF$_6$⊂CAR (CAR = carbazole) in acetonitrile.

To carry out the titration, mixtures of **R**·4PF$_6$ and CAR of different proportions were prepared from appropriate stocks solutions with 2 equivalents of TFA to keep acidic solution.

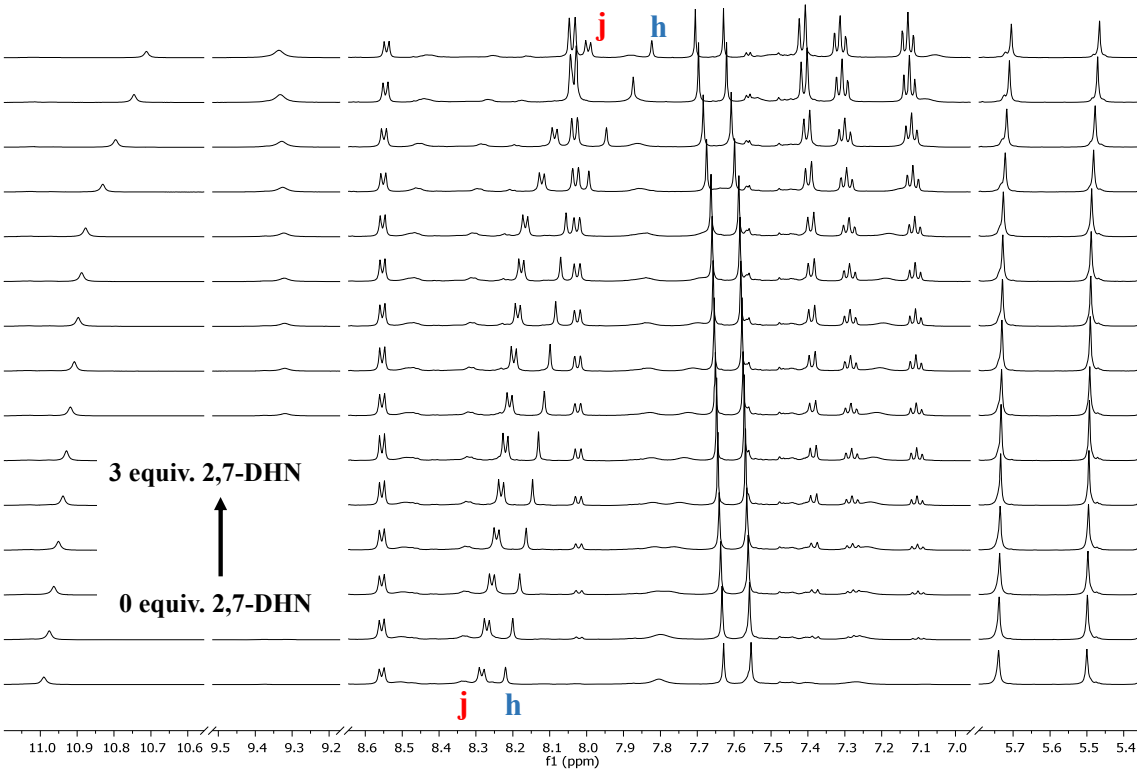

Figure S89. ^{1}H NMR (500 MHz, D$_2$O) spectra of **R**·4PF$_6$ (10 mM) upon titration with CAR (100 mM). The chemical shift of the signals Hj and Hh were used for the fitting.

The mechanism proposed for the fitting process equilibria, and introduced on the software *Dynafit* was the following: **R^{4+} + CAR ⟺ R^{4+}⊂CAR.**

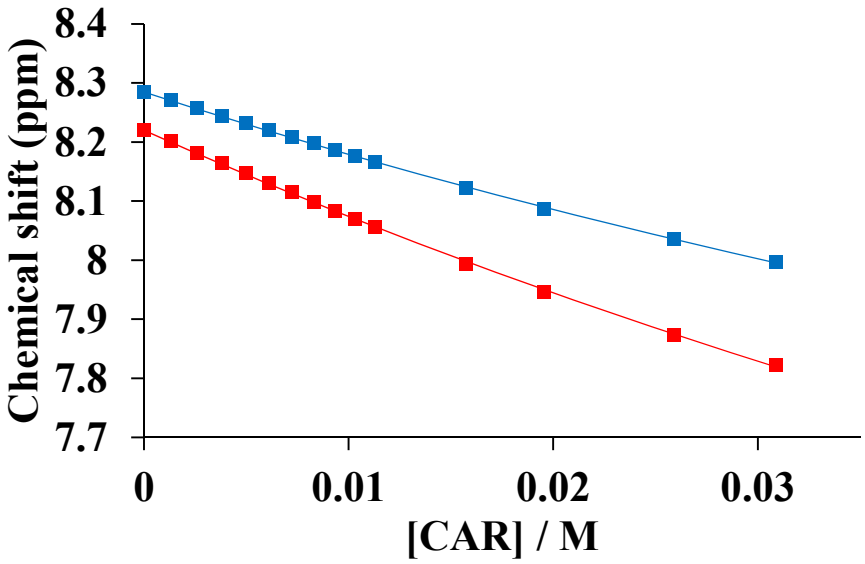

Figure S90. Fitting of the experimental data (squares) of signal Hj and Hh.

Concentration **CAR** (molL^{-1})	Chemical shift (j)	Residual (j)	Chemical shift (h)	Residual (h)
0	8.2843	0	8.2199	0
0.00131	8.2706	8.39E-04	8.2006	8.49E-04
0.00257	8.2568	8.01E-04	8.1815	8.20E-04
0.00379	8.2441	0.00122	8.1638	0.0013
0.00497	8.2317	0.00133	8.1466	0.00143
0.00611	8.2202	0.00174	8.1305	0.00184
0.00722	8.2087	0.00168	8.1148	0.00199
0.00828	8.1974	0.00116	8.099	0.00113
0.00932	8.1866	8.02E-04	8.0839	5.09E-04
0.01032	8.177	0.00112	8.0705	8.57E-04
0.01129	8.1663	-6.61E-05	8.0557	-7.63E-04
0.01572	8.1216	-0.00269	7.994	-0.00415
0.01956	8.0868	-0.00273	7.9465	-0.00349
0.02589	8.036	5.46E-04	7.8737	-0.00134
0.03089	7.9958	4.54E-04	7.8232	0.00374

Table S7. Experimental data for the titration.

9. Determination of K_a value for inclusion complex R·4PF$_6$⊂PYR (PYR = pyrene) in acetonitrile.

To carry out the titration, mixtures of **R**·4PF$_6$ and PYR of different proportions were prepared from appropriate stocks solutions with 2 equivalents of TFA to keep acidic solution.

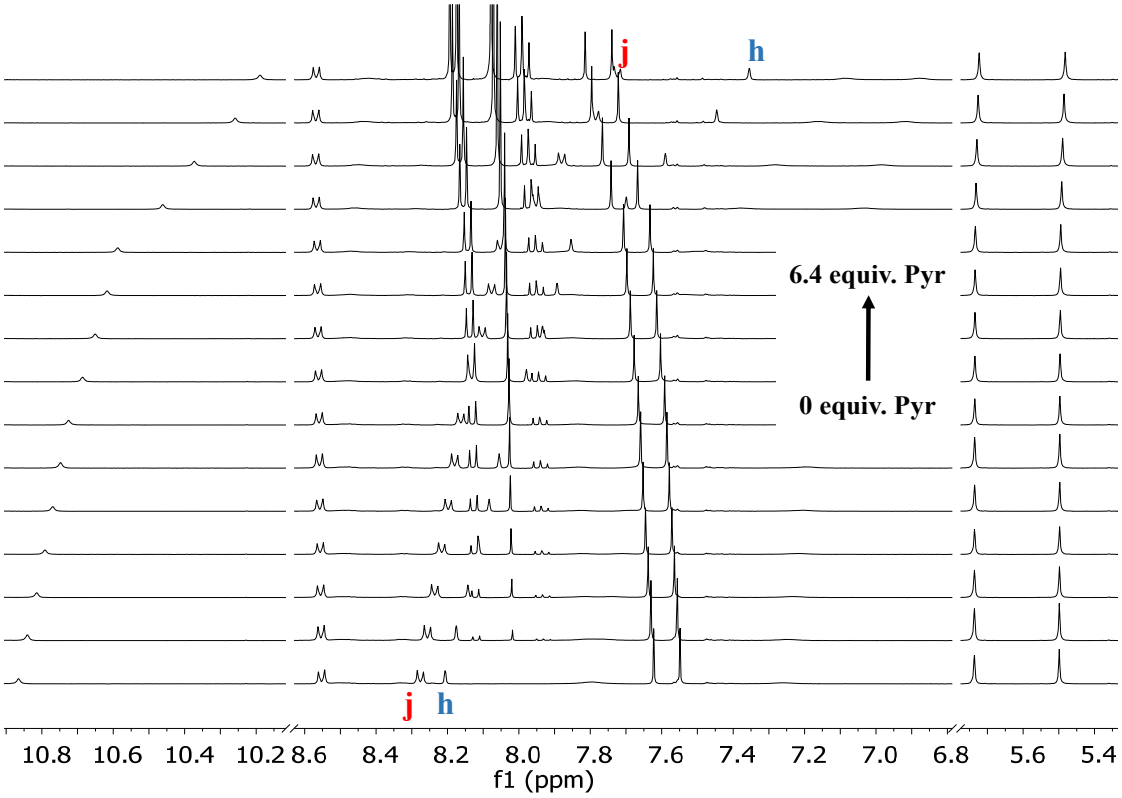

Figure S91. ^{1}H NMR (500 MHz, D_2O) spectra of **R**·4PF$_6$ (2.5 mM) upon titration with Pyr (20 mM). The chemical shift of the signals Hj and Hh were used for the fitting.

The mechanism proposed for the fitting process equilibria, and introduced on the software *Dynafit* was the following: **R^{4+} + Pyr ⟺ R^{4+}⊂Pyr.**

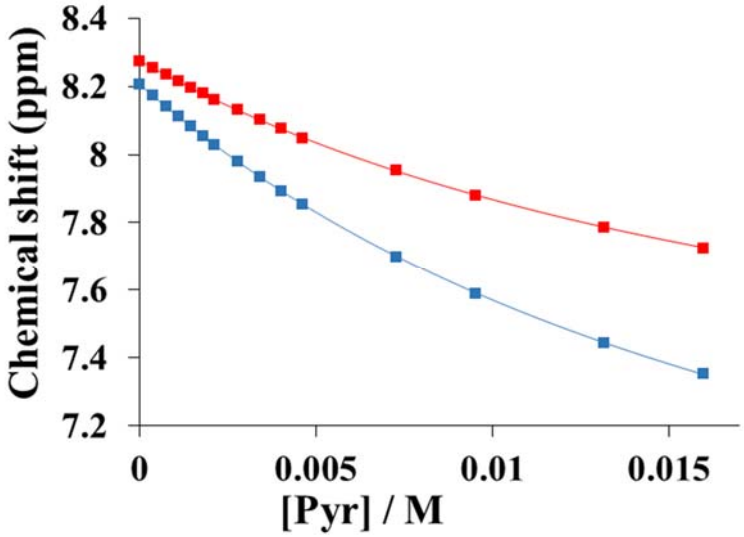

Figure S92. Fitting of the experimental data (squares) of signal Hj and Hh.

Concentration **Pyr** (molL^{-1})	Chemical shift (j)	Residual (j)	Chemical shift (h)	Residual (h)
0.00000	8.2758	0.00000	8.2066	0.00000
0.00037	8.2563	0.00189	8.1753	0.00206
0.00074	8.2358	0.00174	8.1428	0.00128
0.00109	8.2162	0.00151	8.1136	0.00228
0.00144	8.1980	0.00177	8.0835	0.00097
0.00179	8.1799	0.00128	8.0552	0.00013
0.00212	8.1627	0.00090	8.0280	-0.00085
0.00278	8.1341	0.00375	7.9793	-0.00051
0.00341	8.1028	0.00128	7.9342	-0.00066
0.00402	8.0765	0.00150	7.8930	-0.00052
0.00461	8.0501	-0.00044	7.8538	-0.00159
0.00726	7.9536	0.00141	7.6995	-0.00254
0.00951	7.8804	-0.00120	7.5899	-0.00208
0.01315	7.7866	-0.00077	7.4458	0.00075
0.01595	7.7254	-0.00210	7.3548	0.00310

Table S8. Experimental data for the titration.

10. Spectroscopy study of R^{4+} and R^{2+} in water.

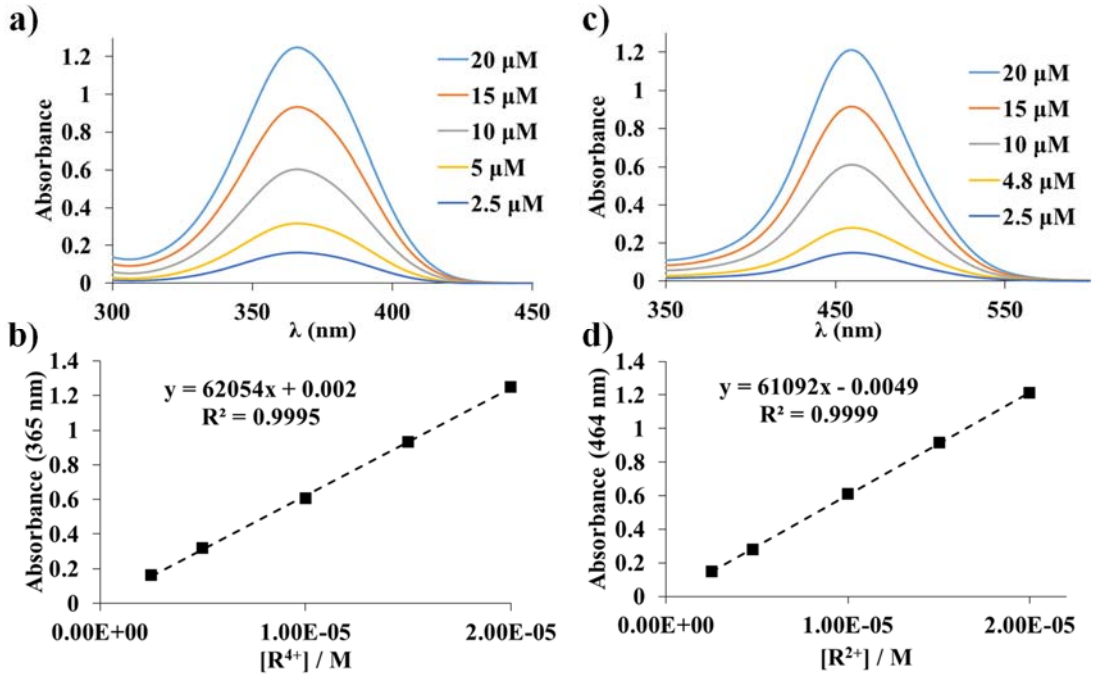

Figure S93. a) UV-Vis spectra of $\mathbf{R^{4+}}$ at pH 7 from 2.5 µM to 20 µM. b) Linear relationship between absorbance at 365 nm and concentration of $\mathbf{R^{4+}}$ where ε = 62054 $Lmol^{-1}cm^{-1}$. c) UV-Vis spectra of $\mathbf{R^{2+}}$ at pH 10.5 from 2.5 µM to 20 µM. d) Linear relationship between absorbance at 464 nm and concentration of $\mathbf{R^{2+}}$ where ε = 61092 $Lmol^{-1}cm^{-1}$.

11. Spectroscopy estudy R^{4+} and R^{2+} in acetonitrile.

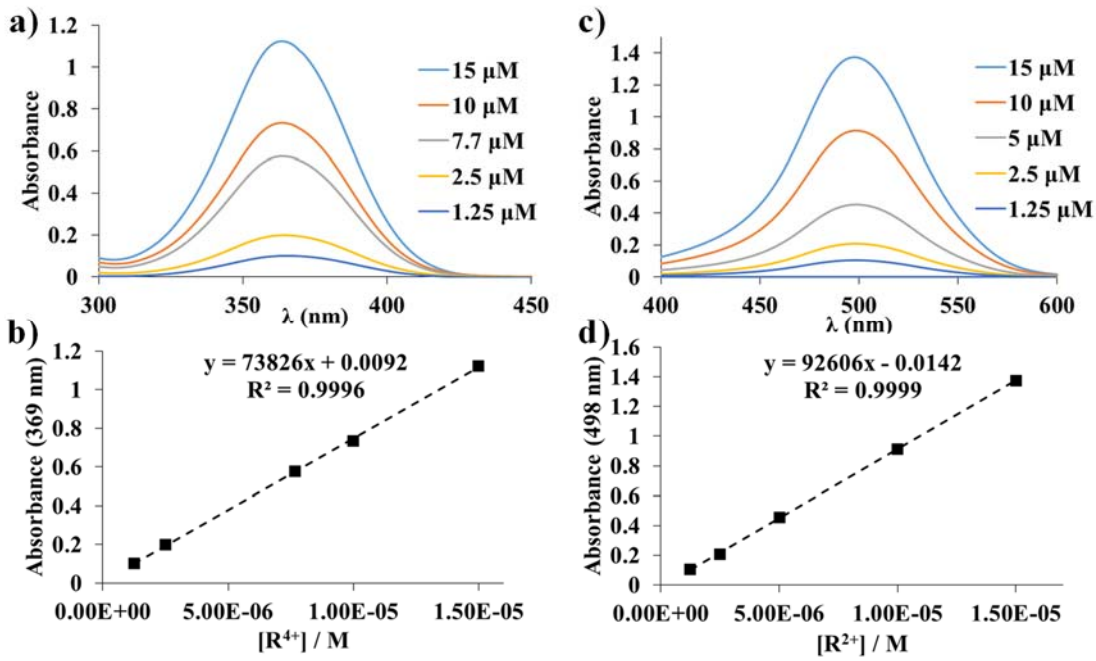

Figure S94. a) UV-Vis spectra of $\mathbf{R^{4+}}$ at pH 7 from 1.25 µM to 15 µM. b) Linear relationship between absorbance at 369 nm and concentration of $\mathbf{R^{4+}}$ where ε = 73826 $Lmol^{-1}cm^{-1}$. c) UV-Vis spectra of $\mathbf{R^{2+}}$ at pH 10.5 from 1.25 µM to 15 µM. d) Linear relationship between absorbance at 498 nm and concentration of $\mathbf{R^{2+}}$ where ε = 92606 $Lmol^{-1}cm^{-1}$.

12. pK_a determination for R^{4+} by UV-vis.

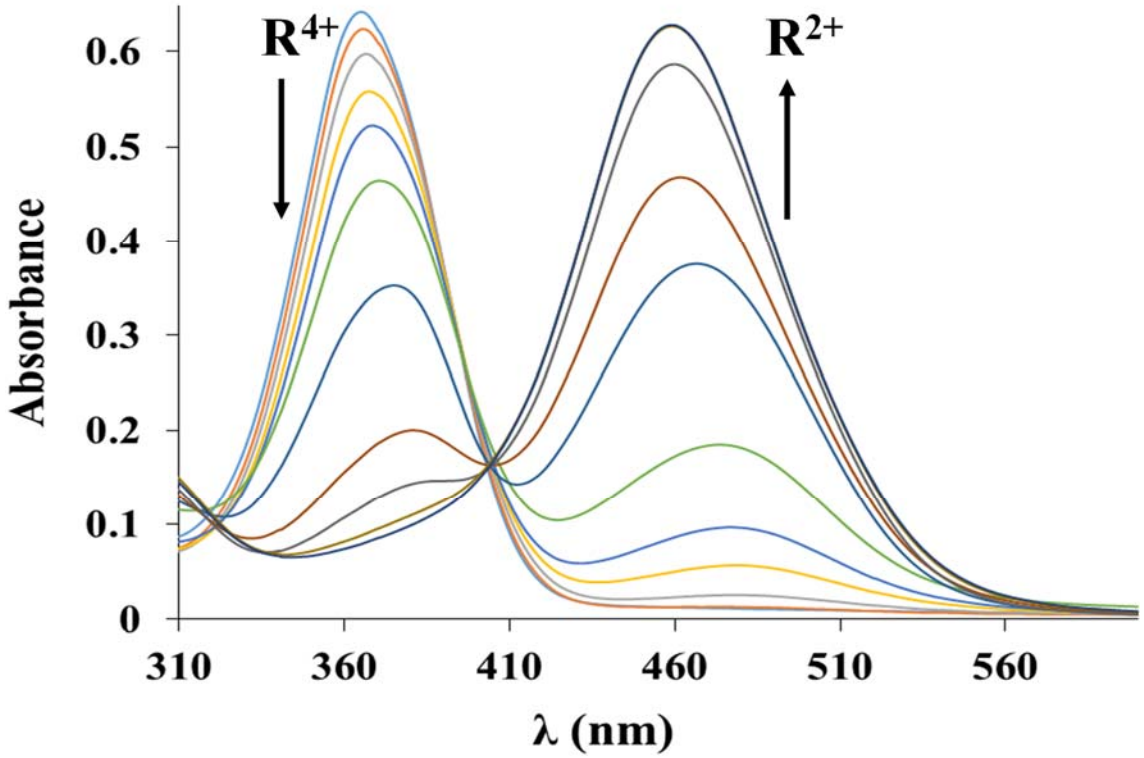

Figure S95. UV-Vis spectra for the titration of **R**·4Cl at 10 μM in NaH_2PO_4/Na_2HPO_4 and $NaHCO_3/Na_2CO_3$ buffer.

pH (measured)	V (mL) of solution A	V (mL) of solution B	V (mL) of solution C	V (mL) of solution D	ABS (464nm)	$\log[(A_{464}-A_{R4+})/(A_{R2+}-A_{464})]$
4.53 (**R^{4+}**)	2	-	-	-	0.0123	-
6.04	1.76	0.24	-	-	0.0131	-28.794
6.69	1.25	0.75	-	-	0.0240	-17.064
7.23	0.56	1.44	-	-	0.0525	-11.490
7.57	0.30	1.70	-	-	0.0903	-0.8312
7.98	0.12	1.88	-	-	0.1784	-0.4238
8.38	-	-	2	-	0.3748	0.1714
8.85	-	2	-	-	0.4667	0.4744
9.3	-	-	1.8	0.2	0.5808	11.715
10	-	-	1	1	0.6182	18.282
10.37 (**R^{2+}**)	-	-	0.4	1.6	0.6191	-

Solution A: 10 μM of R·4Cl and 0.05 M of NaH_2PO_4. Solution B: 10 μM of R·4Cl and 0.05 M of Na_2HPO_4. **Solution C:** 10 μM of R·4Cl and 0.05 M of $NaHCO_3$. Solution D: 10 μM of R·4Cl and 0.05 M of Na_2CO_3.

Table S9. Experimental data obtained for the UV.-Vis. titration of **R**·4Cl at 10 μM in NaH_2PO_4/Na_2HPO_4 and $NaHCO_3/Na_2CO_3$ buffer.

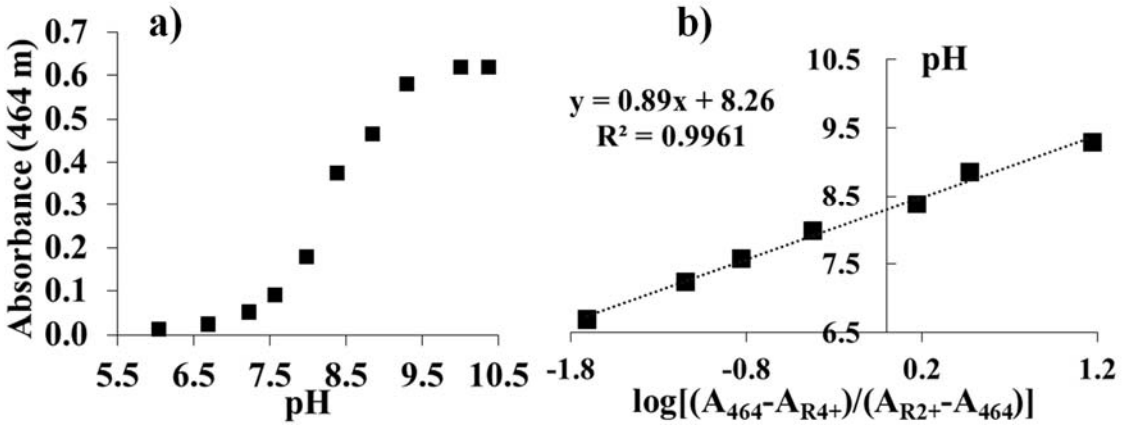

Figure S96. a) Absorption of $\mathbf{R^{2+}}$ at λ = 464 nm plotted against pH. b) Linear fitting of pH plotted against $\log[(A_{464}-A_{R4+})/(A_{R2+}-A_{464})]$, where p$K_a$ value is 8.26.

13. Spectroscopy study of L^{2+} and L^{+}.

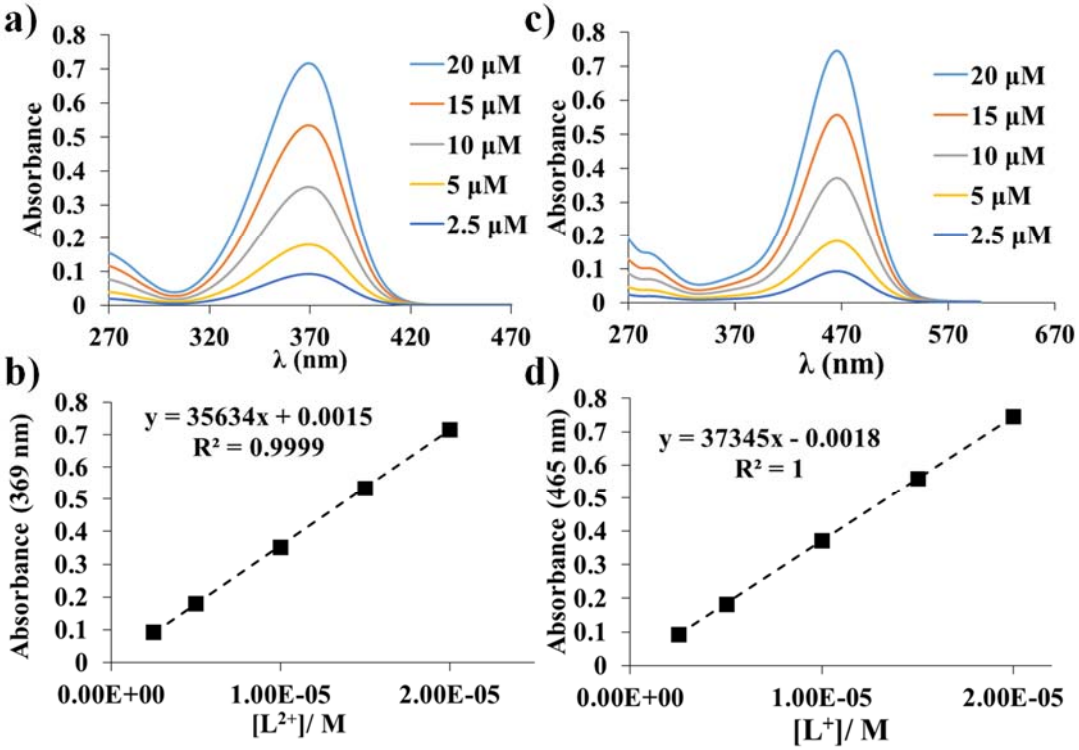

Figure S97. a) UV-Vis spectra of $\mathbf{L^{2+}}$ at pH 6 from 2.5 µM to 20 µM. b) Linear relationship between absorbance at 369 nm and concentration of $\mathbf{L^{2+}}$ where ε = 35634 $Lmol^{-1}cm^{-1}$. c) UV-Vis spectra of $\mathbf{L^{+}}$ at pH 10.3 from 2.5 µM to 20 µM. d) Linear relationship between absorbance at 465 nm and concentration of $\mathbf{L^{+}}$ where ε = 37345 $Lmol^{-1}cm^{-1}$.

14. pK_a determination for L^{2+} by UV-vis.

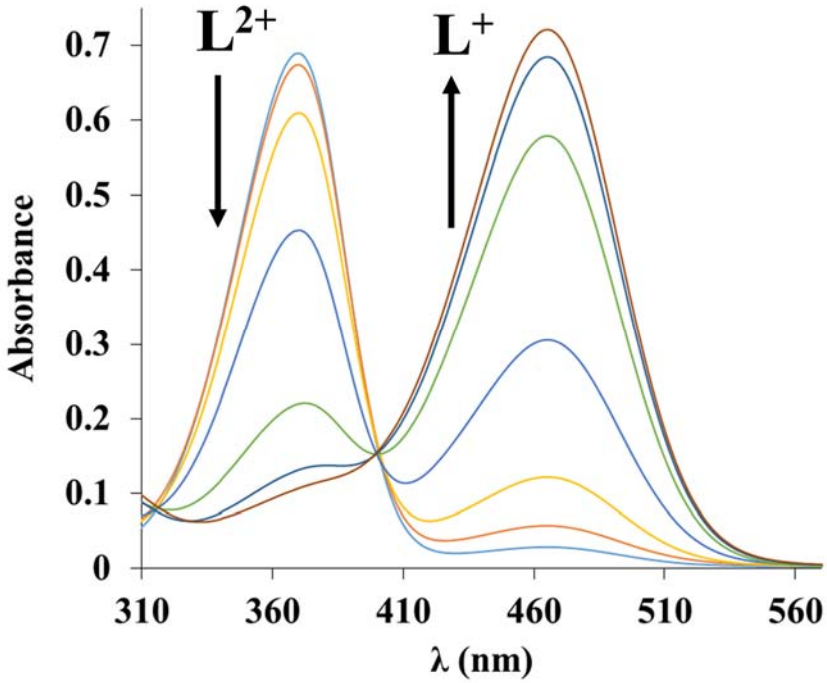

Figure S98. UV-Vis spectra for the titration of **L**·2Cl at 20 μM in NaH_2PO_4/Na_2HPO_4 and $NaHCO_3/Na_2CO_3$ buffer.

pH (measured)	V (mL) of solution A	V (mL) of solution B	V (mL) of solution C	V (mL) of solution D	ABS (464nm)	$\log[(A_{464}-A_{L2+})/(A_{L+}-A_{464})]$
7.45 (**L^{2+}**)	1.40	3.60	-	-	0.0289	-
7.83	0.75	4.25	-	-	0.0574	-1.367
8.26	0.30	4.70	-	-	0.1220	-0.8088
8.80	-	-	5	-	0.3059	-0.1757
9.49	-	-	4.5	0.5	0.5790	0.5881
10.03	-	-	3.5	1.5	0.6845	1.253
10.41 (**L^{+}**)	-	-	2.5	2.5	0.7211	-

Solution A: 20 μM of **L**·2Cl and 0.05 M of NaH_2PO_4. **Solution B:** 20 μM of **L**·2Cl and 0.05 M of Na_2HPO4. **Solution C:** 20 μM of **L**·2Cl and 0.05 M of $NaHCO_3$. **Solution D:** 20 μM of **L**·2Cl and 0.05 M of Na_2CO_3.

Table S10. Experimental data obtained for the UV.-Vis. titration of **L**·2Cl at 20 μM in NaH_2PO_4/Na_2HPO_4 and $NaHCO_3/Na_2CO_3$ buffer.

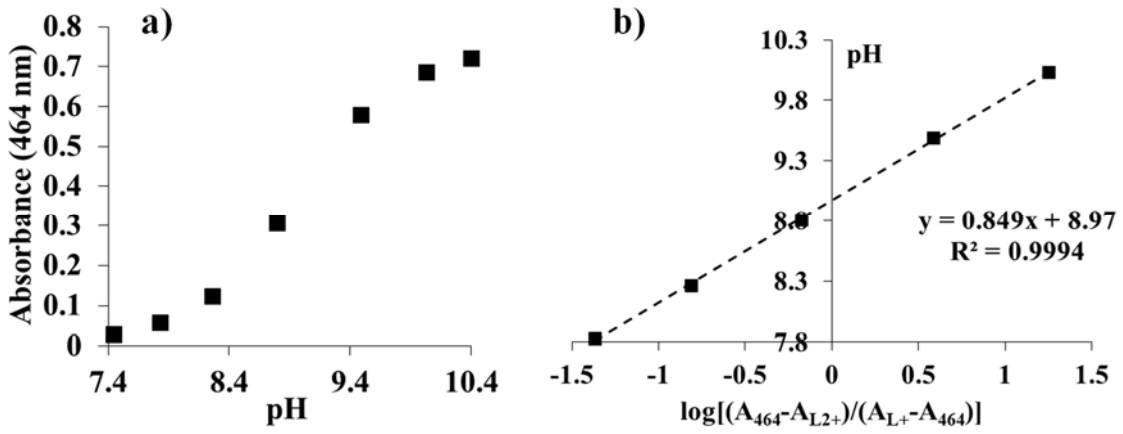

Figure S99. a) Absorption of **L⁺** at λ = 464 nm plotted against pH. b) Linear fitting of pH plotted against $\log[(A_{464}-A_{L2+})/(A_{L+}-A_{464})]$, where p$K_a$ value is 8.97.

15. pK_a determination of L^{2+} by potentiometric titration.

All solutions was prepared with CO_2 free water and ionic strength at 0.2 M with KCl. 10 mL of **L**·2Cl at 0.0082 M was titrated with 0.0402 M KOH solution under inert atmosphere (N_2). Fitting process was done with Hyperquad program.

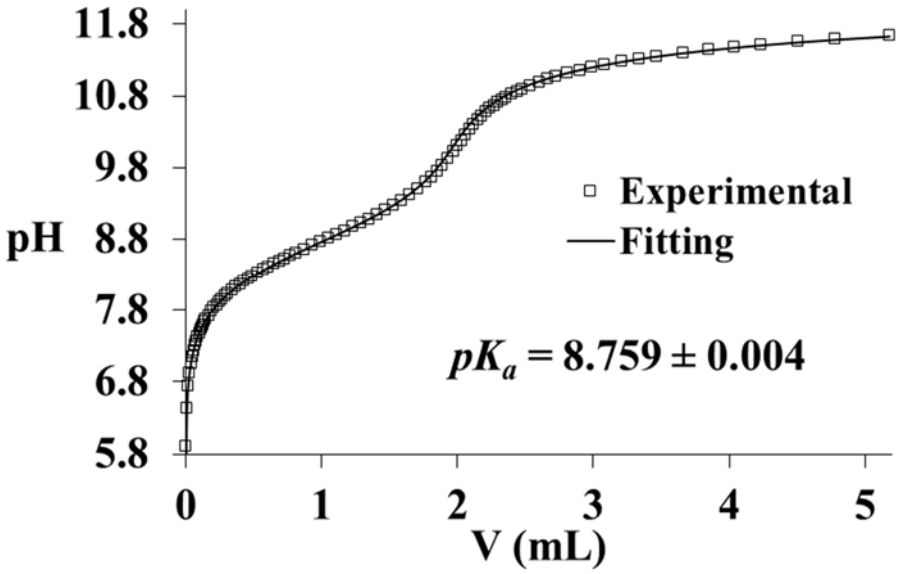

Figure S100. Potentiometric titration curve of **L**·2Cl with KOH.

Volume of KOH (mL)	pH	Residual
0	5.9127	0.4837
0.01	6.4244	-0.0435
0.02	6.7339	-0.0346
0.03	6.9185	-0.0276
0.04	7.0500	-0.0232
0.05	7.1540	-0.0182
0.06	7.2354	-0.0182
0.07	7.3095	-0.0133
0.08	7.3697	-0.0135
0.09	7.4252	-0.0113
0.1	7.4731	-0.0114
0.11	7.5195	-0.0087
0.12	7.5604	-0.0079
0.13	7.5983	-0.0071
0.14	7.6340	-0.0060
0.15	7.6663	-0.0059
0.17	7.7271	-0.0043
0.19	7.7826	-0.0017
0.21	7.8309	-0.0018
0.23	7.8760	-0.0011
0.25	7.9182	-0.0001
0.27	7.9575	0.0005
0.29	7.9954	0.0023
0.31	8.0293	0.0022
0.34	8.0778	0.0028
0.37	8.1233	0.0035
0.4	8.1657	0.0040
0.43	8.2069	0.0055
0.46	8.2451	0.0059
0.49	8.2814	0.0062
0.53	8.3275	0.0065
0.57	8.3714	0.0067
0.61	8.4139	0.0073
0.65	8.4548	0.0078
0.69	8.4932	0.0072
0.73	8.5308	0.0067
0.77	8.5689	0.0076
0.81	8.6049	0.0072
0.87	8.6584	0.0070
0.93	8.7115	0.0073
0.99	8.7628	0.0060
1.05	8.8146	0.0058
1.11	8.8674	0.0057
1.17	8.9190	0.0040
1.23	8.9721	0.0027
1.29	9.0274	0.0021

Volume of KOH (mL)	pH	Residual
1.35	9.0845	0.0010
1.41	9.1437	-0.0006
1.47	9.2053	-0.0032
1.53	9.2710	-0.0064
1.59	9.3415	-0.0104
1.65	9.4190	-0.0149
1.71	9.5042	-0.0215
1.77	9.5994	-0.0307
1.81	9.6699	-0.0387
1.85	9.7471	-0.0485
1.89	9.8323	-0.0591
1.93	9.9236	-0.0717
1.97	10.0228	-0.0815
2	10.1000	-0.0859
2.03	10.1781	-0.0867
2.06	10.2544	-0.0847
2.09	10.3286	-0.0791
2.12	10.3964	-0.0740
2.15	10.4611	-0.0663
2.18	10.5194	-0.0598
2.21	10.5734	-0.0531
2.24	10.6222	-0.0473
2.27	10.6668	-0.0425
2.3	10.7092	-0.0367
2.33	10.7459	-0.0340
2.36	10.7807	-0.0307
2.4	10.8246	-0.0256
2.44	10.8634	-0.0224
2.48	10.8985	-0.0202
2.54	10.9482	-0.0151
2.6	10.9922	-0.0118
2.66	11.0313	-0.0095
2.72	11.0673	-0.0072
2.81	11.1152	-0.0050
2.9	11.1585	-0.0025
2.99	11.1958	-0.0022
3.08	11.2312	-0.0004
3.21	11.2757	0.0004
3.34	11.3173	0.0029
3.47	11.3536	0.0041
3.66	11.4006	0.0053
3.85	11.4412	0.0056
4.04	11.4784	0.0070
4.23	11.5111	0.0072
4.505	11.5547	0.0093
4.78	11.5911	0.0089
5.18	11.6384	0.0100

Table S11. Experimental data for the titration.

16. Determination of the energy of the rotational barrier ($\Delta G^{\neq}$).

The coalescence temperature (T_c) could be estimated for different protons on VT NMR experiments. This provides, in association with the maximum peak separation ($\Delta\nu$ in Hz) at slow exchange between **c – c'** and **d – d'**, the energy of the rotational barrier using Equation (1).[S3]

$$\Delta G^{\neq} = 4.57 \cdot 10^{-3} T_c (9.972 + \log T_c/\Delta\nu) \quad (1)$$

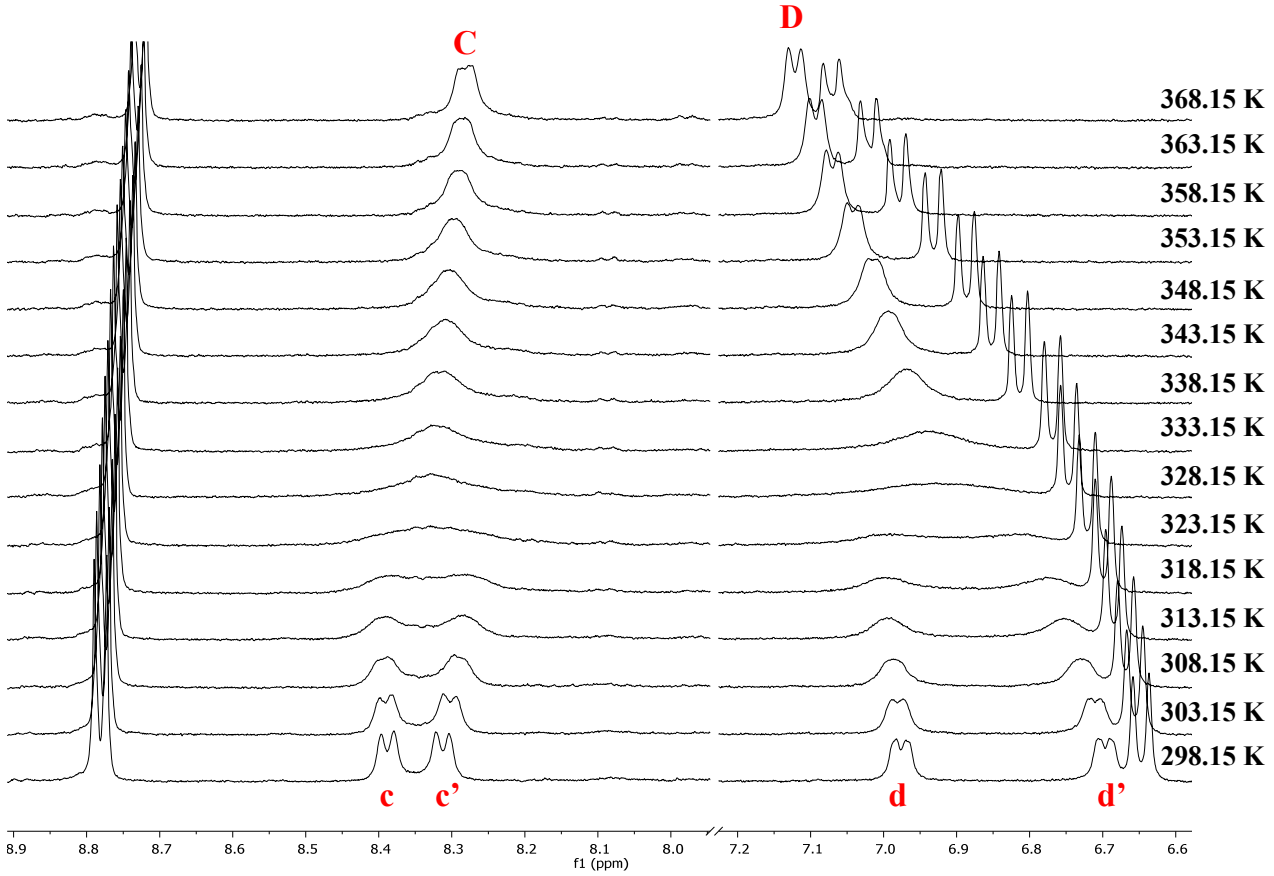

Figure S101. VT ^{1}H NMR (500 MHz, D_2O) stacked spectra for $\mathbf{R}^{4+}\subset$.2,7-DHN.

Signal	$\Delta\nu_c$ (Hz)	T_c (K)	$\Delta G^{\neq}$ (kcal mol^{-1})
c – c'	31.08	323.15	16.23
d – d'	111.83	333.15	16

Table S12. Experimental data obtained for the calculation of $\Delta G^{\neq}$ via coalescence temperatures of various signals on the VT ^{1}H NMR of **R**·4Cl⊂.2,7-DHN in water.

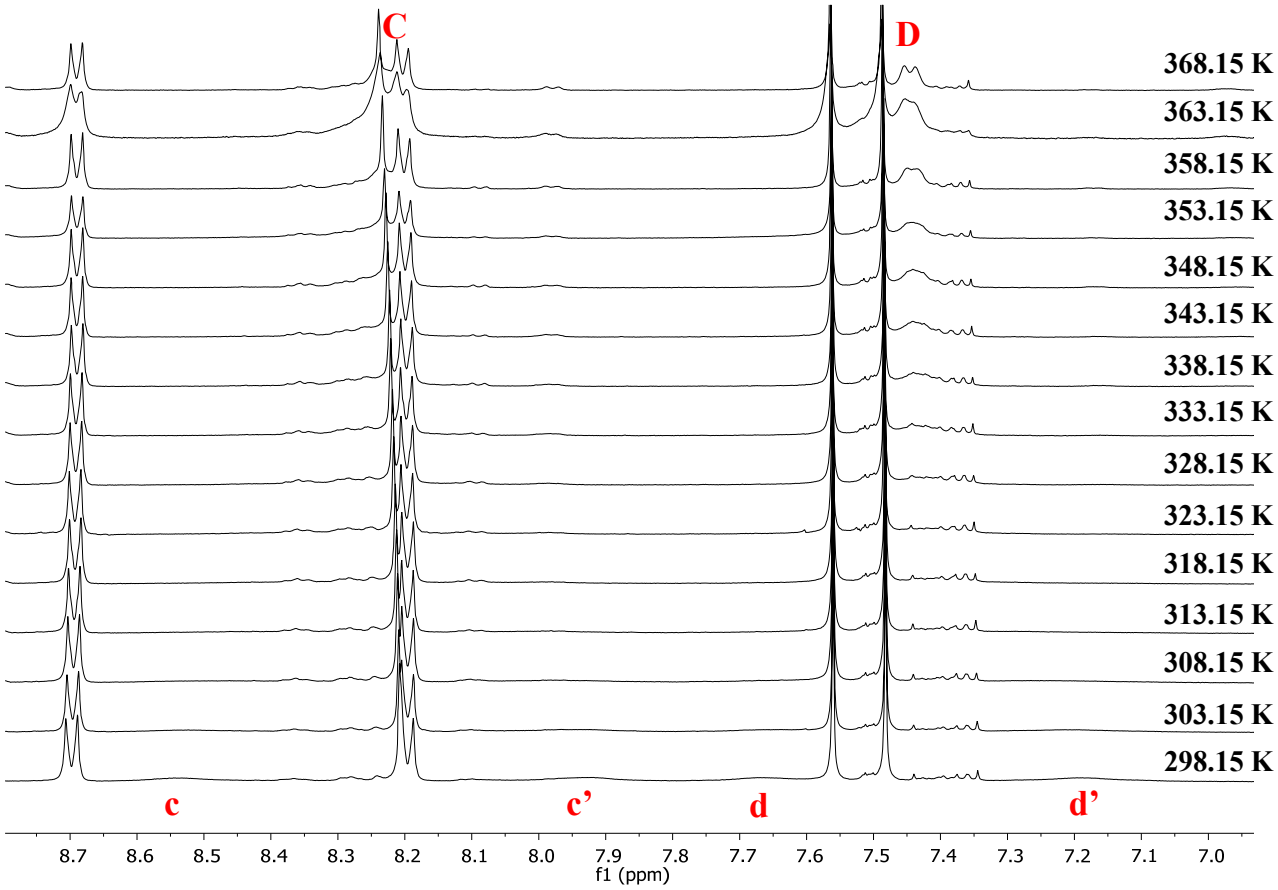

Figure S102. VT ^{1}H NMR (500 MHz, D_2O) stacked spectra for **R**$^{4+}$.

Signal	$\Delta\nu_c$ (Hz)	T_c (K)	$\Delta G^{\neq}$ (kcal mol^{-1})
c – c'	212	333.15	15.5
d – d'	250	333.15	15.4

Table S13. Experimental data obtained for the calculation of $\Delta G^{\neq}$ via coalescence temperatures of various signals on the VT ^{1}H NMR of **R**$^{4+}$ in water.

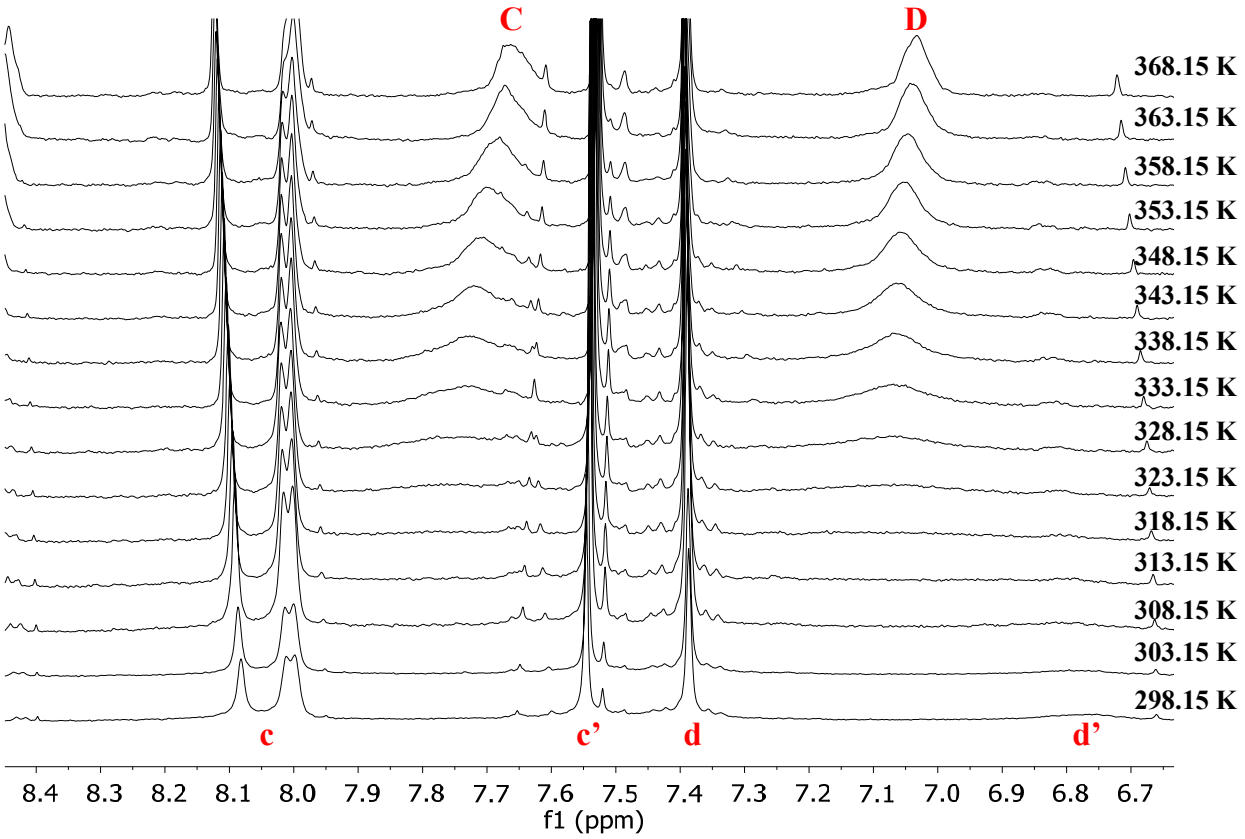

Figure S103. VT ^{1}H NMR (500 MHz, D_2O) stacked spectra for **R**$^{2+}$.

Signal	$\Delta\nu_c$ (Hz)	T_c (K)	$\Delta G^{\neq}$ (kcal mol^{-1})
c – c'	243	328.15	15.2
d – d'	190	333.15	15.5

Table S14. Experimental data obtained for the calculation of $\Delta G^{\neq}$ via coalescence temperatures of various signals on the VT ^{1}H NMR of **R**$^{2+}$ in water.

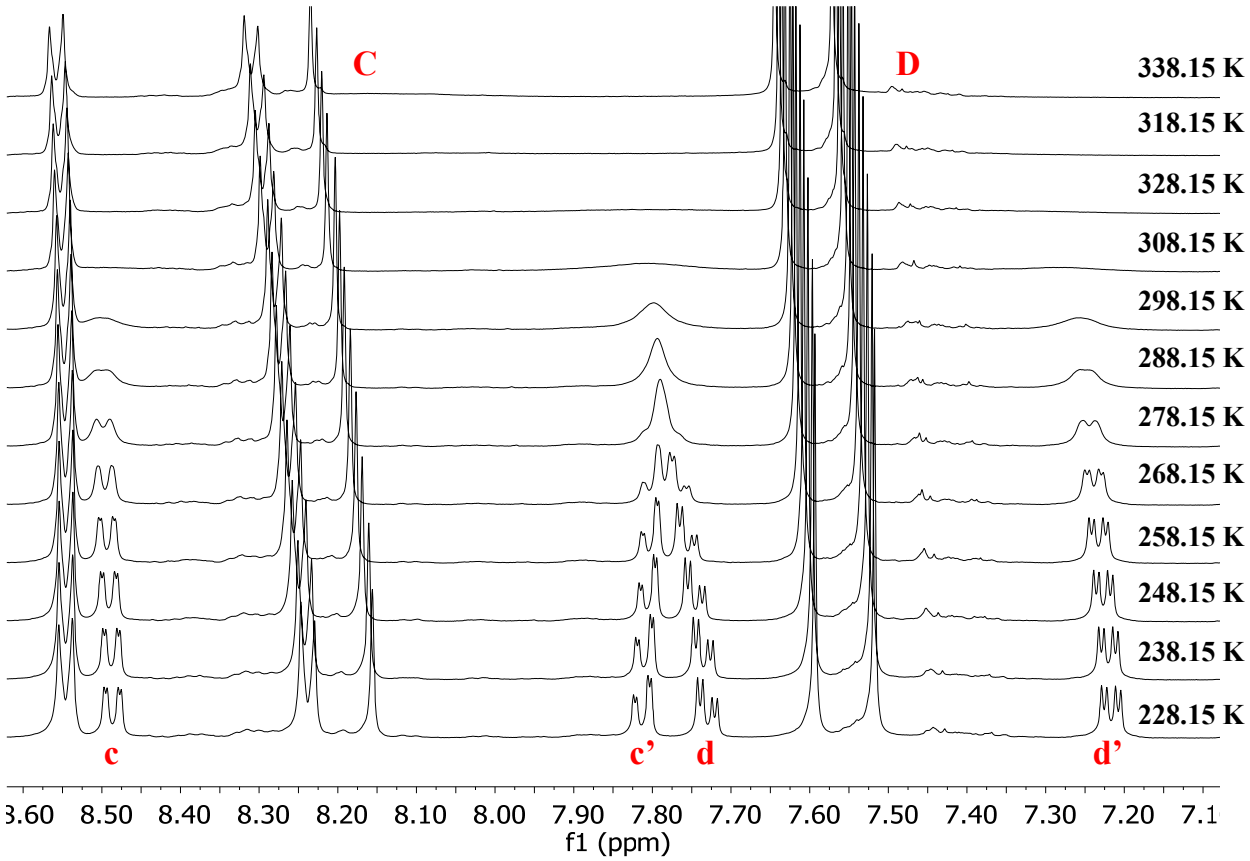

Figure S104. VT ^{1}H NMR (500 MHz, CD_3CN) stacked spectra of **R**$^{4+}$.

Signal	$\Delta\nu_c$ (Hz)	T_c (K)	$\Delta G^{\neq}$ (kcal mol^{-1})
c – c'	270	328.15	15.1
d – d'	205	328.15	15.3

Table S15. Experimental data obtained for the calculation of $\Delta G^{\neq}$ via coalescence temperatures of various signals on the VT ^{1}H NMR of **R**$^{4+}$ in CD_3CN.

17. Kinetic stability of R^{4+}.

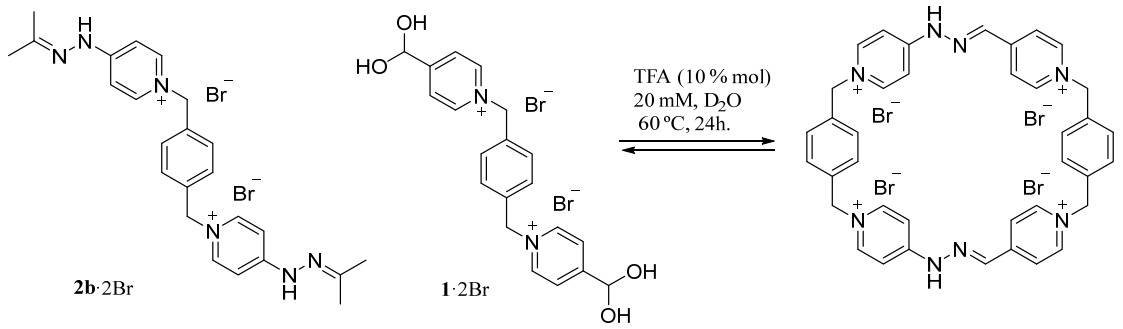

A solution of **1**·2Br (20 mM) and **2b**·2Br (20 mM) with a catalytic amount of TFA-d (10% molar) in D_2O were heated at 60 ºC over 18 h. After this time, $\mathbf{R}^{4+}$ was the main species in solution (**Figure S105b**). On this solution, an excess of 1,5-DHN$_c$ was added, and the concomitant formation of $\mathbf{R}^{4+}\subset$1,5-DHN$_c$ could be observed (**Figure S105c**).

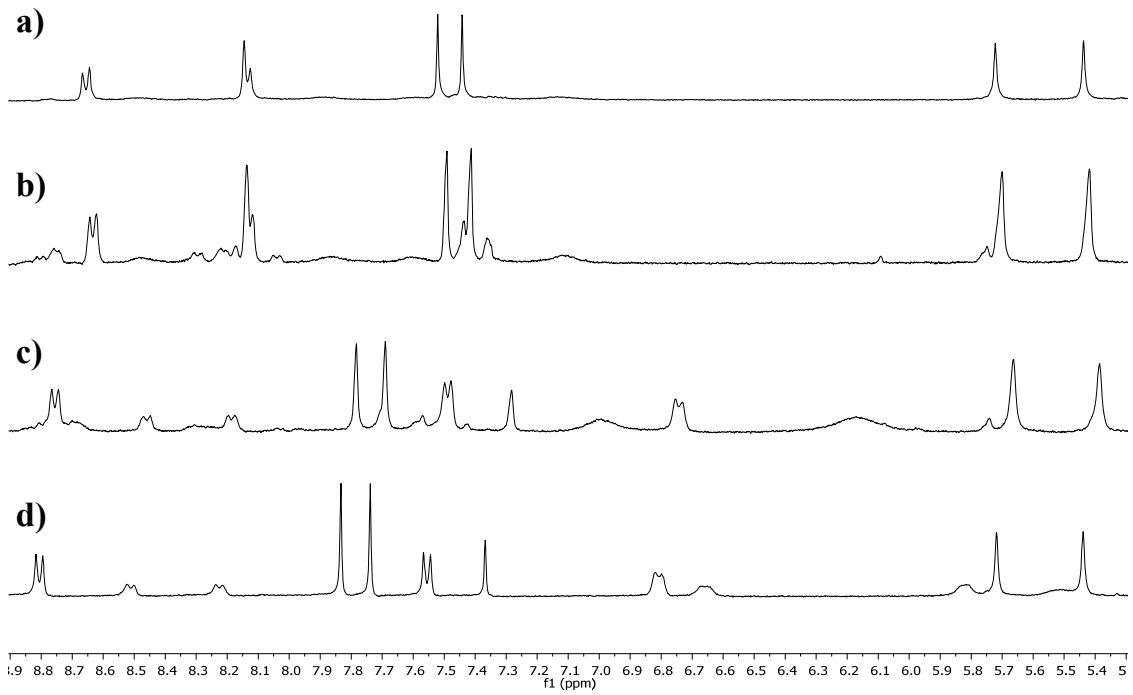

Figure S105. ^{1}H NMR (300 MHz, D_2O) of: a) $\mathbf{R}^{4+}$ self-assembled at 1.5 mM, b) $\mathbf{R}^{4+}$ self-assembled at 20 mM, c) inclusion complex of $\mathbf{R}^{4+}\subset$1,5-DHNc at 20 mM, d) inclusion complex of $\mathbf{R}^{4+}\subset$1,5-DHNc at 1.5 mM.

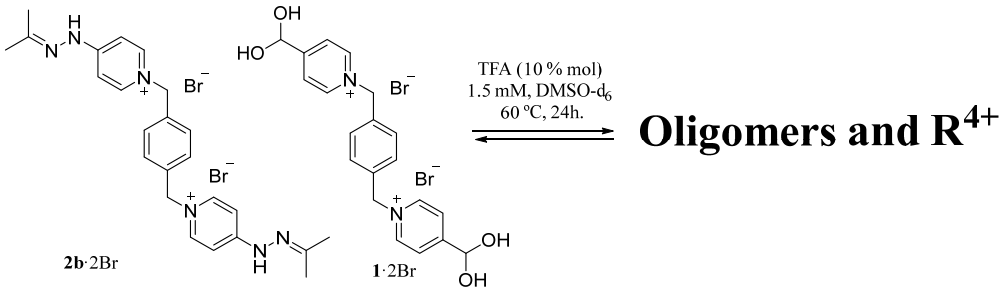

An equimolar solution of **1**·2Br (1.5 mM) and **2b**·2Br (1.5 mM) with a catalytic amount of TFA-d (10% molar) in DMSO-d_6 were heated at 60 ºC over 24 h. After this time, a mixture of oligomers and $\mathbf{R^{4+}}$ were observed in solution (**Figure S106b**).

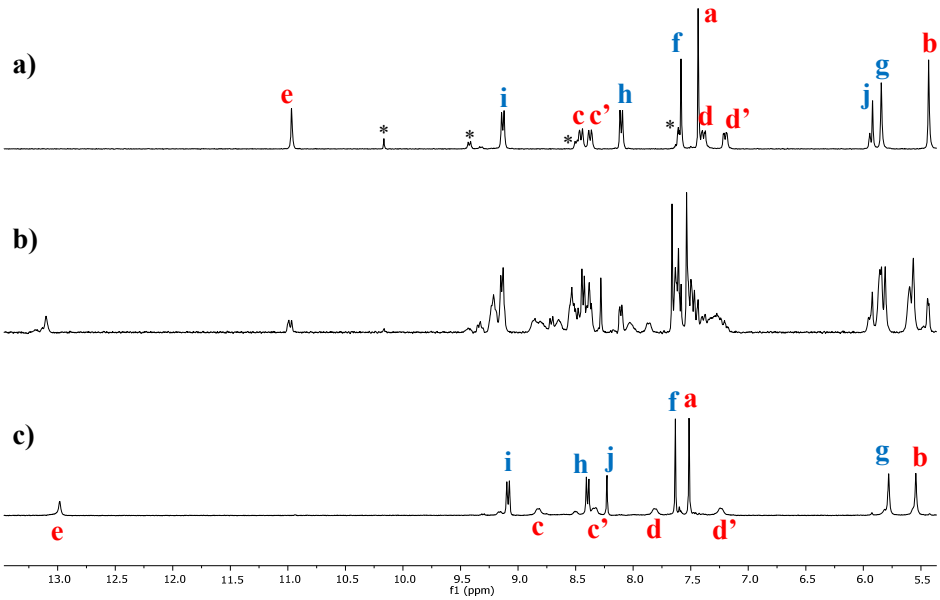

Figure S106. ^{1}H NMR (300 MHz, DMSO-d_6) of: a) equimolar mixture of **1**·2Br and **2b**·2Br at t = 0 min., b) mixture a) after 24 h heating at 60 ºC, c) solution of **R**·4Cl.

The solution of oligomeric species and $\mathbf{R^{4+}}$ in DMSO-d_6 was concentrated and redissolved in D_2O at 1.5 mM with a catalytic amount of TFA-d (10 % molar), and heated at 60 ºC over 24 h (**Figure S107a**). No changes on the NMR signals were observed after 11 days (**Figure S107b**).

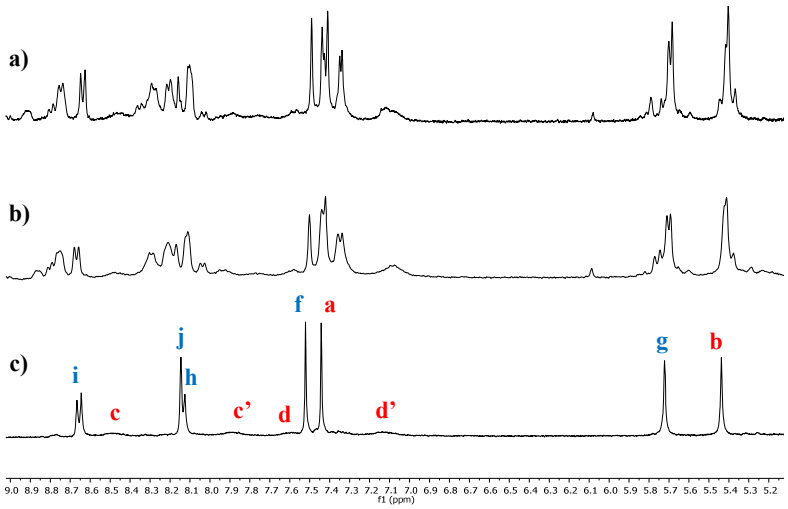

Figure S107. ^{1}H NMR (300 MHz, D_2O) of: a) $\mathbf{R^{4+}}$ after 24 h heating at 60 ºC, b) mixture a) after 11 days heating at 60 ºC, c) solution of **R**·4Cl.

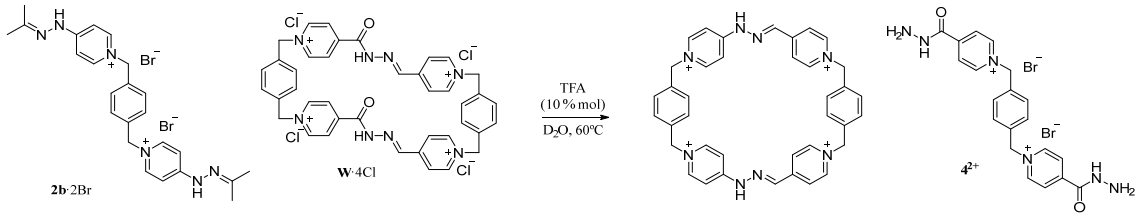

An equimolar solution of **2b**·2Br (1.5 mM) and **W**·4Cl was heated at 60 ºC with a catalytic amount of TFA-d in D_2O for 24 h.

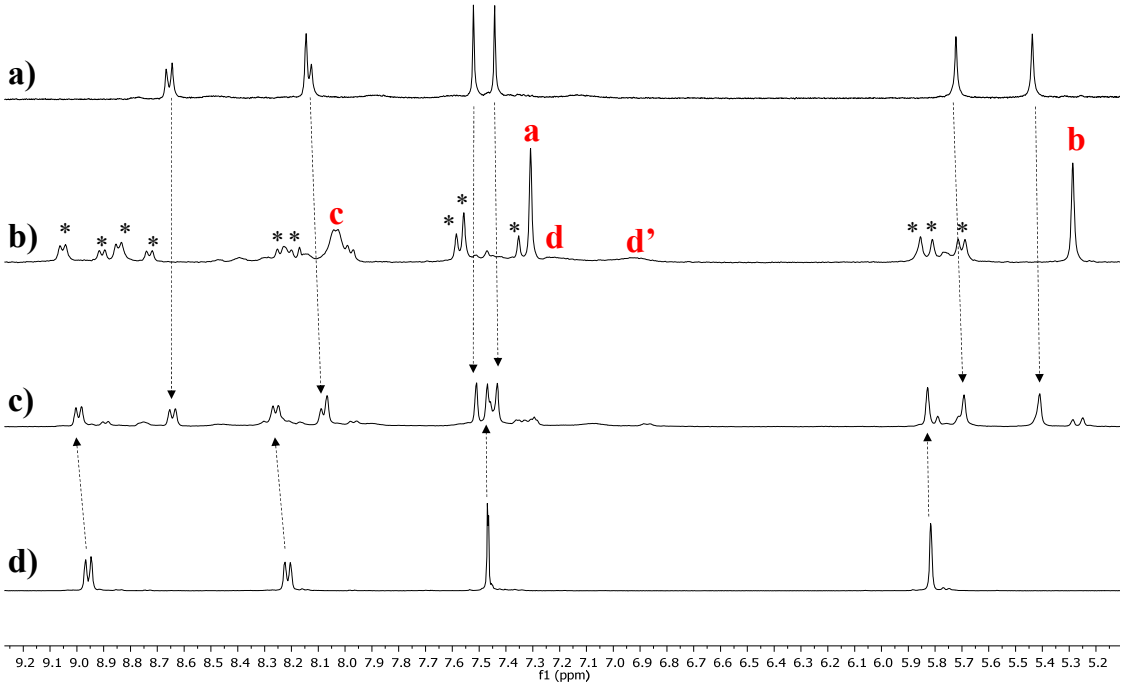

Figure S108. ^{1}H NMR (300 MHz, D_2O) of : a) solution of **R**·4Cl, b) equimolar mixture of **W**·4Cl and **2b**·2Br at t = 0 min, c) mixture b) after 24 h heating at 60 ºC, d) solution of **4**$^{2+}$.

18. Computational Methods

Exhaustive conformational searchers and simulated annealing molecular dynamics for the inclusion complexes where performed with the GFN-xTB method (Geometry, Frequency, Non-covalent, eXtended Tight-Binding), a semiempirical method developed by Grimme *et al.*[S4] The energetics for the bond rotation where preliminary screened at the PM6 semiempirical level and later refined with DFT. DFT calculations were performed with the M06-2X functional embedded in a continuum of water and acetonitrile with the SMD procedure and with the 6-31g(d,p) and 6-31+g(d,p) basis sets. This methodology was selected as it reproduced well the Raman and UV-vis spectra of a related system.[S5] All minima molecular geometries were optimized inside water/acetonitrile and checked by the computation of the Hessian. All DFT and PM6 calculations were performed by Gaussian 09.[S6] The Jmol software was used extensively to prepare the figures and analyze graphically the results.[S7] Cartesian coordinates for all molecules are available on request.

18.1. Tautomers

We computed different possible tautomers for **L**$^{2+}$ with and without an explicit water molecule embedded in a continuum of water.

	L^{2+}	**L**$^{2+}$ with 1 water molecula
Tautomers	E / Kcal/mol	E / Kcal/mol
N(P2)-H	54.8	50.4
N(P1)-H	47.6	44.4
LN2-H	17.6	16.6
LN1-H (Min.)	0.0	0.0

Table S16. DFT energy differences for **L**$^{2+}$ the four different tautomers in a water continuum with and without an extra water molecule.

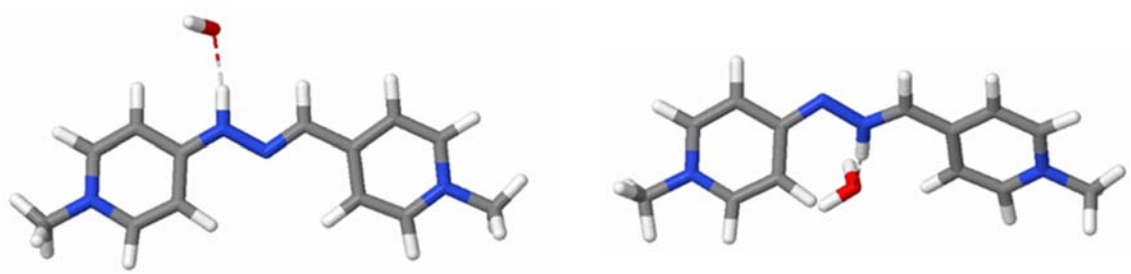

Figure S109. **L**$^{2+}$ possible tautomers modelled with a single water molecule in a water continuum, LN1-H (left) and LN2-H (right).

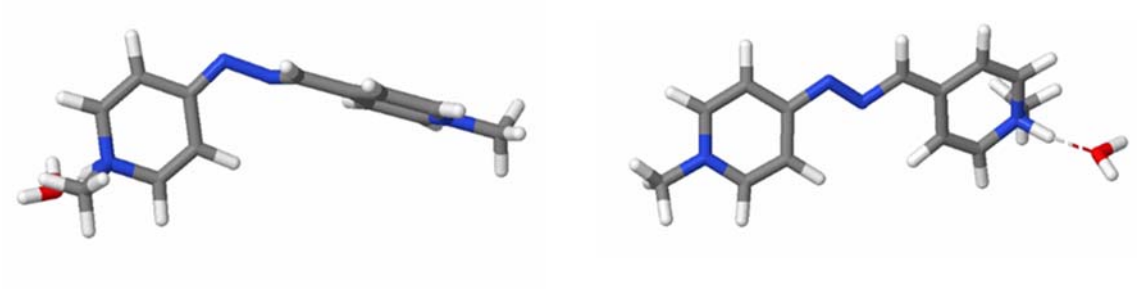

Figure S110. $\mathbf{L}^{2+}$ possible tautomers modelled with a single water molecule in a water continuum, N(P1)-H bent conformation (left) and N(P2)-H (right).

A similar trend was obtained for both models, so for simplicity, the calculations for $\mathbf{R}^{4+}$ and $\mathbf{R}^{3+}$ were performed with the simplest model confirming the same trend: for $\mathbf{R}^{4+}$, $\mathbf{R}^{3+}$ and $\mathbf{L}^{2+}$ only the LN1-H tautomer is thermodynamically populated at room temperature. This was also checked by simulations of the UV-Vis spectra, which showed other tautomers would show different spectral maxima (not shown here).

	$\mathbf{R}^{4+}$	$\mathbf{R}^{4+}$		$\mathbf{R}^{3+}$	$\mathbf{L}^{2+}$
Tautomers	E(rel) / Kcal/mol	E(rel) / Kcal/mol /2	Tautomers	E(rel) / Kcal/mol	E(rel) / Kcal/mol
N(P2)-H N(P2)-H	124.0	62.0	N(P2)-H	55.0	54.8
N(P2)-H N(P1)-H	105.8				
N(P1)-H N(P1)-H	97.1	48.5	N(P1)-H	52.2	47.6
LN2-H LN2-H	46.2	23.1			
LN1-H LN2-H	24.0		LN2-H	17.8	17.6
LN1-H LN1-H (Min.)	0.1		LN1-H (Min.)	0.0	0.0

Table S17. DFT energy differences in water for the different tautomers of $\mathbf{R}^{4+}$, $\mathbf{R}^{3+}$ and $\mathbf{L}^{2+}$.

18.2. Conformational freedom

We screened the activation energy for the rotation of different bonds in the $\mathbf{R}^{4+}$ at the PM6 level. At this level of calculation, the four bonds involving a C*sp*^{3} atom (corner C atoms of the box framework) are rotatable, so the benzene rings are rotating at room temperature with low activation energies, which fits the NMR observations discussed on the manuscript.

There are other four rotatable bonds in the macrocycle, that, for simplicity were explored with the $\mathbf{L}^{2+}$ model molecule. These were initially computed at the PM6 level, and then recomputed at the M06-2X-6-31g(d,p) level. First, the C=N bond barrier was found to be too stiff (with an activation energy > 40 Kcal/mol at the PM6 level). The other three bonds showed two high barriers (~ 14 Kcal/mol) and a low barrier of ~ 7 Kcal/mol at the DFT level.

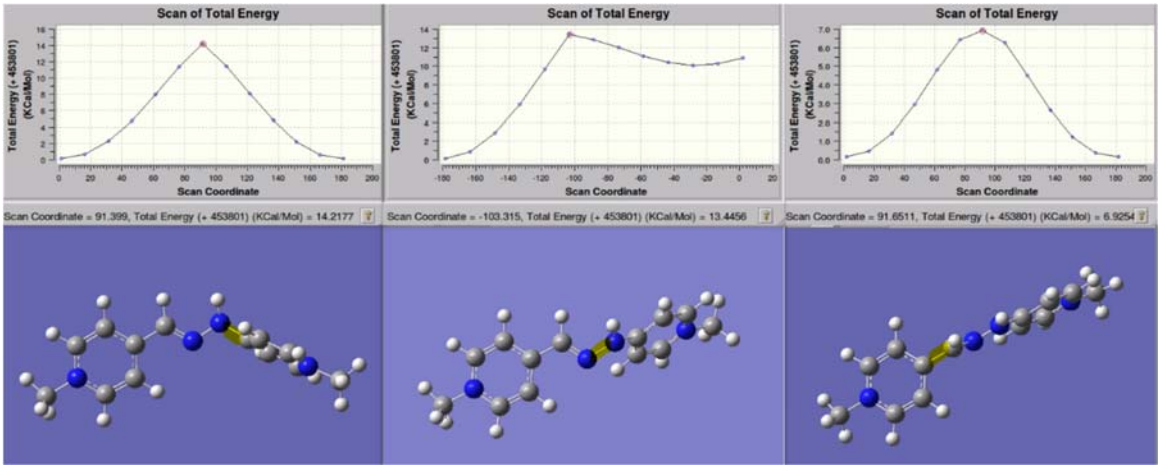

Figure S111. Inflexion point geometries and activation energies for bond rotations for $\mathbf{L}^{2+}$ at the M06-2X-6-31g(d,p) level. Rotating bonds are marked in yellow.

These energies suggest a hindered rotation of the P1 pyridinium ring as observed experimentally. Also, the value obtained by the calculations, 14 Kcal/mol, matches the value estimated experimentally, 15.2 Kcal/mol.

18.3. Conformer exploration

In order to explore the possible minima of the empty macrocycles, we performed a conformation search with the **C**onformer–**R**otamer **E**nsemble **S**ampling **T**ool (**CREST**) software based on the xtb-GFN2 Hamiltonian (see methods) with an implicit water model.

That procedure yielded 6 and 39 distinct conformers for $\mathbf{R}^{4+}$ for $\mathbf{R}^{2+}$, which were reduced to 4 and 14 unique conformers respectively after minimization at the M06-2x-6-31g(d,p) level in water.

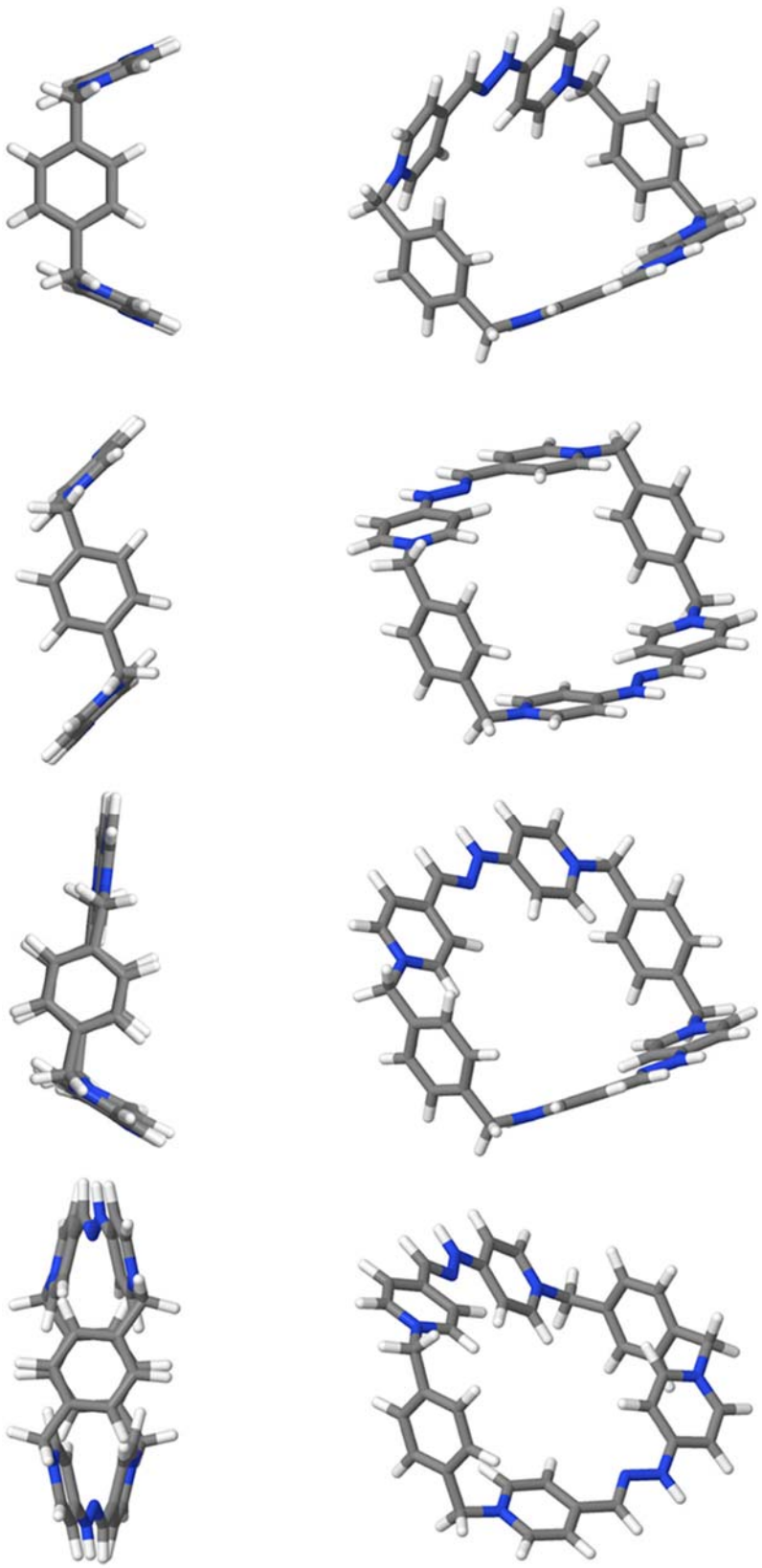

Figure S112. Distinctive low energy **R**$^{4+}$ conformations in water, in order of decreasing stability from top to bottom: ‘C’, ‘Z’, ‘L’, ‘X’.

The ‘C’ and ‘Z’ conformations of the macrocycle are thermodynamically nearly degenerate and populate the ground state of the molecule. The ‘L’ and ‘X’ conformations are higher in energy but might be accessible at room

temperature. The low energy conformers of $\mathbf{R}^{2+}$ show five conformations that resemble the 'C', 'Z', and 'X' of the conjugate acid.

	$\mathbf{R}^{4+}$ 6-31g(d,p) E(rel) / kcal/mol	$\mathbf{R}^{4+}$ 6-31+g(d,p) E(rel) / kcal/mol	$\mathbf{R}^{2+}$ 6-31g(d,p) E(rel) / kcal/mol	$\mathbf{R}^{2+}$ 6-31+g(d,p) E(rel) / kcal/mol	
			22.3	22.9	
			22.2	22.9	
			17.6	18.6	
			13.6	14.1	
			10.8	11.1	
			10.4	10.6	
			10.4	10.6	
			8.7	9.1	
Conformation			8.7	9.1	Conformation
			4.5	4.8	X'
X	4.8	5.1	4.4	4.7	X
L	2.8	3.0	**0.4**	**0.3**	Z'
Z	**0.1**	**0.2**	**0.3**	**0.2**	Z
C	**0.0**	**0.0**	**0.0**	**0.0**	C

Table S18. DFT energy differences in water for the different conformations of $\mathbf{R}^{4+}$ and $\mathbf{R}^{2+}$ with two basis sets.

18.4. pKa estimations from DFT

The ab-initio energies in water of $\mathbf{R}^{4+}$, $\mathbf{R}^{3+}$, $\mathbf{R}^{2+}$ and $\mathbf{L}^{2+}$ and $\mathbf{L}^{+}$ together with the free energy of solvation of the proton [http://mercuryconsortium.org/furman/pubs/AlongiS2010.pdf] were used to estimate the pK_a for $\mathbf{R}^{4+}$, $\mathbf{L}^{2+}$ and $\mathbf{R}^{3+}$. The computed pK_a value for $\mathbf{L}^{2+}$ was 7.8, which compares well to the value of 7.5 obtained using an enhanced model that adds an explicit water molecule embedded in the continuum model. The computed value for $\mathbf{R}^{4+}$ for one and two deprotonations, yielding $\mathbf{R}^{3+}$ and $\mathbf{R}^{2+}$ respectively, 7.4 and 7.5, are very similar and similar to the value obtained for $\mathbf{L}^{2+}$ (7.8).

18.5. UV-VIS Spectra simulation

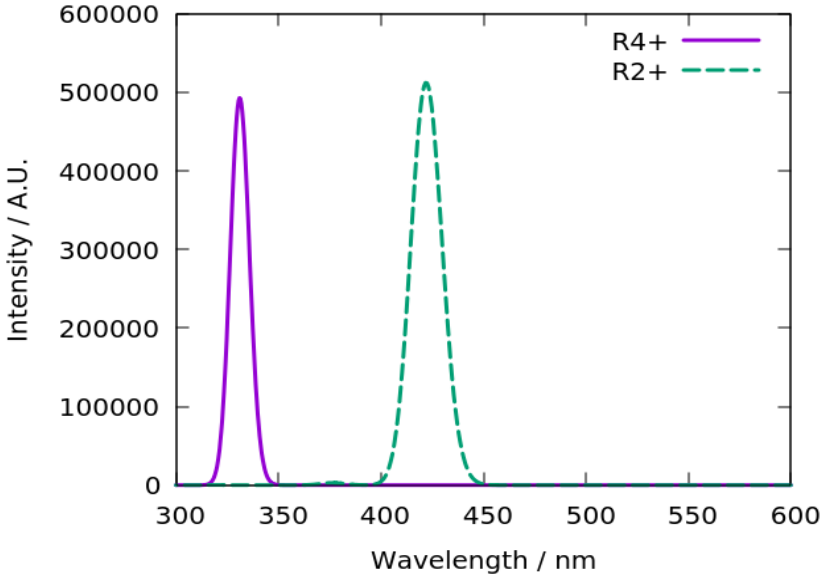

Figure S113. TD-DFT simulated spectrum.

TD-DFT	Wavelength / nm	Osc. Strength / (A.U.)	Experiment / nm
R^{4+}	331	2.27	366
R^{2+}	422	2.36	464
L^{2+}	333	1.16	369
L^{1+}	428	1.19	465

Table S19. TD-DFT first transitions in water for **R**$^{4+}$, **R**$^{2+}$, **L**$^{2+}$ and **L**$^{+}$.

The transitions are very similar between the model compound (**L**$^{2+}$) and the macrocycles, in both cases correspond to transitions between the HOMO and the LUMO orbitals, that in **R**$^{4+}$ and **R**$^{2+}$ are doubly degenerate. In fact, the difference in the optical gap follows the trend in HOMO/LUMO gap for the acid and the basic system for the macrocycle and the model compound, which are also reduced upon deprotonation.

The computed intensities for **R**$^{4+}$ and **R**$^{3+}$ are very similar and roughly double of the intensities for **L**$^{2+}$ and **L**$^{+}$, as it would be expected since the **L**$^{2+}$ moieties are chemically decoupled from the benzene rings by the C*sp*^{3} corner atoms, confirming that that **L**$^{2+}$/**L**$^{+}$ are adequate simplified models to study **R**$^{4+}$/**R**$^{2+}$.

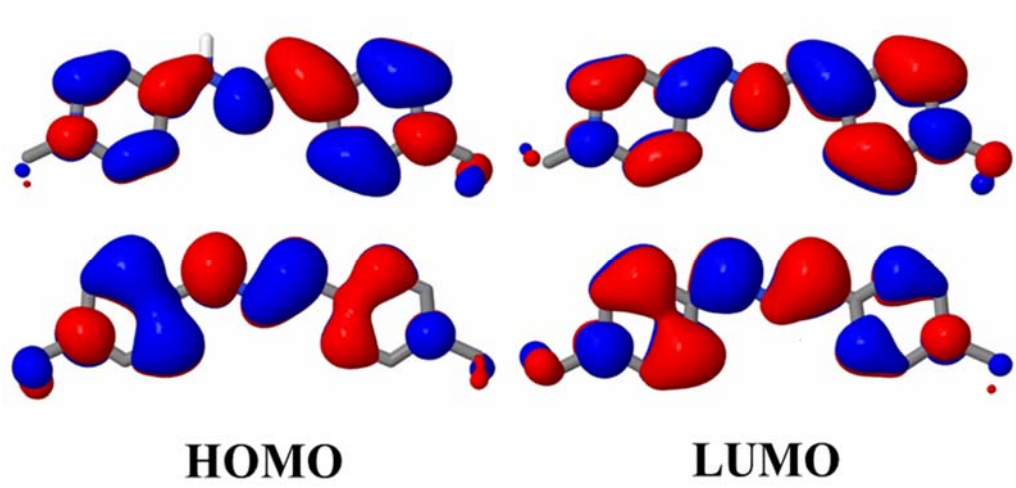

Figure S114. Frontier orbitals of $\mathbf{L}^{2+}$ (left) and $\mathbf{L}^{+}$ (right).

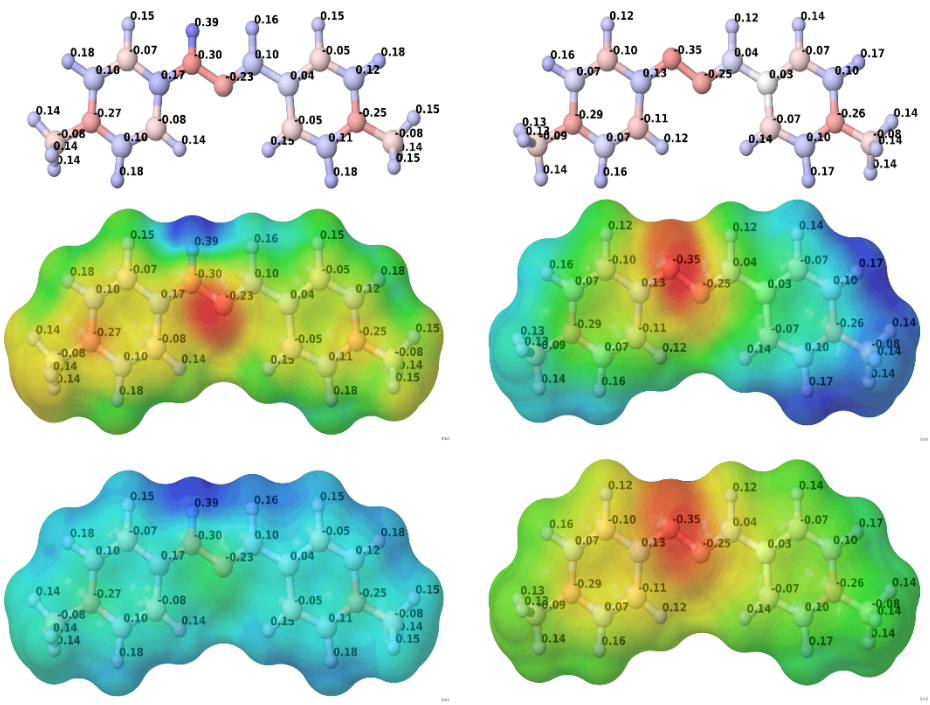

Figure S115. Top: partial DFT charges (Charge Model 5, CM5) in water, $\mathbf{L}^{2+}$ (left) and $\mathbf{L}^{+}$ (right). Middle: Color-coded electrostatic potential on the solvent-accessible-surface of $\mathbf{L}^{2+}$ (left, colored from 0.35 eV to 0.59 eV), and $\mathbf{L}^{+}$ (right, colored from -0.03 eV to 0.34 eV). Bottom: electrostatic field on the solvent accessible surface of $\mathbf{L}^{2+}$ (left) and $\mathbf{L}^{+}$ (right) colored both from -0.05 eV to 0.6 eV).

18.6. Inclusion Complexes

We computed the complexes of 1,5-DHN and pyrene with $\mathbf{R}^{4+}$ and $\mathbf{R}^{2+}$ in water with different procedures and compared the results. The lowest energy complexes were obtained from simulated annealing molecular dynamics at 400 K inside a water continuum for 0.5 ns at the xtb-GFN2 level for $\mathbf{R}^{4+}$ and reoptimized at the DFT level. For $\mathbf{R}^{2+}$, the $\mathbf{R}^{4+}$ geometry was deprotonated and reoptimized at the DFT level. For the geometries in acetonitrile, the water $\mathbf{R}^{4+}$ geometry was used as a reference, after a xtb-GFN2 procedure in acetonitrile yielded comparable results to water.

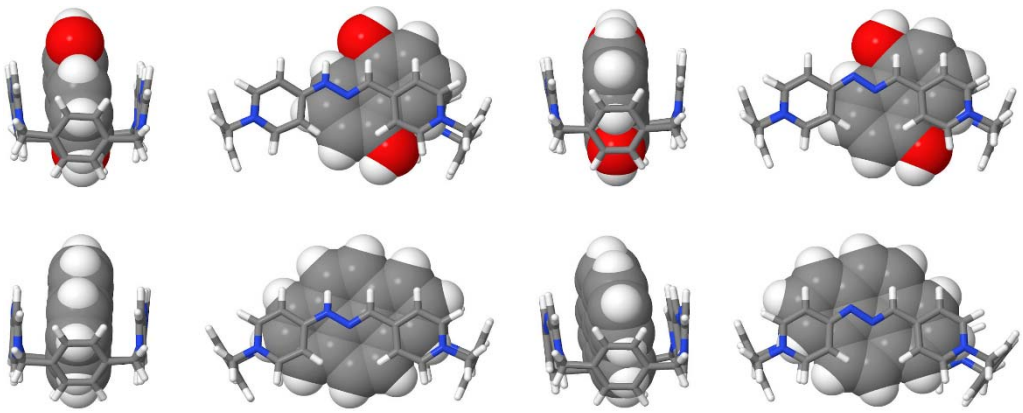

Figure S116. Inclusion complexes with 1,5-DHN (top) and pyrene (bottom) for **R**$^{4+}$ (left) and **R**$^{2+}$ in water (right).

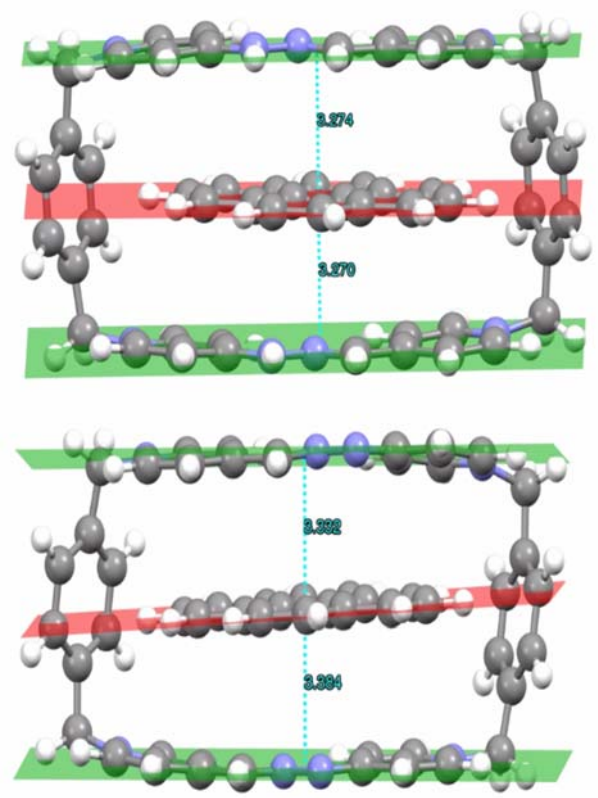

Figure S117. Distance between the average plane of the aromatic moieties of the L fragments and a centroid on pyrene for the inclusion complexes in water of pyrene with **R**$^{4+}$ (top) and **R**$^{2+}$ (bottom).

19. References:

S1 M. J. Plater, P. Barnes, L. K. McDonald, S. Wallace, N. Archer, T. Gelbrich, P. N. Horton, M. B. Hursthouse, *Org. Biomol. Chem.*, **2009**, *7*, 1633-1641.

S2 A. Blanco-Gómez, Á. Fernández-Blanco, V. Blanco, J. Rodríguez, C. Peinador, M. D. García, *J. Am. Chem. Soc.* **2019**, *141*, 3959-3964.

S3 a) J. Sandstrom, *Dynamic NMR Spectroscopy*; Academic Press: New York, NY, USA, **1983**. b) H. Kessler, *Angew. Chem. Int. Ed.* **1970**, *9*, 219-235.

S4 C. Bannwarth, S. Ehlert, S. Grimme, GFN2-xTB - an Accurate and Broadly Parametrized Self-Consistent Tight-Binding Quantum Chemical Method with Multipole Electrostatics and Density-Dependent Dispersion Contributions. ChemRxiv. 2018, D.O.I: https://doi.org/10.26434/chemrxiv.7246238.v1. Preprint.

S5 C. Gozalvez, J. L. Zafra, A. Saeki, M. Melle-Franco, J. Casado, A. Mateo-Alonso, *Chem. Sci.*, **2019**, *10*, 2743-2749.

S6 Gaussian 09, Revision D.01, M. J. Frisch, G. W. Trucks, H. B. Schlegel, G. E. Scuseria, M. A. Robb, J. R. Cheeseman, G. Scalmani, V. Barone, G. A. Petersson, H. Nakatsuji, X. Li, M. Caricato, A. Marenich, J. Bloino, B. G. Janesko, R. Gomperts, B. Mennucci, H. P. Hratchian, J. V. Ortiz, A. F. Izmaylov, J. L. Sonnenberg, D. Williams-Young, F. Ding, F. Lipparini, F. Egidi, J. Goings, B. Peng, A. Petrone, T. Henderson, D. Ranasinghe, V. G. Zakrzewski, J. Gao, N. Rega, G. Zheng, W. Liang, M. Hada, M. Ehara, K. Toyota, R. Fukuda, J. Hasegawa, M. Ishida, T. Nakajima, Y. Honda, O. Kitao, H. Nakai, T. Vreven, K. Throssell, J. A. Montgomery, Jr., J. E. Peralta, F. Ogliaro, M. Bearpark, J. J. Heyd, E. Brothers, K. N. Kudin, V. N. Staroverov, T. Keith, R. Kobayashi, J. Normand, K. Raghavachari, A. Rendell, J. C. Burant, S. S. Iyengar, J. Tomasi, M. Cossi, J. M. Millam, M. Klene, C. Adamo, R. Cammi, J. W. Ochterski, R. L. Martin, K. Morokuma, O. Farkas, J. B. Foresman, and D. J. Fox, Gaussian, Inc., Wallingford CT, 2016.

S7 Jmol: an open-source Java viewer for chemical structures in 3D. http://www.jmol.org/ .

S8 K. S. Alongi, G. C. Shields, *Annu. Rep. Comput. Chem.* **2010**, *6*, 113–138.